Experimental Investigation, Stochastic Modelling and Reliability Analysis of Fatigue Behavior of Tapered Composite Laminates

Xuan Ning Guo

A thesis

in

The Department

Of

Mechanical and Industrial Engineering

Presented in Partial Fulfillment of the Requirements

For the

Degree of Master of Applied Science

At

Concordia University

Montreal, Quebec, Canada

February 2005

Guo Xuan Ning, 2005

Library and Archives Canada

Published Heritage Branch

395 Wellington Street
Ottawa ON K1A 0N4
Canada

Bibliothèque et Archives Canada

Direction du Patrimoine de l'édition

395, rue Wellington
Ottawa ON K1A 0N4
Canada

Your file Votre référence
ISBN: 978-0-494-16250-7
Our file Notre référence
ISBN: 978-0-494-16250-7

NOTICE:
The author has granted a non-exclusive license allowing Library and Archives Canada to reproduce, publish, archive, preserve, conserve, communicate to the public by telecommunication or on the Internet, loan, distribute and sell theses worldwide, for commercial or non-commercial purposes, in microform, paper, electronic and/or any other formats.

The author retains copyright ownership and moral rights in this thesis. Neither the thesis nor substantial extracts from it may be printed or otherwise reproduced without the author's permission.

AVIS:
L'auteur a accordé une licence non exclusive permettant à la Bibliothèque et Archives Canada de reproduire, publier, archiver, sauvegarder, conserver, transmettre au public par télécommunication ou par l'Internet, prêter, distribuer et vendre des thèses partout dans le monde, à des fins commerciales ou autres, sur support microforme, papier, électronique et/ou autres formats.

L'auteur conserve la propriété du droit d'auteur et des droits moraux qui protège cette thèse. Ni la thèse ni des extraits substantiels de celle-ci ne doivent être imprimés ou autrement reproduits sans son autorisation.

In compliance with the Canadian Privacy Act some supporting forms may have been removed from this thesis.

While these forms may be included in the document page count, their removal does not represent any loss of content from the thesis.

Conformément à la loi canadienne sur la protection de la vie privée, quelques formulaires secondaires ont été enlevés de cette thèse.

Bien que ces formulaires aient inclus dans la pagination, il n'y aura aucun contenu manquant.

Canada

ABSTRACT

Experimental Investigation, Stochastic Modelling and Reliability Analysis of Fatigue Behavior of Tapered Composite Laminates

Xuan Ning Guo

The present thesis contains the results of testing, stochastic process modeling and reliability analysis of symmetric tapered laminates with pre-set delaminations. Two laminate configurations, called lay-up A and lay-up B are considered. Lay-up A is a $[0/\pm45/0/(\pm45)_3/\pm45/0_7]_S$ laminate that is reduced to a $[0/\pm45/0/\pm45/0_7]_S$ laminate and lay-up B is a $[0_7/\pm45/0/(\pm45)_3/\pm45/0]_S$ laminate that is reduced to a $[0_7/\pm45/0/\pm45/0]_S$ laminate. Two locations of pre-set delaminations, at the center of the core layer and in between belt and core layers in the thin side of lay-up A tapered laminate, are considered. Two loading conditions, (a) cyclic tension-compression loading and (b) cyclic tension-compression loading with 85% over tension load, are applied for the fatigue tests in the present thesis.

A stochastic approach to model the fatigue damage development based on the test data which has been developed and presented in an existing work is used in the present thesis. The Markov Chain is used to represent the fatigue damage accumulation in this approach, and the differences between the true probability

distribution and the unconditional probability distribution (or predicted unconditional probability distribution) of the fatigue response parameter are determined by using different methodologies, that are, the Maximum Entropy Method (MEM) and, Gaussian (single and bivariate) probability distribution and joint probability density function. The test data on the fatigue response parameter are analyzed based on the reliability function, hazard rate and failure density function.

Dedicated this to my wife and my son……

Acknowledgement

I would like to express my sincere gratitude and thanks to all those who help me to complete this thesis in various ways. In particular, I am deeply indebted to my supervisor Dr. Rajamohan Ganesan whose generous help, valuable suggestions and warmhearted encouragement accompanied me in all the time of research for and writing of this thesis.

I am grateful to many people in the department who have assisted me in the course of this work. Among them, Ming Xie, Robert Oliver, Anandha Kumar Arumugam, and Paul Ouellette have been particularly helpful and generous with their time and expertise.

I would like to give my special thanks to my parents for their generous support, encouragement. Lastly, and most importantly, I wish to thank my wife and my son, Hong Wei Yin and Dong Kun Guo, who supported me with their love, understanding, and encouragement. To them I dedicate this thesis.

TABLE OF CONTENTS

List of Tables

LIST OF FIGURES

Nomenclature

ε	Strain
σ	Stress
S_{thick}	Cross-section square on thick side of specimen
S_{thin}	Cross-section square on thin side of specimen
S_a	Average of cross-section square of specimen
Y_0	Grip position at zero loading
Y	Grip position at any given time
E	Young's modulus
C_i	Compliance
$p_{ij}(n_{k-1}, n_k)$	Transition probability function (TPF)
P	Probability
$f_{ci}(c_i)$	Density function
λ_i	MEM coefficients
σ	Standard deviation
μ	Mean value
$f(x, y)$	Joint probability density function
X	Random variables
Y	Random variables
σ_x	Standard deviations of variables X
σ_y	Standard deviations of variables Y

$[\prod(n_{k-1}, n_k)]$	Transition probability matrix
$[\prod^U(n_0, n_m)]$	Unconditional transition probability matrix
p_m	Match percentage
λ_{t_i}	Hazard rate at any given time
$N_S(t_i)$	Numbers of survived specimens at time t_i
$N_S(t_i + \Delta t_i)$	Numbers of survived specimens at time $t_i + \Delta t_i$
E_0, E_n	Young's modulus at load cycle 0 and n
$R(n)$	Reliability at load cycle n
F_n	Failure probability
f_n	Failure density function at load cycle n

Chapter 1

Introduction

1.1 Literature review

1.1.1 Fracture mechanisms of metal and composite materials

In addition to the conventional metallic materials, laminated composite materials are now being widely used in various applications for the past three decades due to their relatively high strength/stiffness-to-weight ratio, elastic tailoring properties, inherent damping, and capability of anti-corrosion. For example, the application of composite materials can be found in power generation plants, automotive and transportation industry, construction and civil engineering industry, and aerospace industry.

In metallic materials, fracture mechanism is normally concerned about how and where a crack (or cracks) is generated and grows as well as the severity of damage caused by crack growth that leads to final fracture. But the failure mechanisms and damage modes for composite material laminates are more complex than that of metallic materials due to

their anisotropic material properties. One or more of the following failure modes are encountered during any time of service life [1-3]: matrix cracking, de-bonding between fiber and matrix, delamination, fiber cracking, and laminate splitting, etc. A number of researchers derived various models to describe how the factors, such as composite material (including fiber-dominated or matrix-dominated composite material, glass or graphite fiber, etc.), geometry configuration (fiber orientation, stack sequence, tapered laminate, etc.), fatigue loads (stress magnitude, stress ratio, frequency and overload), and environment (thermo and humidity), affect the static fracture and fatigue behavior of composite laminates.

1.1.2 Fatigue damage mechanism and life prediction of composite laminates

For a new structure or new component design procedure, the original experimental data regarding the mechanical properties of the material under both static and fatigue loadings have to be available, which are the key issues of capability and reliability aspects during service, especially for those fatigue data that are directly related to the life time of the structure and component. Therefore, the fatigue behavior of composite laminates, which have been largely investigated in recent years, is considered as one of the most critical properties in automotive and aerospace engineering research and design.

In general, the three typical stages of composite material fatigue damage better show the processes of strength/stiffness degradation and damage accumulation under various cyclic loadings, as descibed by Reifsnider [1] and Jie [2], which are often called:

i) Initiation phase,

ii) Stiffness and strength steady-degradation phase, and

iii) The phase of damage increasing that leads to fracture and failure.

They also mentioned the differences between the damage modes and damage growth rates involved in these three stages although the damage modes and interactions between damage modes can not be separately or precisely described in a certain phase. For example, matrix cracking and fiber breaking are often observed in the initiation phase that may trigger high damage growth rate; crack coupling, interfacial de-bonding, delamination and its growth are the main damage modes in the relative steady-degradation of stiffness and strength phase that occupies the most life time of service; the major damage modes during phase iii) are presented as the rapid growth of delamination, fiber concentrative breaking and local fracture, etc. with high damage growth rate that leads to a complete failure.

Talreja [3] also mentioned that the damage modes showed quite the same routine processes as Reifsnider [1] did in that the matrix cracking appears to be the first mode of damage at the very beginning of service life, then the delamination occurs as a result of stress concentrations at the intersections of matrix cracks and grows into the second

stage, and the large-scale of delamination and matrix cracking leads to fiber breaking and this results in final fracture and failure in the third stage although the damage accumulation and growth rate are always different due to loading history, specimen geometry, stacking sequence and environment. Very often, ultimate failure of laminated composites is caused by large-scale fracture due to fiber cracking at different locations of delaminated layers. Therefore, the onset and propagation of delamination in composite laminates is considered as the critical damage mode during fatigue service time.

Many researchers had worked out some approaches for fatigue damage tolerance and life prediction under some assumptions in the past two decades. Among them, Hwang and Han [4] introduced a new definition, that is called fatigue modulus dF/dN (fatigue modulus F at N cycles), to calculate damage accumulation and life prediction of composite material under single-stress level as well as multi-stress level fatigue loads by using strain failure criterion. O'Brien [5, 6] proposed to establish a damage-threshold/fail-safety approach to predict the tension fatigue life of composite laminates based on the model of dG/dN (Strain energy release rate at N cycles), and it is further applied for compression load conditions. Yang and his associates [7, 8] established a residual strength/stiffness degradation model dE/dN (residual strength E after N cycles) to calculate residual strength after N cycles or to predict fatigue cycles at failure for graphite/epoxy composite laminates under tension-compression cyclic loading based on an appropriate failure criterion. Many researchers, such as Wu et al [9] and Schaff et al [10], used residual strength as a fatigue parameter to predict the fatigue life of composite laminate. The model of da/dN (rate of delamination growth along with fatigue cycles:

crack length a at N cycles) was also used by Komorowski, Lefebvre et al [11] to represent the fatigue damage accumulation and life prediction under the assumption that the major damage mode is delamination.

1.1.3 Delamination sensitive factors of composite laminates in fatigue service

Although the composite laminate's final fatigue failure results from the combined failures of several damage modes like matrix cracking, de-bonding between matrix and fiber, delamination, laminate splitting and fiber fracture, the threshold and propagation of delamination along the thickness of specimen is considered to be the major fatigue damage mode as it directly leads to fiber breaking, laminate splitting and finally laminate fracture. So the sensitive factors that lead to delamination initiation and accelerate its propagation have been largely investigated in recent years.

1.1.3.1 Effectiveness of stacking sequences and tapered laminates

Among the specimen geometry configurations, two structures that are considered more sensitive to initiate delamination are named in the literature as tapered laminates and multi-angle orientation laminates, compared to the uniform thickness and unidirectional laminates respectively, as concentrated shear stresses exist in the interlaminate in both cases that may lead to Mode I (opening) and Mode II (shear opening) failure [12] under simple tension load.

Many papers investigated the onset and propagation of delamination in the tapered composite laminates under static or cyclic tension loading, and the test results were also different for the different types of ply-drop and for different angles of tapered laminate. Those ply- drop types that are presented in Fig.1.1 are often called: i) External-ply-drop-off, ii) Mid-plane-drop-off, and iii) Internal-ply-drop-off [13].

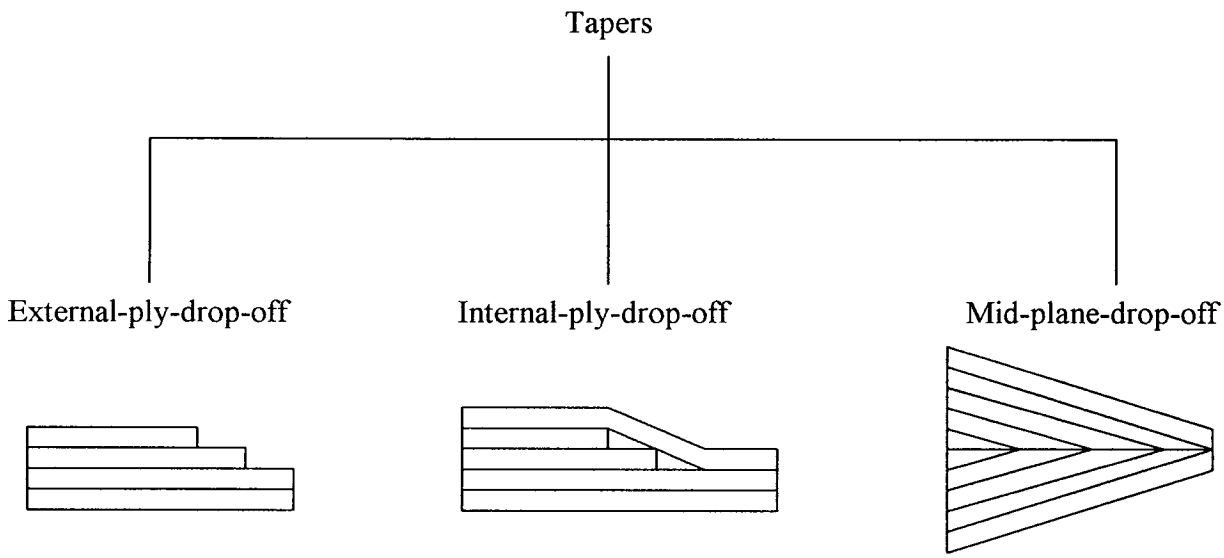

Figure 1.1 Laminate types in terms of ply-drop-off

The Internal-ply-drop-off (see Figure 1.2) has proved to have the least interlaminar residual stress in the ply-dropped area than that of the other two types of ply-drop-off and this was investigated by Ochoa and Chan [14]. Murri, O'Brien et al [15, 16] analyzed the delamination onset and predicted the delamination onset in unidirectional tapered laminates (called hereafter as Internal-ply-drop-off laminates) by using FE (finite element) model and have shown that the most likely place for an opening delamination

(Mode I) is at the junction of the tapered and thin regions, which is shown as a line (BCD) in Figure 1.2 and that the growth occurs in both directions of tapered and thin regions. Erian and Parnas [17] also proved that the initial delamination occurred at the junction of tapered and thin portions and they predicted the growth along both directions using interlaminar stress and strain energy release approach. Of course, from the methods of stress analysis and FEM, it is easy to conclude that the larger the taper angle is, the more sensitivity is for triggering delamination in that tapered area [18].

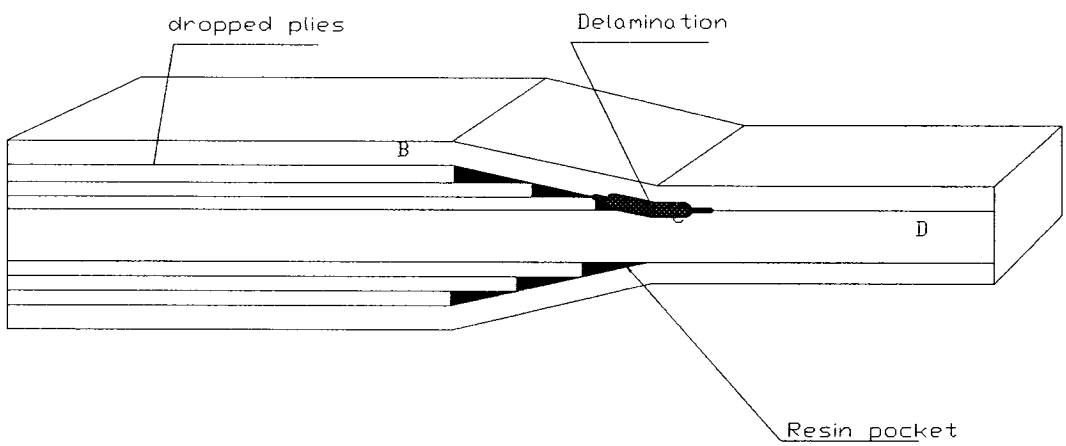

Figure 1.2 Typical schematic of symmetric tapered laminate with internal ply-drop

In another type of study for multi-angle fiber orientation of the graphite epoxy laminates $(0_2/\theta_2/-\theta_2)$ (θ was 15^0, 20^0, 25^0, 30^0) under tension-tension fatigue load that was done

by O'Brien [19] indicated that the onset of matrix cracking in the central $-\theta^0$ plies always preceded the onset of local delamination in the $\theta/-\theta$ interface by calculation of strain energy release rate. Therefore, the manufacturing flaws like air bubbles and contaminations in the interlaminate, which are considered as a kind of pre-set delamination in the laminate plates, are proven to be more dangerous than any other manufacturing flaws in this study.

1.1.3.2 Effect of tension-compression cyclic load and over tension load

The composite laminate fatigue behavior under tensile loading depends mainly on the properties of the fibers (along the fiber direction), while under compression loading, the property of the matrix gets more influence. In another words, the interlaminar stresses under compression load are more severe than tension load and certainly have more chances to de-bond the interface between fiber and matrix or break the matrix directly, which leads to delamination locally in any case, therefore, the compression load is always regarded as more sensitive to generate delamination and accelerate the growth of delamination than that of tension load during composite laminate's service life. Furthermore, the tension-compression fatigue load has significant influence on initiating delamination at any weakened interlaminar and makes it grown faster than that of tension-tension load, or further leading to buckling failure [20, 21] and global structural failure. In order to prevent delaminating and buckling in earlier damage stages both under static and cyclic loading, the anti-buckling guide had to be used in most experiments with compression load. The anti-buckling guide is normally used in the relative high

compression load condition, whose stress ratio is in the range of R<-1 (tension-compression load case) or R>1 (compression-compression load case) [22]. The compression behavior of delaminated/buckled composite laminates dealt with an ideal case of single delamination is largely investigated by use of FE method since the past two decades, and then it was developed for the multi-delamination case by Woo-Min Kyoung et al and Hiroshi Suemasu [23, 24].

The fatigue damage model and life prediction of unidirectional laminates under tension-tension load have been largely investigated [4, 25, 26, 27] by calculation of fatigue modulus and strain energy release rate under assumption of steady-accumulation damage theory. With the increasing use of composite laminates in recent years, more and more authors involved in the research composite material field of tension-compression loading conditions. For example, Yang and Liu et al [6, 28, 29] worked out a residual strength degradation model for fiber dominated graphite/epoxy composites under tension-compression cyclic loading, and later on they also developed a fatigue stiffness degradation model [7]. Jerzy P. Komorowski et al [11] derived a delamination propagation rate (da/dn) as a function of strain energy release rate G to estimate the valid service time under compression-dominated fatigue loading.

On the other hand, unlike the metallic materials for which the tension overload leads to the creation of plasticity and damage retardation in the fatigue service, in the case of composite laminates it definitely accelerates damage scale by heavily triggering the various forms of damage modes, such as matrix cracking, de-bonding, fiber cracking and

delamination, comparing with the normal failures under normal tension-tension or tension-compression loading. Only few researchers are working on that aspect to analyze its effects on the fatigue behavior of composite laminates.

Overall, the tapered laminates are reckoned on less fatigue life than uniform thickness laminates under cyclic loading, especially under compressive loads or even over tension load based on normal tension-compression, since there are more chances of delamination occurrence in the tapered area [14, 18, 25] during fatigue life. Joakim [26] and Komorowski et al [11] proposed that the fatigue life is mainly related to the delamination growth rate for the laminated composite, so based on that, it would be much more interesting to know how the artificial delamination (pre-set delamination) affects the fatigue life. And more interesting parts here would be, how the delamination sensitive factors, such as multi-directional tapered laminates, compression load, tension overload and pre-set delamination, synthetically affect the stiffness/strength degradation as well as fatigue life. Some of these effects have been investigated and associated with some experiments done in this thesis.

1.1.4 Environmental and frequency effects

The environmental conditions, on the other hand, are also considered as an important factors to affect the composite laminate's fatigue behavior as the fiber and matrix are sensitive to temperature and humidity, but very often this kind of environmental problem can be easily avoided by simply choosing high-temperature resistance composite material

such as CSPI (Chung Shan modified Poly-Imide) [30] or painting the surface of composite structures to prevent moisture absorption.

Ignoring the heat effects due to increasing test frequency, the strength and stiffness of composite materials under strain-controlled fatigue test is proved to be a nonlinear response of test frequency in the earlier studies of Stinchcomb, Reifsnider et al [31]. The following studies by Sun et al [32] show that the frequency effects enter only in stress controlled fatigue test and they have derived a stiffness equation as a function of test frequency. Of course, another part of frequency effects on fatigue damage is from heating that is generated by the increased load frequency. So Barron et al [33] concluded that the effects of test frequency for the matrix-dominated orientations such as angle-ply on fatigue behavior are much greater than that for the fiber-dominated laminates such as unidirectional and cross ply specimens according to their experiments, and more important is that they also proved that the test frequency effects on fatigue behavior are mostly due to hysteretic heating.

1.1.5 Stochastic approach to model the fatigue damage process

Even though the above models for fatigue damage accumulation processes and fatigue life prediction have been established and developed in recent years, it is still hard to determine precisely how these failure mechanism damage modes, which are considered very complex [1, 2, 3] as mentioned in the above, and their occurrences individually or synthetically contribute to the composite laminate fatigue damage [3]. One complexity is

how these failure modes and their occurrences contribute to fatigue damage that can not be quantified precisely [3]. Other complexities, like failure mode changing from one to another, crack jumping, many failure modes active at the same time and viscoelastic response, also can not be presented precisely. Therefore, the Markov process modeling, which can better represent the composite material's fatigue damage accumulation process under such mentioned complexities through the entire service, has been developed in the recent years.

In the research paper by Bogdanoff and Kozin [34], the Markov Chain Model was first proposed to represent the probabilistic behavior of the cumulative damage of fatigue failure and fatigue crack growth of metals. Then Wen-Fang Wu et al's studies [9] on probabilistic modeling of Young's residual stiffness degradation by using lognormal and Weibull distribution showed a reasonable fit to the probability distributions of life times that have been obtained from fatigue tests and service operations. But considering the two limiting states of Weibull probabilistic distribution on the fatigue parameters, which are satisfactory (no damage) and failure (completely damaged), they certainly could not represent precisely the fatigue damage accumulation states. Moreover, the parameters used in the above models were for the crack length as fatigue response parameter and the parameters were estimated from test data by using statistical parameter estimation procedures. The true probability distributions (both individual and joint distribution) as well as the reliability of the above mentioned fatigue response parameters have not been considered or calculated so far.

The stochastic approach has been investigated in recent years for knowing or predicting the possibilities of fatigue damage or distribution of fatigue response parameter during cyclic tests. Ganesan's [35] "Data-driven stochastic approach" precisely and truly employs the probability distribution of fatigue response parameter at a certain damage state and the estimated states are based on the establishment of a structural-level response parameter, which is sensitive to various damage modes and is better to describe and quantify the fatigue damage. This approach is used in the present work. Due to limited test data, the individual and joint probability distributions corresponding to the experimental data do not always follow certain distributions like Normal Distribution and Weibull Distribution. Therefore, different standard distributions such as Gaussian distribution, Maximum Entropy distribution, and the combination of these have been determined and used in the present thesis.

The aim of the present thesis is to use a stochastic approach to model and analyze the fatigue damage accumulation processes for tapered composite laminates with the pre-set delamination under the conditions of normal tension-compression loading and the normal tension-compression load with over tension load.

1.2 Objective of the thesis

A better understanding of fatigue behavior of composite laminates is a key issue for the reliable and safe engineering design. From literature survey, it can be observed that the delamination through laminate thickness as well as its growth is identified as the major

damage modes in composite material's service life. Therefore, many researchers and investigators work on how the delamination sensitive factors affect the fatigue response parameters and how differences are influenced individually or synthetically by those factors, but none of them conducted the following aspects, which are all investigated in the present thesis:

a) How the thickness of core part of tapered laminate affects the fatigue response parameter in terms of same overall dimensions of the specimen with different lay-up sequences shown in Figure 1.2.

b) The effect of different pre-set delamination locations in the tapered laminates.

c) The effect of over tension load in terms of normal tension-compression load.

Accordingly, three phases of test with two groups of specimens in each phase have been carried out in the present work. The organization of tests is shown in Fig. 1.3. Phase One considered the tapered laminate specimens with same overall dimensions but with two types of lay-up sequences, which are lay-up A that is a $[0/\pm45/0/(\pm45)_3/\pm45/0_7]_S$ laminate that reduced to a $[0/\pm45/0/\pm45/0_7]_S$ laminate and lay-up B that is a $[0_7/\pm45/0/(\pm45)_3/\pm45/0]_S$ laminate that reduced to a $[0_7/\pm45/0/\pm45/0]_S$ laminate; Phase Two includes the tapered laminate specimens with the same lay-up sequence (lay-up B) but with different locations of pre-set delamination; In Phase Three, a total of 40 tapered specimens with same lay-up sequence (lay-up B) and delamination location (in between

belt and core layers in the thin side) are tested under normal tension-compression fatigue loading and normal tension-compression loading with regular over tension load, with 20 specimens in each group.

From reliability and safety point of view, the successful expression and prediction of probability distribution of fatigue response parameter at a certain load cycle is considered as a good reference for mechanical design. Therefore, the following two objectives are also considered in the present thesis:

d) To use a stochastic approach to model and analyze the fatigue damage accumulation processes in the tapered composite laminates with the pre-set delamination under the conditions of normal tension-compression loading and the normal tension-compression load with regular over tension load.

e) To analyze the reliability distribution corresponding to different load cycles of the test data from Phase Three using the reliability function, hazard rate and failure density function.

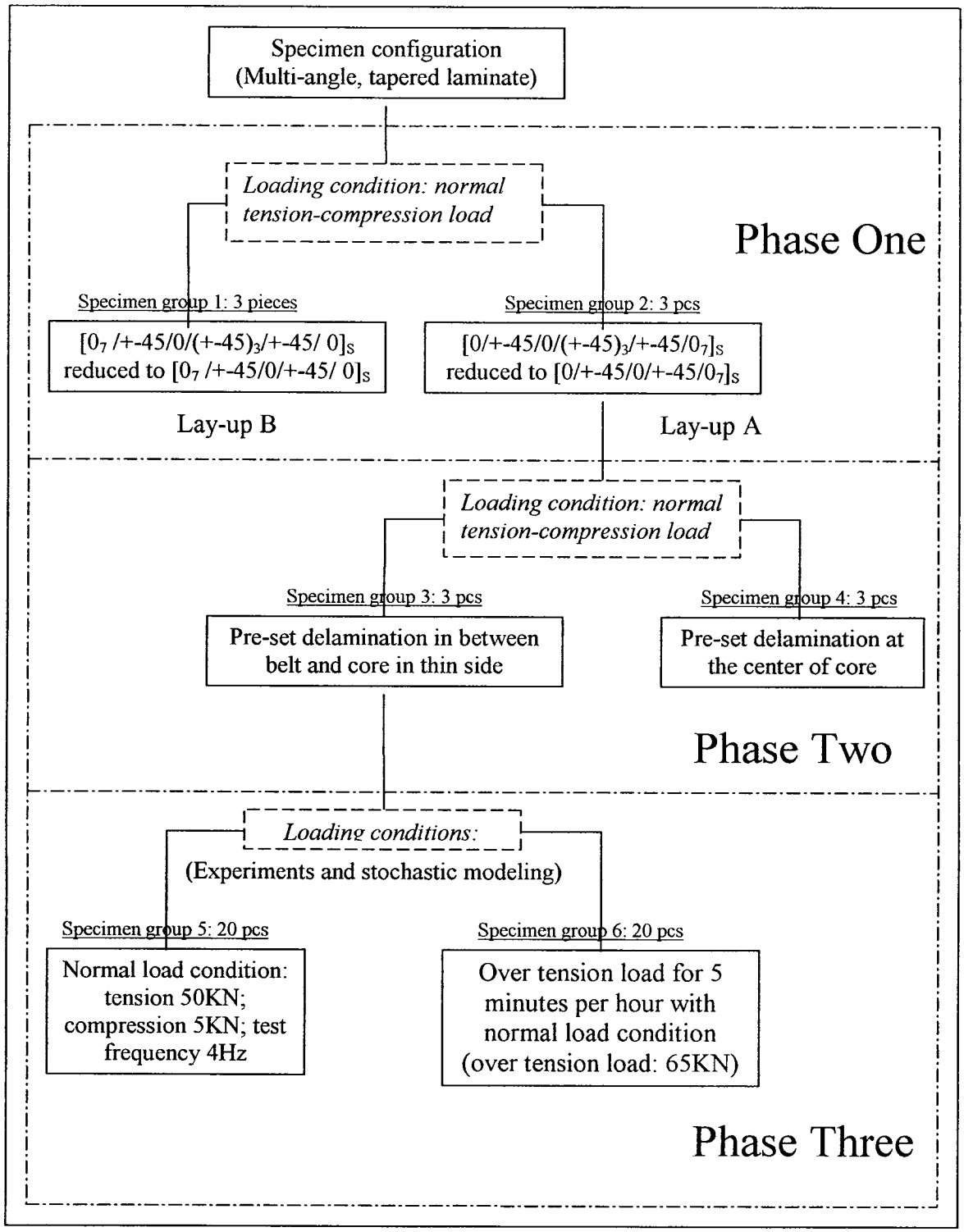

Figure 1.3 Organization of fatigue tests

1.3 Organization of thesis

The present chapter provides a brief introduction and literature review regarding failure modes and fatigue damage calculation or prediction for the composite laminates, and stochastic approach to determine the fatigue damage probability distribution and prediction as well as reliability distribution. The scope and objectives have been presented in section 1.2.

In chapter 2, the processes and procedures as to how the tapered composite laminates with pre-set delamination have been manufactured and the experimental program including three phases of tests with two groups of specimens in each phase are presented in detail.

In chapter 3, the test results of first two groups of specimens with different stack sequences are presented and it is shown that the specimens with thicker core laminate are much stronger than the specimens with thinner core laminate. The next two groups of tests concerning the effect of different locations of delamination are also presented and it is shown that when the pre-set delamination is more close to the middle of symmetric laminate, more fatigue damage will occur. The 5^{th} and 6^{th} groups of specimens with the same location of pre-set delamination are tested under two load conditions: normal tension-compression load (load condition one: LCO) and regular over tension load based on normal tension-compression load (load condition two: LCT). The results are given and

it is shown that the LCT has significant impact on the composite laminate's fatigue damage process.

In chapter 4, Markov process modeling is used to calculate the probability distribution of fatigue damage parameter at a certain cycle and to estimate the probability distribution after certain cycles. A MATLAB® code has been developed for this purpose. Different ways are used to derive individual and joint probability density functions including MEM (maximum entropy method) and Gaussian distribution. The advantages and disadvantages of these methods are described in this chapter. The final part of this chapter provides a sample application of the above investigation and discussion.

In chapter 5, Markov process modeling of reliability is presented based on reliability function, hazard rate and failure density function. Further discussion about the reliability of composite laminate is also provided in this chapter using the sample application.

The thesis ends with chapter 6, which provides conclusions of present thesis work and some recommendations for future work.

Chapter 2

Manufacturing and testing of composite laminates

2.1 Introduction

Symmetric tapered laminates with internally dropped plies are fabricated by using NCT-301 graphite/epoxy prepreg and they are laid-up manually followed by a vacuum-bag air-pressure autoclave cure. The two different types of lay-up configurations with the same number of layers and same dimensions are manufactured and tested in terms of the experimental program mentioned in the previous chapter. Lay-up A is a $[0/\pm45/0/\ (\pm45)_3/\pm45/0_7]_S$ laminate that reduced to a $[0/\pm45/0/\pm45/0_7]_S$ laminate, while lay-up B is $[0_7/\pm45/0/(\pm45)_3/\pm45/0]_S$ that reduced to a $[0_7/\pm45/0/\pm45/0]_S$ laminate. The specimen configurations A and B are shown by the cross-section drawing in Fig.2.1 and the photograph of cross-section in Fig.2.2. The typical difference between the two lay-ups is that lay-up A is with 18 core layers and only 4 belt layers in each side of symmetric laminate while lay-up B is with 6 core layers and 10 belt layers in each side of symmetric laminate. Based on the Phase Two of experimental program, the two locations of pre-set delamination that was made by

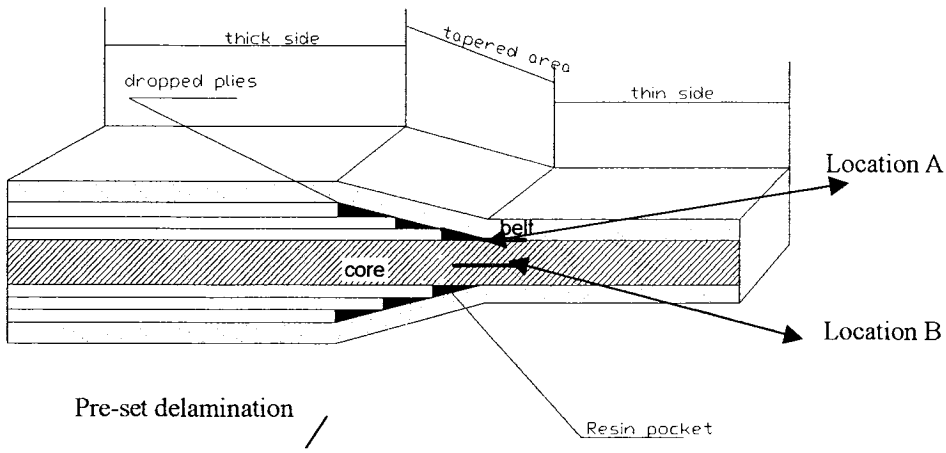

Figure 2.1 Tapered laminate configuration

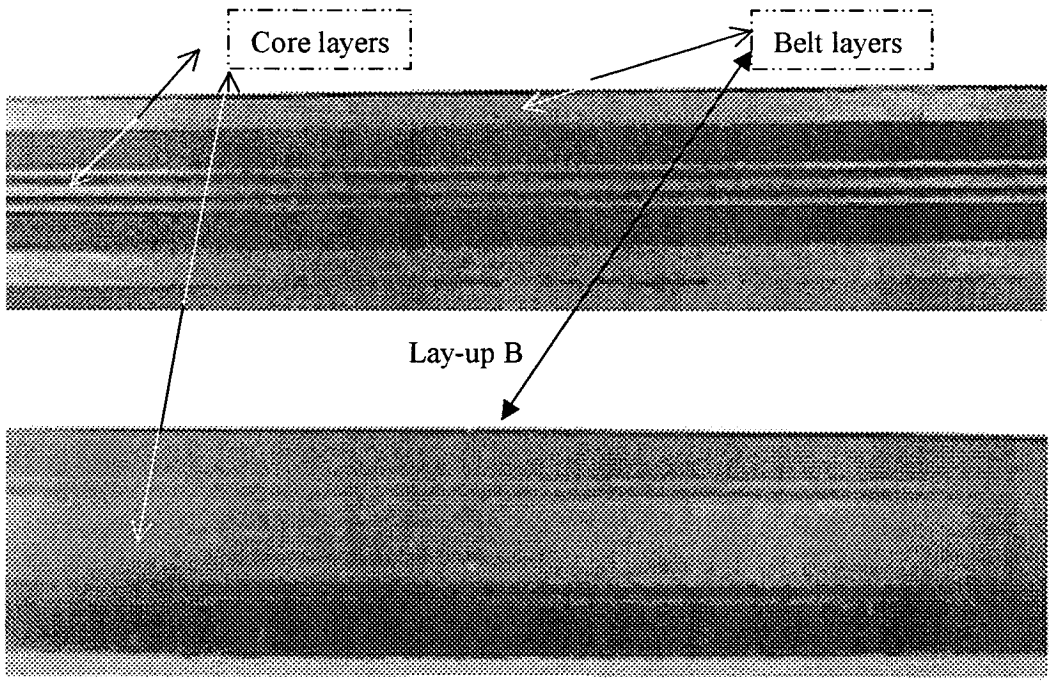

Figure 2.2 Photograph of specimen cross-section

using TEFLON are marked by bolder lines in Fig.2.1, which is about 10mm wide and at the Core center for one location (I) and in between Core and Belt layers for another location (II). The Figure 2.1 shows a schematic diagram of the symmetric tapered laminate with internal ply drops and two different locations of delamination.

2.2 Tools and auxiliary material

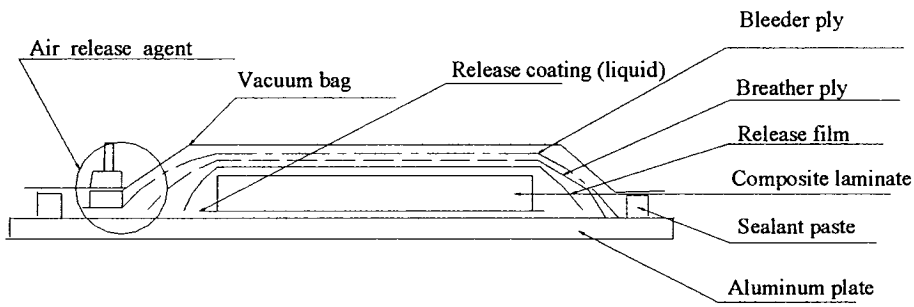

Figure 2.3 Typical laminate structure that is ready for autoclave process.

All necessary tools and materials are made ready before starting manual fabrication of the composite laminate. The main tools are the marble roller, which is used to squeeze the air from the interlayer by rolling on the prepreg surface; and a flat aluminum plate, which is used to support the laminates; and an air release agent, which is used to create vacuum in the vacuum bag with the vacuum pump. An iron is necessary to help

plies stick together when the room temperature is relatively low. Many auxiliary materials like release coating (liquid), bleeder plies, breather plies, release films, vacuum bag films and sealant paste are used to build-up the laminate structure that is the original specimen laminate, which is ready for autoclave process. The figure 2.3 shows the cross section of typical composite laminate structure prepared for autoclave processing.

2.3 Manual lay-up process

Composite laminate is manufactured by hand lay-up of prepregs that are cut according to the required size and fiber orientation. The detailed manual lay-up processes are described as follows: first, the aluminum plate has to be cleaned before the release coating is applied on the surface. After the coating dries, the first layer of prepreg is laid-up according to stack sequence, and the marble roller is used (or warm iron applied first in case of low room temperature) to roll and press the surface of prepreg to make sure that air has been removed from interlayer, which could avoid any voids or delaminations in the interlayer. After that, the sticky preventive paper of prepreg is removed from the rolled prepreg and the second layer is laid-up. The above process is repeated until the last ply is laid-up according to the specimen stacking sequence. Then the release film, bleeder ply, and breather ply are placed on top of the laminate and the vacuum bag is constructed by using sealant paste, vacuum bag film, and release agent according to figure 2.3. Now the composite laminate structure is ready

for cure in the autoclave.

2.4 The symmetric tapered laminate lay-up process

The symmetric tapered laminate fabrication process is a little bit different from the above process. The symmetric tapered laminate is manufactured in two separate parts namely the upper part and lower part. The detailed procedure is explained below as shown in Fig.2.4:

i. First place the release film over the aluminum plate, which is used to remove and turn upside down the whole lower part.

ii. Then lay-up the lower part starting from middle layer according to stacking sequence as per lay-up procedure.

iii. Lay-up the dropped plies as per the required dimension of the specimen configuration and keep the cut-off plies as fill-in layers for the missing material part.

iv. After laying-up the belt plies, one layer of release film is placed over it in order to remove the fill-in layers after curing process.

v. Then the cut-off plies are laid-up over the release film in the missing material area.

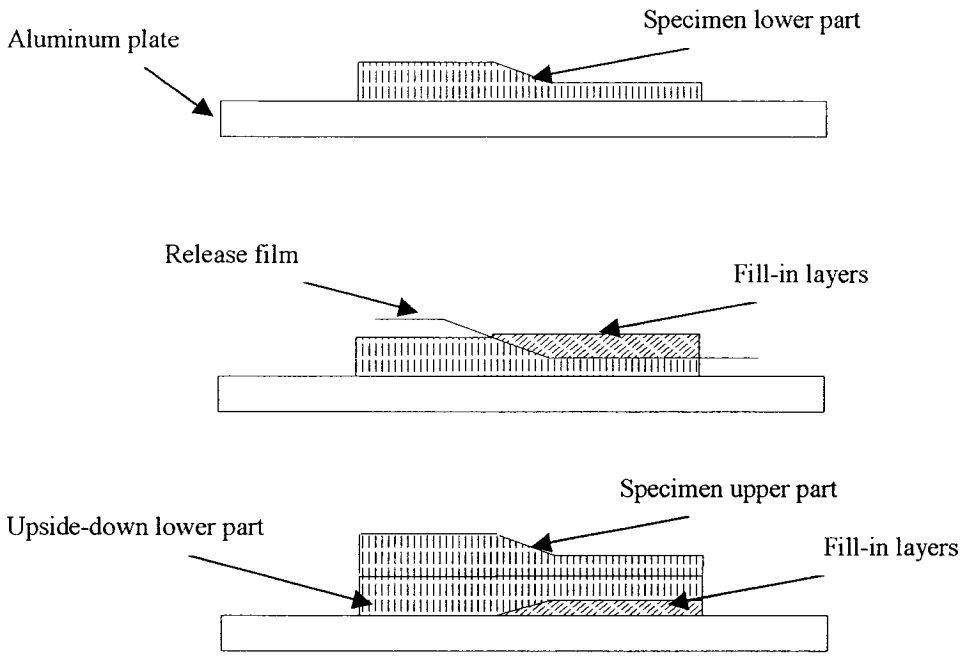

Figure 2.4 The symmetric tapered laminate manufacturing procedure

vi. Then remove the lower part from the aluminum plate and apply the release liquid coat on the surface of aluminum plate.

vii. Then turn the lower part upside-down (the middle layers will be on the top) and place it on the surface of coated aluminum plate.

viii. Continue to lay-up the upper part of tapered laminate as per stacking sequence until the last ply of laminate is finished.

ix. Repeat the sealing and vacuum processes as mentioned above. Then the laminate structure is ready for the cure process.

2.5 Cure process in autoclave

Put the finished laminate structure in the autoclave, and connect the air release agent with the vacuum pump. Then start the vacuum pump and make sure the pressure of the vacuum bag is at 30 psi, and then close the door of autoclave with the bolts. Open the valve of air pressure of autoclave until the pressure inside the autoclave reaches 80 psi, and then start curing program that is shown in Figure 2.5. In the curing process, the temperature of laminate is increased from room temperature to 106^0C within 40 minutes, and the temperature is maintained at 106^0C for about 15 minutes. Again the temperature is increased from 106^0C to 145^0C in 30 minutes and kept at that temperature for about 50 minutes. And then the curing program will automatically stop. The cured laminate in the autoclave should cool down naturally to the room temperature with the autoclave closed. Now the laminate is ready for cutout and test.

The purpose of increasing the temperature from room temperature to 106^0C and keeping it constant for 15 minutes at that temperature is to allow the gases (entrapped air, water vapor or volatiles) to escape from inside the laminate. Then increasing the temperature from 106^0C to 145^0C and keeping it constant for 50 minutes at that temperature allows the matrix to flow and for cross-linking of the resin. The main purpose for maintaining a constant temperature at 145^0C is to develop and build the mechanical properties of the composite laminate.

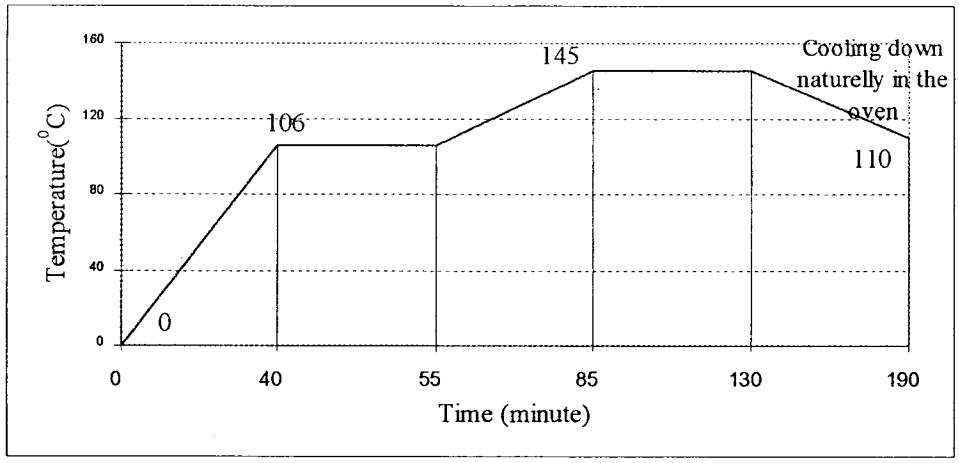

Figure 2.5 Cure process chart

2.6 Specimen configuration and preparation

The specimen is cut by high-speed diamond wheel/water cooled cut-off saw in order to avoid any surface defects/damage and keep free edge according to the following dimensions shown in Figure 2.6. The fabrication method and testing of the specimen meets the requirements of ASTM standards D 3479/D 3479M-96 and D 3039/D 3039M-00, although the specimen geometry is different from the ASTM recommendation due to the small size of raw material used in the laboratory, which could not be cut to obtain the recommended dimensions with 45 degrees fiber orientation.

The length and width of the specimen should meet the tolerance requirements of the ASTM standards because these two dimensions will influence the test results much when compared to other dimensions.

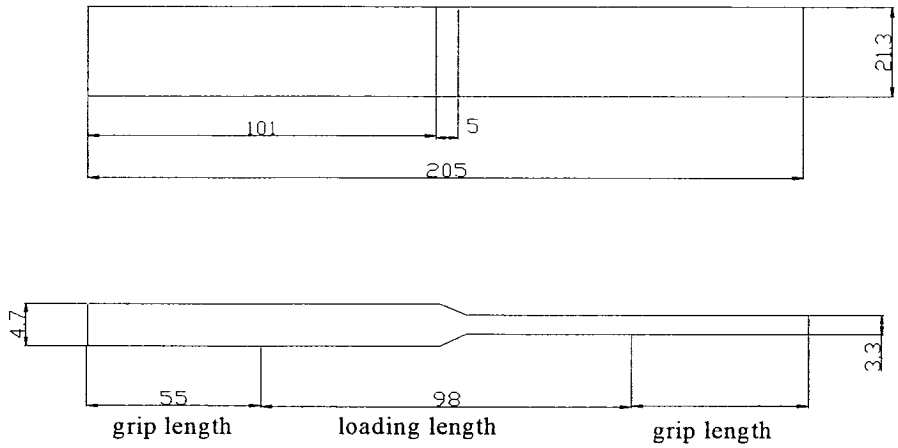

Figure 2.6 Test specimen dimensions

2.7 Fatigue test configuration and data collecting

The fatigue testing of the specimen is done using the MTS machine (computer controlled hydraulic test equipment) with force-controlled mode. The hydraulic controlled wedged grips with flat surface are used for gripping the test specimen instead of manual fasten grips by using the tabs at specimen ends, which has been proved to have high possibility to damage the specimen at root of tab or the slip failure of specimen. The test specimen that is loaded by the hydraulic controlled wedged grips in MTS machine is shown in Fig. 2.7.

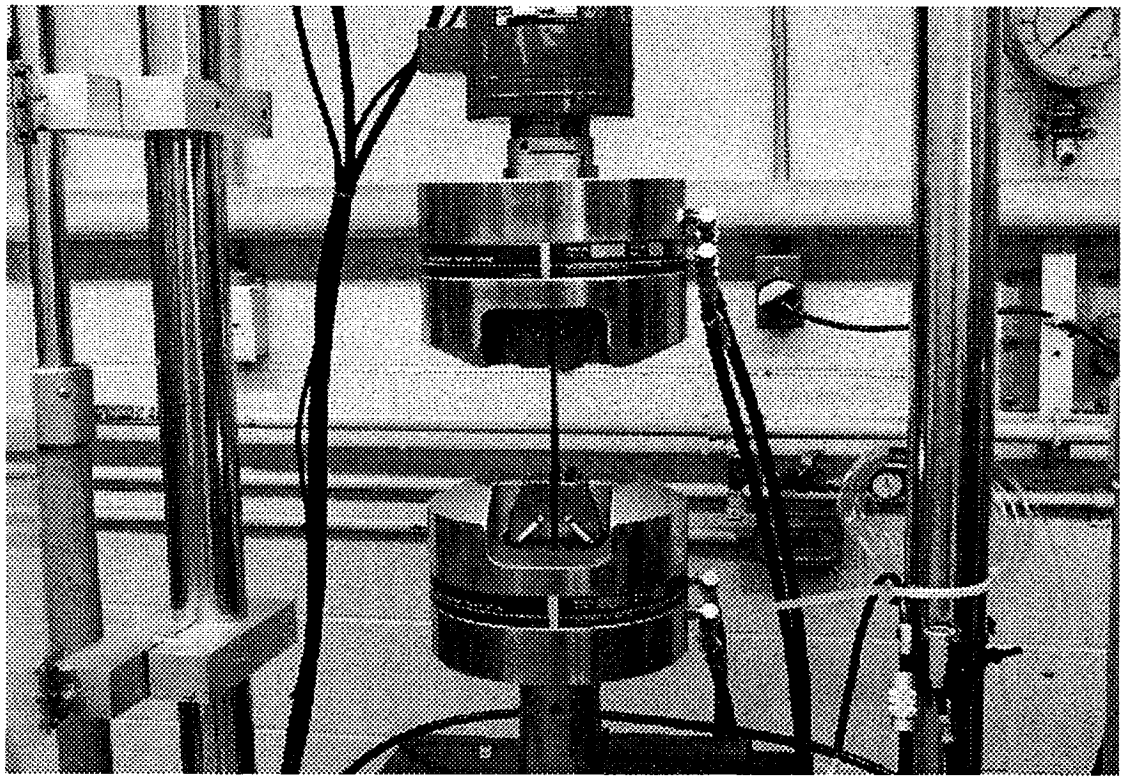

Figure 2.7 Photograph of test specimen in MTS test machine

In order to fix the fatigue test load parameters, the ultimate load of tapered laminates with stack sequence A ($[0/\pm45/0/(\pm45)_3/\pm45/0_7]_S$ laminate that is reduced to $[0/\pm45/0/\pm45/0_7]_S$) under the quasi-static loading has to be determined first. For instance, 3 pieces tapered laminates with lay-up A were tested under the quasi-static loading with 3mm/min ramp speed of test frame and the average ultimate load is about 75,000 Newton. So the tension load of fatigue test is determined as 50,000 N that is about 65% of the average ultimate load, and compression load is selected as 5,000 N when the stress ratio is defined as R=–0.1.

The following two load conditions are used for all the tests listed in the organization

of fatigue test (Fig. 1.3) in the section 1.2, which are in terms of the ultimate loading:

- Load Condition One (LCO: Normal tension-compression fatigue load):

  Test frequency: 4 Hz;

  Tension load: 50,000 N (65% of ultimate load);

  Compression load: -5,000 N (i.e. stress ratio R=–0.1.)

- Load Condition Two (LCT: see Fig. 2.8):

  Over tension load: 65 KN, that is about 85% of ultimate load;

  5 minutes of over tension load for every one-hour based on LCO.

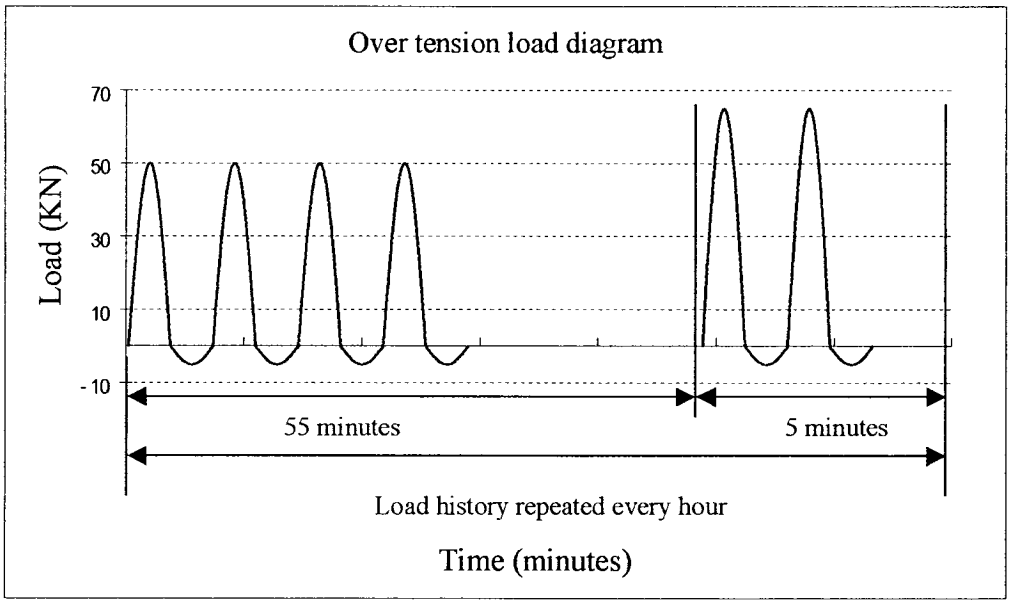

Figure 2.8 Load Condition Two: over tension load diagram

The following fatigue test phases are set-up in test according to the organization of

tests (Fig. 1.3):

Phase One:

Two groups (groups 1 and 2) of tapered laminate specimens with same overall dimensions but with different types of lay-up sequence (A and B) are tested subject to LCO (normal tension-compression load).

Phase Two:

Two groups (groups 3 and 4) of tapered laminate specimens with the same lay-up sequence (A) but with different locations of pre-set delaminations are tested under LCO. The pre-set delaminations are in between Core and Belt layers in the thin side of specimen and at the center of Core layers of specimen as shown in Figure 2.1.

Phase Three:

Another two groups of tapered laminate specimens, groups 5 and 6, with 20 specimens in each group are tested under both the loading conditions (LCO and LCT).

The test program is set to record 100 test data points within 2 seconds in every hour for one data collection point, which includes two fatigue cycles in each group of data. So a total of 40 groups of collection points are recorded for each specimen in the 40

hours test period. Considering the stability of test system, the test program is also set to start the data collection at 2800 cycles, which means that the 40 groups of data are at 2800, 17280, 31680, ... , 578880 cycles respectively. The three parameters which are recorded in each test data group are test times, forces and the displacements of specimen.

2.8 Calculation using test data

Since the stress and strain are different at different locations of the specimen such as the thicker side, thinner side and tapered area of specimen, the average stress and strain are considered in the present thesis.

For calculating the average strain of the tapered laminate, the displacement and loading length are considered, which is expressed by the formula:

$$\varepsilon = \frac{\Delta L}{L_0} \tag{2.1}$$

$$\Delta L = Y - Y_0 \tag{2.2}$$

where L_0 is the measurement of specimen's loading length; ΔL is the displacement difference, which represents the difference between the grip position at any given time (Y) and the position at zero loading (Y_0), that is shown in Fig. 2.9.

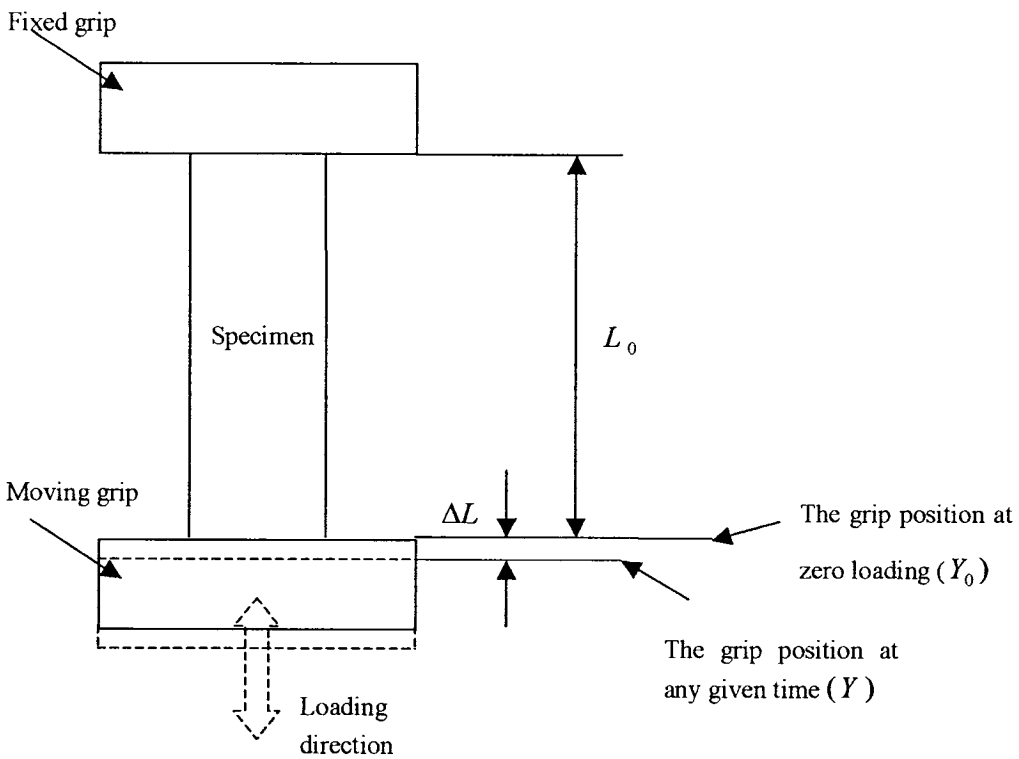

Figure 2.9 Specimen's displacement at any given time in MTS machine

The average stress is defined as the force divided by average cross section of the specimen:

$$\sigma = \frac{F}{S_a} \tag{2.3}$$

where F is the force of tension or compression; S_a is the average cross section of the specimen that is calculated by:

$$S_a = \frac{S_{thick} + S_{thin}}{2} \tag{2.4}$$

where S_{thick} is the cross sectional area of the thicker side of the specimen; S_{thin} is the cross sectional area of the thinner side of the specimen.

For example, from one specimen's original data file that is listed in the table 2.1, one can find from data point 16 that the load at that time point is 18 N that is close to zero, therefore, Y_0 is 0.09707055 as defined in the above, and L_0 is 97.32 mm that is the measurement of specimen loading length. And S_a is known by the measurements of S_{thick} and S_{thin}. So the average values of specimen strain ε and stress σ are listed in the table 2.2 based on equations (2.1), (2.2), (2.3) and (2.4).

Table 2.1 The recorded original data of one specimen from MTS machine:

Data points	Time Sec	Position(Y) mm	Load N
...	...	...	...
9	689.77252	-0.0132785	-4079.2393
10	689.77753	-0.0098301	-4044.7788
11	689.78235	-0.0132785	-4034.4409
12	689.78754	-0.0098301	-4017.2109
13	689.79254	-0.0098301	-3727.7444
14	689.79755	0.01775716	-2866.2368
15	689.80255	0.05224124	-1539.5154
16	689.80756	0.09707055	18.05347
17	689.81238	0.14879666	2182.1965
18	689.81757	0.22466162	4697.7983
19	689.82257	0.29362977	7358.1333
20	689.82758	0.37294316	10201.108
21	689.83258	0.45570493	13230.168
...	...	...	...

Table 2.2 The strain and stress calculation results of one test specimen:

Data points	Time Second	Position (Y) mm	Load N	Position (Y_0) mm	L_0 mm	S_a m^2	ε	σ Pa
...	...	...	...	...	...	...	...	...
10	689.7775	-0.00983	-4044.78	0.097071	97.32	8.97E-05	-0.0011	-4.5092E+07
11	689.7824	-0.01328	-4034.44	0.097071	97.32	8.97E-05	-0.00113	-4.4977E+07
12	689.7875	-0.00983	-4017.21	0.097071	97.32	8.97E-05	-0.0011	-4.4785E+07
13	689.7925	-0.00983	-3727.74	0.097071	97.32	8.97E-05	-0.0011	-4.1558E+07
14	689.7976	0.017757	-2866.24	0.097071	97.32	8.97E-05	-0.00081	-3.1954E+07
15	689.8026	0.052241	-1539.52	0.097071	97.32	8.97E-05	-0.00046	-1.7163E+07
16	689.8076	0.097071	18.0535	0.097071	97.32	8.97E-05	0	2.0073E+05*
17	689.8124	0.148797	2182.197	0.097071	97.32	8.97E-05	0.000532	2.4328E+07
18	689.8176	0.224662	4697.798	0.097071	97.32	8.97E-05	0.001311	5.2372E+07
19	689.8226	0.29363	7358.133	0.097071	97.32	8.97E-05	0.00202	8.2030E+07
20	689.8276	0.372943	10201.11	0.097071	97.32	8.97E-05	0.002835	1.1372E+08
21	689.8326	0.455705	13230.17	0.097071	97.32	8.97E-05	0.003685	1.4749E+08
...	...	...	...	...	...	...	...	...

*: Since Y_0=0.097071, then ε =0, can be viewed as a reference value.

Note: E+n represents 10^n for any value of n

Then the Young's modulus is determined using the formula:

$$\sigma = E\varepsilon \tag{2.5}$$

where E represents the Young's modulus.

Since there are 100 data points that are captured in each data group, there are 100 values of Young's modulus available based on the 100 pairs of values of σ and ε in each data group within two seconds as defined in the previous section. The Young's modulus of specimen at load cycle 2880 is defined as the slope of linear trend of the 100 data points that is 38815068059.20 Pa (38.82 GPa), which is shown in Fig. 2.10.

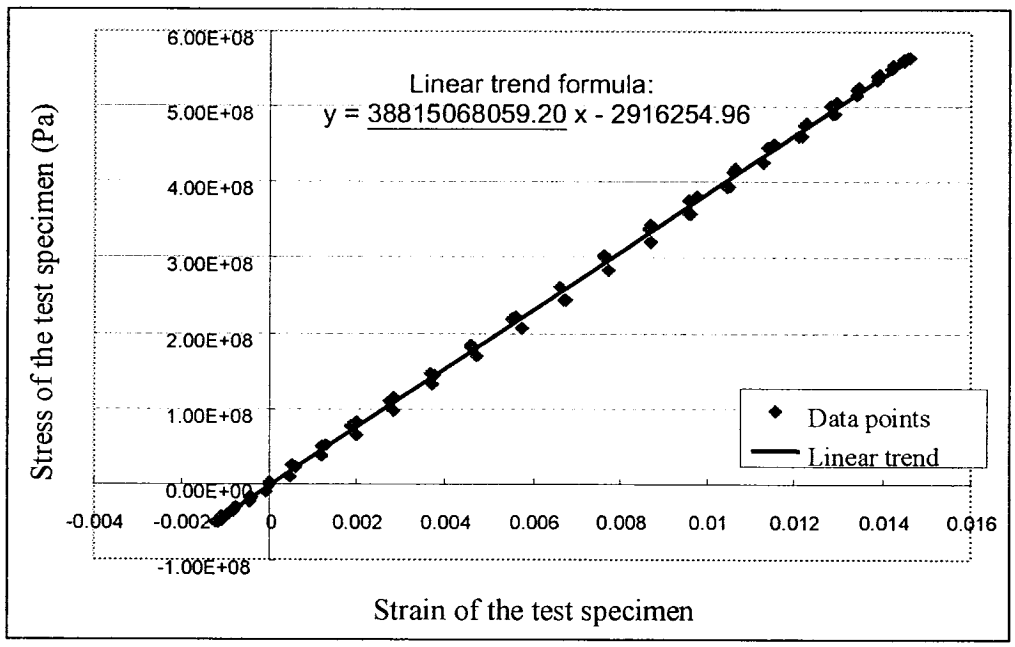

Figure 2.10 Linear trend of 100 data points at load cycle 2880

In the same manner, we can calculate 40 values of Young's modulus from 40 groups of data for one specimen in its whole fatigue life. Then the Young's modulus values corresponding to the fatigue load cycles for 20 specimens can be calculated and the results are presented in the graph in Fig. 2.11.

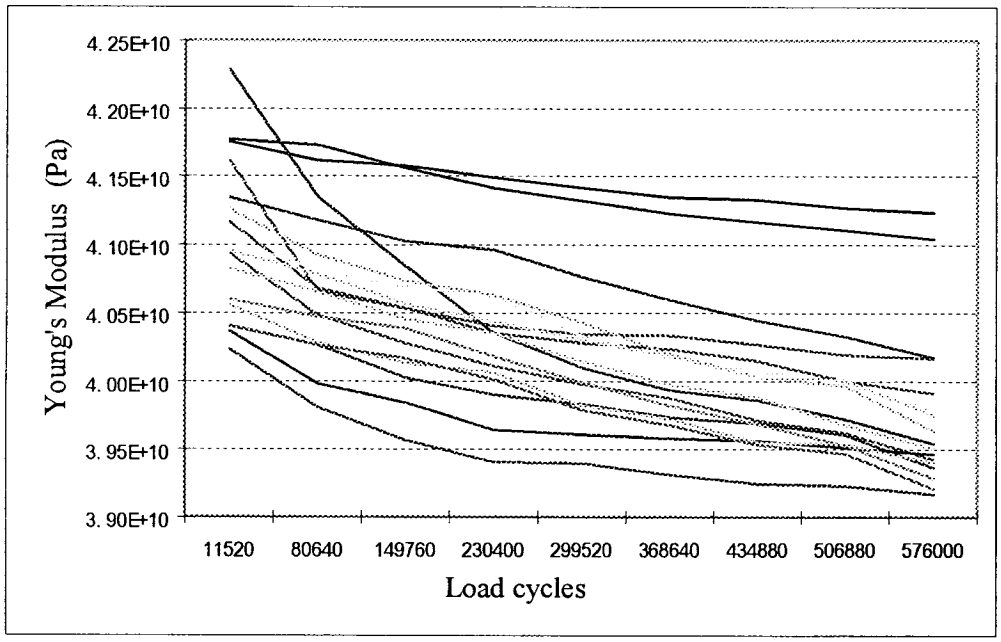

Figure 2.11 Young's modulus versus load cycles

Chapter 3

Fatigue test data and failure analysis of experimental results

3.1 Introduction

In order to investigate i) how the change in the numbers of core and belt layers in the tapered laminate configuration; ii) how the locations of pre-set delaminations; and iii) how the over tension load based on normal tension-compression load, affect the strength and stiffness of composite laminates, the three phases of test that are shown in Fig. 1.3 in the previous chapter had been planned and carried out on a uniaxial hydraulic test frame (MTS) in the present work. The three test phases included two specimen configurations (lay-up A and lay-up B), two locations of pre-set delaminations (at the center of core layers and in between core and belt layers) and two loading conditions (LCO and LCT). There were at least three specimens of each test group that were tested subjected to cyclic loading and the results were recorded and analyzed accordingly, and for the test specimens whose data will be proceeded for further stochastic analysis at least 20 pieces were tested for each group (groups 5 and 6).

3.2 Effect of laminate configurations

The specimen groups 1 and 2 with two kinds of configurations, which are called lay-up A tapered laminate ($[0/\pm45/0/(\pm45)_3/\pm45/0_7]_S$ that is reduced to $[0/\pm45/0/\pm45/0_7]_S$) and lay-up B tapered laminate ($[0_7/\pm45/0/(\pm45)_3/\pm45/0]_S$ that is reduced to $[0_7/\pm45/0/\pm45/0]_S$), were tested under fatigue LCO according to Phase One described in section 1.2.

3.2.1 Observations

The visual inspection of test specimens after 40 hours of testing shows that the laminates with lay-up A were without any local delamination or de-bond of the fiber and matrix, and did not even have visible failures, but Young's modulus was gradually degraded as load cycles increase. This was clearly shown in Fig. 3.1. For the laminates with lay-up B, the Young's modulus dropped largely after certain cycles, although the initial value of Young's modulus for both configurations almost had the same level of values. It was also observed that a delamination at the tapered area between core and belt layers in the thin side of specimen occurred in all three specimens at the moment when Young's modulus suddenly dropped, and then grew between $\pm45^0$ layers along axial direction as load cycles further increased. The expended delamination triggered some other defects such as de-bonding of fiber and

matrix, and breakage of matrix and fiber, or some other local delamination occurred. Therefore, from the moment of delamination onset, the specimen enters an unstable stage, which means that the specimen could break at any time depending on manufacturing quality of specimen, load conditions, and environmental conditions, etc.

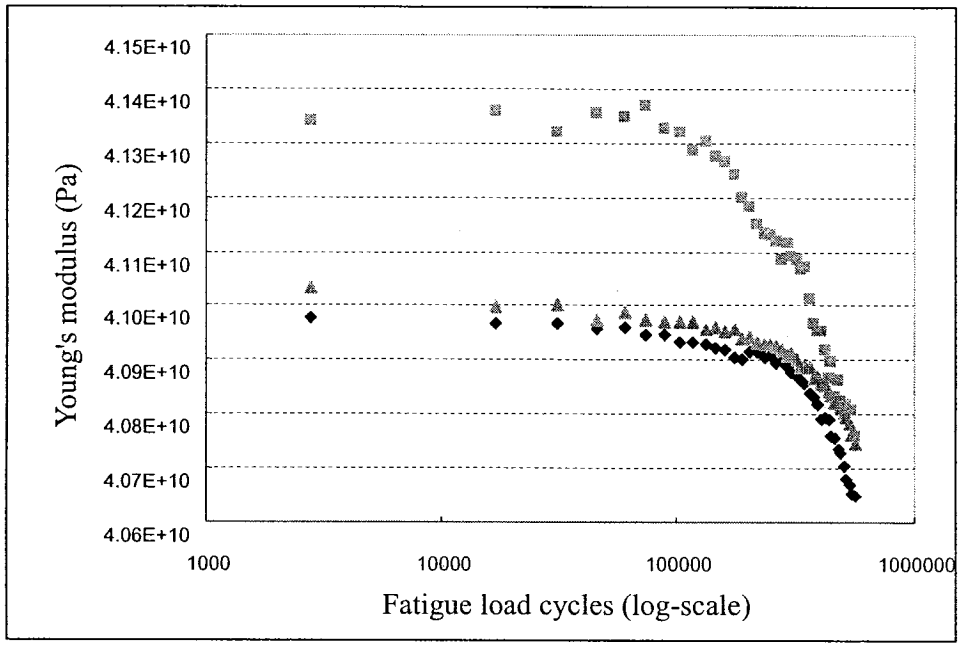

Figure 3.1 Young's modulus versus load cycles for laminates with lay-up A

For example, Specimen One with lay-up B represented with triangle symbol in Fig. 3.2 shows the typical fatigue damage accumulation process that was divided into several damage stages, which are marked with circles *a, b, c,* and *d*. At each stage, the change in the values of Young's modulus was very small. But between the two conjunction stages, a relatively big drop exists as load cycles increase until the final failure. The explanation of this phenomenon, which was proved by observations, was

that the delamination occurred and expanded at one side of tapered area of symmetric laminate when stage changed from *a* to *b*; and then another delamination occurred in the other side of tapered laminate after some damage accumulation with the growth of primary-delamination, and this is explained by the large Young's modulus drop from *b* to *c*; and further damage accumulation triggered large scale of failures, such as the delamination expansion along the axial direction of the specimen, some other local delamination onset, fiber breakage along the delaminated layers, and layers splitting etc. till the specimen was totally broken (see Fig. 3.3). The whole damage accumulative processes were shown clearly as the drops from *a* to *b*, *b* to *c*, *c* to *d*, and finally to *e* and it lasted as long as 15 hours from the primary-delamination-occurrence to the final failure of the specimen.

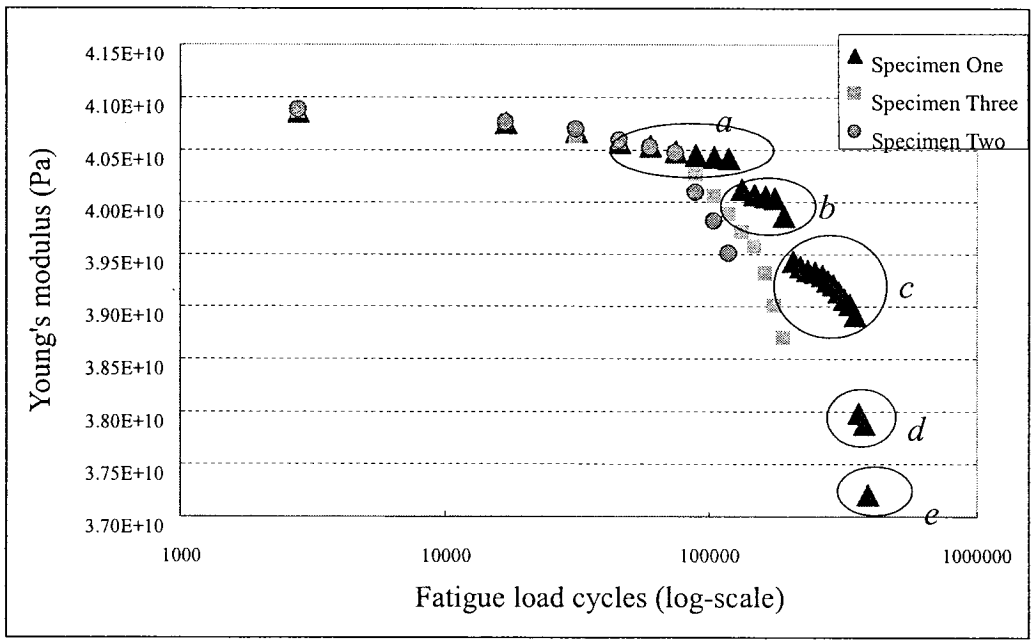

Figure 3.2 Young's modulus versus load cycles for the laminates with lay-up B under LCO

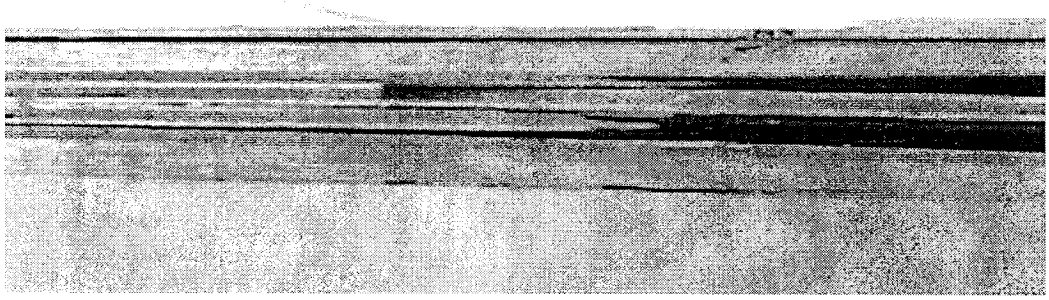

Figure 3.3 Photograph of the broken specimen with lay-up B

Specimen Two marked with round circle shown in Fig. 3.2 presents that the values of Young's modulus of laminates with lay-up B continuously dropped largely after certain cycles until the final failure. The cumulative process, in this case, was 5 times shorter compared to that of the specimen One, which means that this random damage accumulation process could only last about 3 to 4 hours because the onset and propagation of primary-delamination in the tapered symmetric laminate must have triggered large scale of failures immediately, that leads to final failure which can be read through the chart. One can also notice from Fig. 3.2 that the onset of delamination for specimen Two is 3-hour-cycle earlier than that of specimen One because of the uncertainties of environmental conditions existing in the test that are mentioned above.

The damage accumulation process of Specimen Three was just in between Specimen One and Specimen Two that lasted about 7 hours to the final failure after the primary-delamination onset.

3.2.2 Conclusions

From the test results of Phase One, the following conclusions had been drawn:

- The initial values of Young's modulus of tapered laminate with lay-ups A and B are much similar as they both have the same ply groups, the same fiber orientation angles, and the same overall dimensions with the difference between them being the number of plies in the core and belt layers of composite laminate.
- For the same thickness of composite tapered laminate, the probability of delamination occurrence could be largely decreased by increasing the numbers of prepreg in the core layer and reducing the same numbers of prepreg in the belt layer simultaneously.
- The unstable and random damage accumulation process of tapered laminate exists after the primary-delamination-occurrence, since the primary delamination will trigger the large scale of failures when the cyclic tension-compression loading is applied.
- The area between the core and the belt layers in the thin side of the composite laminate (around the point C of Fig. 2.1) becomes relatively less stress concentrated by decreasing the numbers of belt layer and increasing the numbers of core layer, even though that area still carries more stress concentration compared to the other area in the specimen

according to FEM analysis results from [9].

3.3 Effect of pre-set delaminations at different locations

In test Phase Two, the effect of pre-set delaminations at different locations of composite laminates has been investigated subject to the tension-compression cyclic loading. Therefore, two groups of specimens with lay-up A and pre-set delamination (one group has pre-set delamination at the center of core layers near the tapered area and another group has pre-set delamination in between core and belt layers near the tapered area), were tested and analyzed together with the results from test Phase One.

3.3.1 Observations

All the three specimens with pre-set delamination at the center of core layers delaminated along the pre-set delamination layer only after few thousand cycles, and then entered the unstable damage process immediately as mentioned in previous section. During that unstable process, it also showed the occurrence of various failure modes. Furthermore, this unstable damage process occurs not only earlier but also acts more severely compared to that in the laminates with lay-up B in Phase One. For instance, the tests only lasted about 5 hours that is one third of minimum hours of life of the laminates with lay-up B. But for the specimens with pre-set delamination in between the core layers and belt layers near the tapered area, there is no delamination

or other visible failures that occurred after 40 hours of test. The complete differences among the two cases are shown in Fig. 3.4.

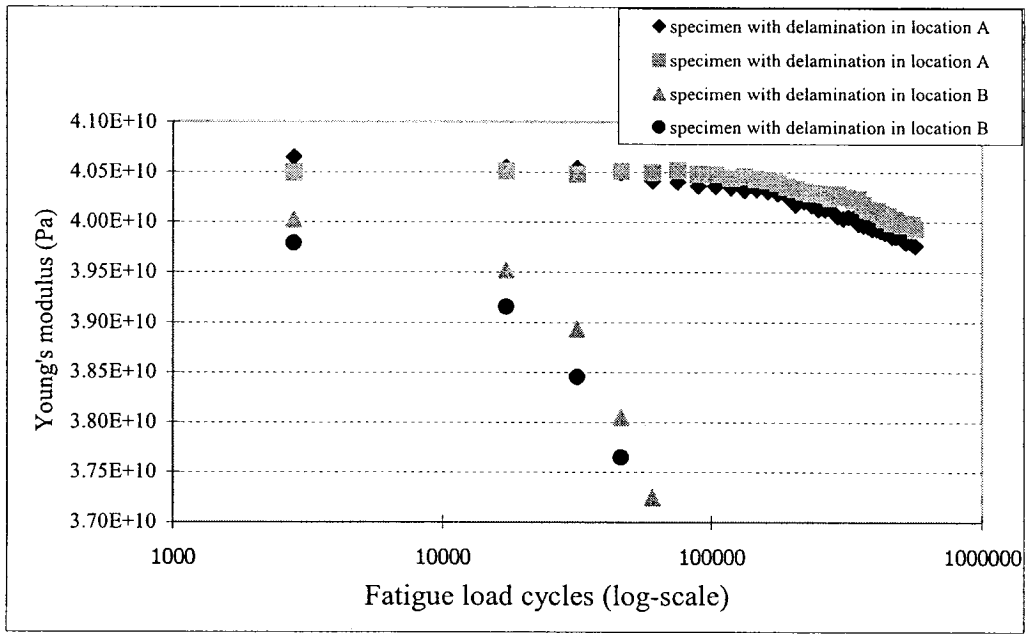

Figure 3.4 Comparison of Young's modulus values with two locations of delamination

3.3.2 Conclusions

Comparing the results from the above two test phases, one can conclude that:

- The initial strength and stiffness of various types of tapered laminates (with lay-up-A or lay-up-B, with or without pre-set delamination, with different locations of pre-set delamination) are almost at the same level.
- The closer the delamination occurs towards the center of tapered laminates, the more severe the damage will be when subjected to cyclic tension-compression loading.

- There is not enough damage to initiate the delamination in the stress concentrated area between core and belt layers even with the Teflon as the pre-set delamination in that area for specimen group 3 under cyclic tension-compression loading.

3.4 Effect of over tension load

Unlike metallic material, the over tension load shall trigger more failure occurrences instead of producing plastic zone to prevent further crack growth in metal. This can be proven by the following tests according to the test Phase Three of experimental program described in Fig. 1.3:

- Two groups of test specimens (groups 5 and 6) with pre-set delamination in between core and belt layers near the tapered area in lay-up A were tested under LCO & LCT (Load Condition One and Load Condition Two).

3.4.2 Observations

For the specimens under LCO, there were no visible failures in the tested specimens after 40 hours of test, and the strength/stiffness was degraded gradually as the hazard rate remained nearly unchanged. But when they were tested under LCT, the test

results of laminates indicate that Young's modulus drops largely with a relatively large slope in the range of certain cycles. For example, from Fig. 3.5, one can see that the slope in the range of 1000 - 200,000 cycles is bigger than that in the range from 200,000 cycles to the end for the specimens under LCT, because the 85% ultimate over tension load may lead to the occurrence of some initial failures of laminates (such as de-bonding of matrix and fiber, delamination, etc.). Although most specimens were without any visible failures on the surface for both cases, few specimens under LCT had cracks located in the tapered area where the pre-set delamination has been placed.

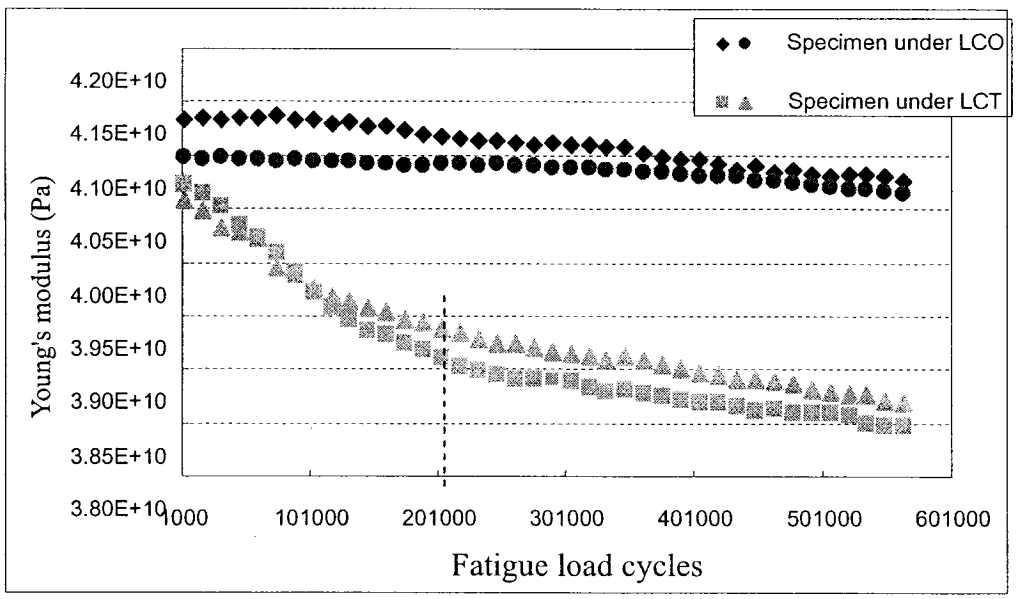

Figure 3.5 Comparison of Young's modulus values corresponding to two load conditions

3.4.2. Conclusions

The conclusion we now have for the case of over tension load based on normal tension- compression load is:

- The regular over tension load based on normal tension-compression load will have big impact on the acceleration of the stiffness and strength degradation of tapered composite laminates and shorten their fatigue life.

3.5 Discussion and conclusion

We may have the following conclusions from the above test results regarding Phases One, Two, and Three subjected to cyclic tension-compression loading:

- The stress concentration in the area between core and belt layers may be reduced by decreasing the number of belt layers. Therefore, the probability of delamination occurrence as well as fatigue damage accumulation may be less because of that change.
- The delamination plays an important role in fatigue damage process, especially the locations of delamination. The closer the delamination is to the center of specimen laminate, more severe the damage will be. Furthermore, the specimen tends to become unstable as soon as the primary delamination occurred.
- The influence of over tension load for composite laminates is different from

that of metallic material in that it will trigger more occurrences of failure modes so as to accelerate the damage accumulation and shorten service life.

Chapter 4

Stochastic Approach to Model and Analyze Test Data

4.1 Introduction

Unlike the metallic material, the composite laminate has more complexity and uncertainty during the entire service life in terms of its materials, configurations and test environment. Some of the complexity and uncertainty is related to the damage mechanism and failure modes, like de-bonding between fiber and matrix, delamination, matrix cracking, fiber breaking, and laminates splitting, etc.; another complexity and uncertainty is the occurrences of these failure modes and their contributions to the fatigue damage, as well as the complexity and uncertainty in failure mode changes, crack (fiber or matrix) jumping, simultaneous occurrence of more than one failure modes, etc. The influences from these complexities and uncertainties can largely affect the fatigue test results, but they can not be quantified precisely. Therefore, the structural-level fatigue response parameter, which is sensitive to various damage modes, is established and used to quantify the fatigue damage process. The reciprocal of the Young's modulus of composite laminate subjected to

the axial tension-compression loading is used as a structural-level fatigue response parameter in the present thesis.

A Stochastic Modeling methodology based on Markov Chain process has been developed in the work of Ganesan [35] for the structural-level fatigue response parameter to model and analyze fatigue damage accumulation in the composite laminates considering the following two aspects: 1) the damage probability distribution at any given cycles; 2) the prediction of damage probability distribution after certain cycles. This methodology is applied in the present thesis for the tapered laminates that were tested.

A finite discrete Markov Chain is established to quantify the fatigue damage accumulation process in this approach. The differences between the probability distribution of the fatigue damage response parameter obtained using different methods such as the Maximum Entropy Method (MEM), Gaussian (Single and Bivariate) probability distribution method and the statistical joint probability density function are also presented and discussed in the present thesis. In the following sections, the approach and methodology that have been developed by Ganesan [35] are reproduced for the purpose of clarity and continuity.

4.2 Markov process modeling of fatigue damage process

The fatigue test, no matter whether the material is metallic or composite, or what kind of failure modes and their occurrences, is regarded as a damage accumulation process, and it can be well modeled by Markov Chain in terms of the structural-level fatigue parameter. For example, the test results of fatigue response parameters are considered as the random variables since they always showed differences from specimen to specimen due to the complexities and uncertainties that are presented in composite material properties (batches) and the quality of laminate (manufacturing and process parameters), failure modes and their occurrence as well as the service loading and environmental conditions. So when a number of specimens are tested, a group of fatigue response parameter values that are called random variables, which fluctuated as the load cycle increases, are presented as the fatigue process chain. The compliance values of composite laminate (reciprocal of the Young's modulus) corresponding to load cycle values are used to represent the fatigue response parameter in the present thesis.

4.2.1. Markov Chain

A Markov Chain Model has been established in the work of Ganesan [35] to simulate the real cumulative damage process based on the establishment of the discrete set of damage states corresponding to the fatigue cycles. That means at any particular

number of load cycles n_1, there exists the corresponding value of fatigue response parameter C_1. For any two numbers of load cycles n_1 and n_2, there exists two values of C_1 and C_2 respectively. The "Duty Cycle" (DC) [35, 37] is introduced and denoted here as the repetitive deviation of two consecutive load cycles n_1 and n_2. Then the fatigue response parameter can be written as C_{m+1} subjected to load cycle n_{m+1} after m DC. Certainly, the whole range of fatigue response parameter can then be divided into m number of equal or non-equal intervals, like $(C_2 - C_1)$, $(C_3 - C_2),\ldots,(C_{i+1} - C_i),\ldots,(C_{m+1} - C_m)$, where C_{m+1} is the maximum value of the fatigue response parameter. In another words, if the fatigue parameter at load cycle n is in the range $(C_{i+1} - C_i)$, then the composite laminate is considered to be in the damage state i when load cycle is at n. And if the load cycle is further increased, then the damage stage of specimen is to be transformed from current stage to a high-level damage stage until it reaches the maximum damage stage m in the range of $C_{m+1} - C_m$ at the maximum load cycle $n_{\max}$. Also, the random variables of specimen compliances C_i are treated as non-homogenous because of their continuous function of the number of loading cycles $(n_0, n_1, n_2,\ldots,n_{j-1}, n_j,\ldots,n_{\max})$ at the damage stages $(1,2,3,\ldots,j-1,j,\ldots,m)$ of the entire service life. It is also noted that the compliance of composite laminate as well as damage accumulation continuously increase when DC is applied.

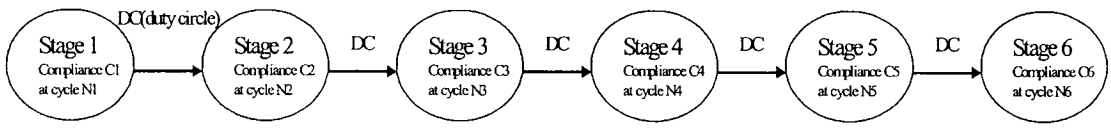

Figure 4.1 Finite Markov Chain diagram

As the two index sets, the loading cycles and the damage stages, are discrete and finite, the fatigue response parameter process becomes a Finite Markov Chain. The Finite Markov Chain, including discrete damage stages, fatigue response parameter values, and repetitive constant DC that is shown in Figure 4.1, is established under the following assumptions:

- ✓ There is a repetitive constant DC.
- ✓ Fatigue parameter values are discrete.
- ✓ Damage accumulation in a DC depends only on the damage stage at the start of that particular DC.

4.2.1.1 Concept of damage stage and damage state

Damage stages are regarded as a discrete damage accumulation chain in the service life of specimen, which is directly related to the DC. Two parameters are available in each damage stage called specimen compliance and corresponding cycles. The compliance of specimen in further damage stage is counted on the former damage stage after one DC. This means that whatever numbers of damage stages exist, the

same numbers of Transition Probability Matrices are available. While damage states represent the continuous ranges that can be divided by any number from minimum to maximum values of fatigue response parameter, which only depend on how many orders of Transition Probability Matrix one wants. The more states are divided, the smaller range of each state is, and more precise the estimated probability distribution will be. In other words, the value of response parameter in each damage stage will fall only in a part of the whole damage states that can be shown in Figure 4.2.

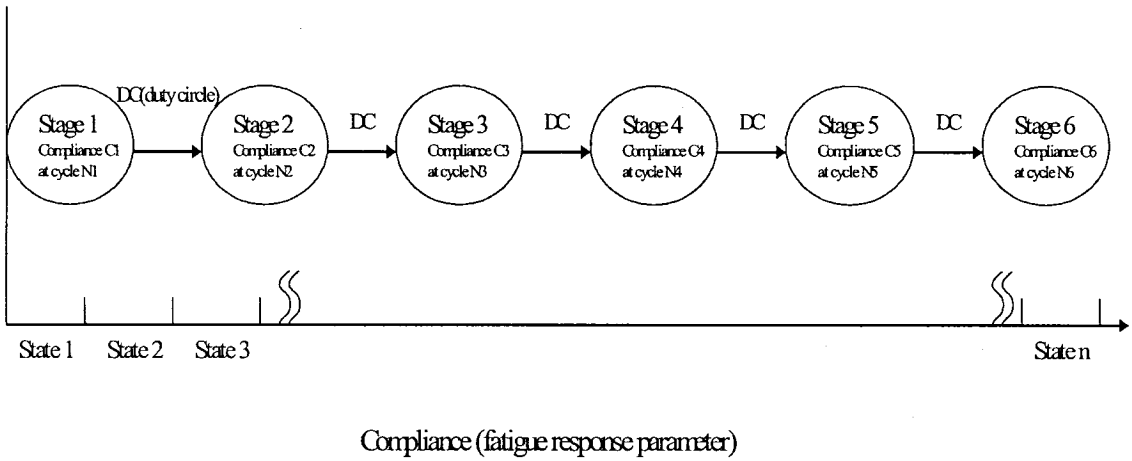

Figure 4.2 Damage stage and damage state in Markov Chain for one specimen

4.2.2. Transition probability function (TPF)

As a result of the Markovian property and non-homogeneity of the stochastic process, the probability at any damage stage is mathematically represented using the Conditional Probability Density Function as

$$p_{ij}(n_{k-1},n_k)=p\left[C_{(nj)}=j/C_{nj-1}=i\right]n_k\rangle n_{k-1} \tag{4.1}$$

where $p_{ij}(n_{k-1},n_k)$ is the Transition Probability Function (TPF), which is denoted as the probability distribution of the specimen compliance (fatigue response parameter) entering a new damage stage j at loading cycle n_k from its current damage stage i at loading cycle n_{k-1}. Based on the definition of the conditional probability density function, joint probability density function, and Bayes' theorem, then the TPF between damage stages i and j can be recast in the following formula:

$$p_{ij}(n_k-1,n_k)=\frac{P\{[C_j\langle C(nk)\le C_{j+1}]\cap[C_i\langle C(nk)\le C_{i+1}]\}}{P[C_i\langle C(nk)\le C_{i+1}]} \tag{4.2}$$

As the specimen compliance at any load cycle is a random variable and then compliances C_{k-1},C_k at load cycles n_{k-1} and n_k denote two correlated random variables. Then the individual and joint probability distributions can be re-written in terms of individual probability density functions $f_{c_{k-1}}(c_{k-1})$ and $f_{c_k}(c_k)$ for random variables of C_{k-1} and C_k, and joint probability density function $f_{c_{k-1}c_k}(c_{k-1},c_k)$ for these two correlated random variables. Then the equation (4.2) of TPF between the damage stage i and j can be determined as following:

$$p_{ij}(n_{k-1}, n_k) = \frac{\int_{C_j}^{C_{j+1}} \int_{C_i}^{C_{i+1}} f_{C_{k-1}C_k}(c_{k-1}, c_k)\, dc_{k-1}\, dc_k}{\int_{C_i}^{C_{i+1}} f_{C_{k-1}}(c_k)\, dc_k} \tag{4.3}$$

where $f_{C_{k-1}}(c_{k-1})$ represents probability density function of random variable C_{k-1} at damage stage i to $i+1$ or n_{k-1} cycles, and $f_{C_{k-1}C_k}(c_{k-1}, c_k)$ represents the joint probability density function of two correlated random variables C_{k-1} and C_k.

4.2.3. MEM for calculation of individual probability density function

Maximum Entropy Method (MEM) [36] is used for the calculation of individual probability density function from the above equation (4.3), as it is a closer match with the true distribution (relative frequency histogram) instead of other probabilistic methods like Weibull, Gamma, etc. because of fewer specimens' values (20 specimens' values in each case) and relative dispersion of the data values. The individual probability density function can be calculated using MEM as shown below:

$$f_{C_{k-1}}(c_{k-1}) = \exp\left[\lambda_0 + \sum_{i=1}^{p} \lambda_i c_{k-1}^i\right] \tag{4.4}$$

where $\lambda_i (i = 0,1,2..p)$ are the MEM coefficients (the mathematical details are given in [36]) ; p is the order of moment used in maximum entropy distribution calculation.

In most cases, the combination of random variables always tends to become a normal distribution when the number of random variables increases due to the Central Limit Theorem of probability theory [38, 44]. Therefore, another consideration of calculation of individual probability density function is the Gaussian distribution, which is presented as follows:

$$f_{c_{k-1}}(c_{k-1}) = \frac{1}{\sigma\sqrt{2\pi}} \exp\{-\frac{[(x-\mu)/\sigma]^2}{2}\} \tag{4.5}$$

where σ and μ represent the standard deviation and mean value of compliance values at a given cycle.

4.2.4. Calculation of joint probability density function

The joint probability density function $f_{c_{k-1}c_k}(c_{k-1}, c_k)$ corresponding to two random variables C_k and C_{k-1} of specimen fatigue response parameter at n_{k-1}, n_k cycles can be calculated and presented by following ways based on different approaches.

4.2.4.1. Joint probability density function estimation

The joint probability density function estimation for a pair of specimens' time-history records from two stationary random variables $x(t)$ and $y(t)$ [37] is given by the following equation:

$$f(x,y)=\frac{N_{X,Y}}{NW_XW_Y} \tag{4.6}$$

where $N_{X,Y}$ is the number of pairs of data values that simultaneously fall within these two narrow intervals W_X, W_Y that stands for the range of damage states (C_i, C_{i+1}) and (C_j, C_{j+1}), and N is the total number sets of specimen compliance. As in case of joint probability density function of specimen compliance at load cycles n_{k-1} and n_k, the above equation can be re-written as

$$f_{C_{k-1}C_k}(c_{k-1},c_k)=\frac{N_{C_{K-1},C_K}}{N} \tag{4.7}$$

where $N_{ck-1,ck}$ represents the number of pairs of specimen whose compliances simultaneously fall within these two damage stages i and j, and N is the total number of specimens tested.

4.2.4.2. Bivariate Gaussian distribution

Another method of estimating joint probability density function is considered by using Bivariate Gaussian probability density function for two random variables X and Y (representing compliances C_k and C_{k-1} at n_{k-1} and n_k cycles respectively), which is written as below:

$$f(x,y)=\frac{1}{2\pi\sigma_x\sigma_y\sqrt{1-\rho^2}}\exp\{-\frac{1}{2(1-\rho^2)}[(\frac{x-\mu_x}{\sigma_x})^2-2\rho(\frac{x-\mu_x}{\sigma_x})(\frac{y-\mu_y}{\sigma_y})+(\frac{y-\mu_y}{\sigma_y})^2]\} \quad (4.8)$$

where σ_x and σ_y are standard deviations of variables X and Y, and μ_x, μ_y are the mean values of those two variables, ρ stands for the correlation coefficient between X and Y. Then the integration of the above density function at any small rectangle area of two variables X and Y (or damage stages we divided in the above) can be determined.

4.2.4.3. Combined methods and discussion

Compared to the histogram of real frequency for specimen fatigue response parameter at certain load cycles, the most accurate method is to combine the joint probability density estimation and Gaussian distribution. For example, if the relative frequency distribution of specimen fatigue response parameter at load cycle k and its next cycle $k+1$ are represented using normal distribution, then bivariate Gaussian distribution method will be applied for joint probability distribution at load cycles k and $k+1$; while, if the frequency distributions at load cycle k and its next cycle $k+1$ show non-reasonable match with any standard distribution, then joint probability density estimation method is applied.

But considering small number of specimens in the test, the method of equation (4.6) is always selected as a more accurate way to calculate the joint probability density

estimation since the less number of test specimens and dispersal of data could largely influence the estimated probability density functions.

Furthermore, the divided damage states can be increased by the use of combined methods, which then more accurately represent the probability distribution (see the examples and more discussion in section 4.5).

4.2.5. Transition probability matrix (TPM)

Transition Probability Matrix is defined as generalizing the probabilities at all damage stages, denoted by $[\prod(n_{k-1}, n_k)]$, when the load cycle is increased from n_{k-1} to n_k. Then the TPM can be written as

$$[\prod(n_{k-1}, n_k)] = \begin{bmatrix} p_{11}(n_{k-1}, n_k) & p_{12}(n_{k-1}, n_k) & . & . & p_{1m}(n_{k-1}, n_k) \\ p_{21}(n_{k-1}, n_k) & p_{22}(n_{k-1}, n_k) & . & . & p_{2m}(n_{k-1}, n_k) \\ . & . & . & . & . \\ . & . & . & . & . \\ p_{m1}(n_{k-1}, n_k) & p_{m2}(n_{k-1}, n_k) & . & . & p_{mm}(n_{k-1}, n_k) \end{bmatrix} \quad (4.9)$$

where m is the number of damage states in the whole fatigue life of specimen and $p_{mm}(n_{k-1}, n_k)$ denotes TPF. Since the specimen's fatigue response parameter values at cycles increasing from n_{k-1} to n_k will be within the full damage state range, the sum of probabilities of any row of TPM is equal to unity, that is:

$$\sum_{j=1}^{m} p_{ij}(n_{k-1}, n_k) = 1 \qquad i, k = 1,2,3,\ldots,m; n_k > n_{k-1} \quad (4.10)$$

And since we assume that the damage accumulation is increasing from cycles n_{k-1} to n_k, so the probability of $p_{ij}(i>j)=0$ is always true. Furthermore, when the specimen has entered the new damage state from state m, p_{mm} can not make a transition to any other future stage and so $p_{mm}(n_{k-1},n_k)=1$. Then TPM can be rewritten as

$$[\Pi(n_{k-a},n_k)]=\begin{bmatrix} p_{11}(n_{k-1},n_k) & p_{12}(n_{k-1},n_k) & . & . & p_{1m}(n_{k-1},n_k) \\ 0 & p_{22}(n_{k-1},n_k) & . & . & p_{2m}(n_{k-1},n_k) \\ 0 & 0 & . & . & . \\ 0 & 0 & . & . & . \\ 0 & 0 & . & . & 1 \end{bmatrix} \quad (4.11)$$

4.2.6 M-step transition probability matrix

Based on the Chapman-Kolmogorov Theorem and the non-homogenous Markov Chain property, the Transition Probability Matrix from load cycles n_0 to n_m that is called M-step transition probability matrix can be calculated by the TPMs at all previous damage states, which are denoted by $[\Pi(n_0,n_1)]$, $[\Pi(n_1,n_2)]$,..., $[\Pi(n_{m-1},n_m)]$. The equation is given below:

$$[\Pi(n_0,n_m)] = [\Pi(n_0,n_1)]\times[\Pi(n_1,n_2)]\times.....\times[\Pi(n_{m-1},n_m)] \quad (4.12)$$

where $[\Pi(n_{m-1},n_m)]$ denotes TPM from load cycle n_{m-1} to n_m; $[\Pi(n_0,n_m)]$ denotes

M-step transition probability matrix (M-Step TPM), and the physical meaning here is that the probabilities of specimen fatigue response parameter in any of the damage states 1,2,3,...,m at load cycle n_m is given by the initial state of specimen at load cycle n_0.

The unconditional probabilities of the fatigue parameter in any of the damage states, when load cycle is increased from n_0 to n_m, are denoted by $[\Pi^U(n_0, n_m)]$ that can be derived from equation (4.12) using the given initial damage state distribution:

$$[\Pi^U(n_0, n_m)] = [\Pi(0)] \times [\Pi(n_0, n_1)] \times [\Pi(n_1, n_2)] \times ..... \times [\Pi(n_{m-1}, n_m)] \qquad (4.13)$$

where $[\Pi(0)]$ represents the probability distribution of fatigue response parameter of specimen in any damage states at load cycle n_0.

4.2.7 Prediction of probability distribution of fatigue response parameter

In order to predict the probability distribution of fatigue response parameter after certain cycles, we need to determine the procedure for estimating the TPM, when the specimen enters a new damage state, which is given as follows:

- ✓ Determination of appropriate constant DC for the fatigue response parameter

in the whole damage range. Say dividing into m number of damage states.

- ✓ Calculation of each TPM from initial damage state to the final damage state by using MEM, Gaussian distribution or/and combined methods in the previous section. Say m number of TPM will be available.
- ✓ Then there will be m number of probability values of p_{ij} available. For example, the value of $1p_{ij}, 2p_{ij}, 3p_{ij}, ..., mp_{ij}$. Certainly these numbers can be considered as constituting a random variable, and it is assumed that this random variable follows Gaussian distribution.
- ✓ Then use Gaussian Distribution Model to predict the transition probability matrix at further damage state. For example at $m+1$ state, the $p_{ij}(n_m, n_{m+1}) = Z_{90}\sigma_{ij} + \mu_{ij}$ where Z_{90} stands for the value of the standardized random variable when reliability is 90%, which is approximately equal to 1.3 [35]; σ_{ij} is a standard deviation of the values in all known transition probability matrices and μ_{ij} is the mean value. In this way, the TPM for further load cycle increasing from n_m to n_{m+1} is finally obtained by calculation of each $p_{ij}(n_m, n_{m+1})$.

Then the Transition Probability Matrix for further load cycle that is increased from n_m to n_{m+1} can be re-written as following:

$$[\Pi(n_m, n_{m+1})] = \begin{bmatrix} p_{11}(n_m, n_{m+1}) & p_{12}(n_m, n_{m+1}) & . & . & p_{1m}(n_m, n_{m+1}) \\ 0 & p_{22}(n_m, n_{m+1}) & . & . & p_{2m}(n_m, n_{m+1}) \\ 0 & 0 & . & . & . \\ 0 & 0 & . & . & . \\ 0 & 0 & . & . & 1 \end{bmatrix} \quad (4.14)$$

Similarly, the predicted unconditional probabilities of the fatigue parameter at $m+1$ state (after another DC from damage state m) can be derived from equation (4.13):

$$\left[\Pi^U(n_0, n_{m+1})\right] = [\Pi(0)] \times [\Pi(n_0, n_1)] \times [\Pi(n_1, n_2)] \times \ldots\ldots \times [\Pi(n_{m-1}, n_m)] \times [\Pi(n_m, n_{m+1})] \quad (4.15)$$

4.3 Flow chart and organization of MATLAB program for computing TPMs

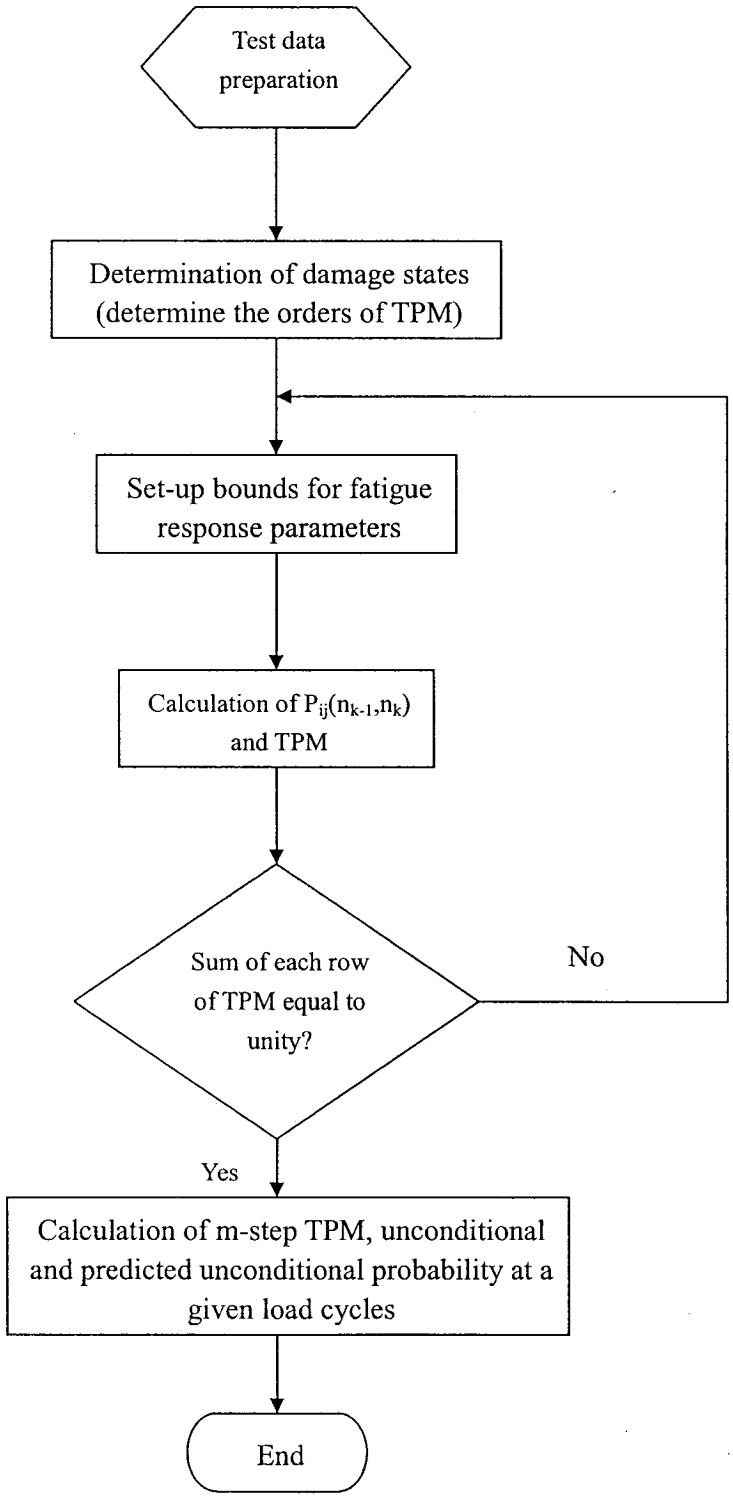

4.4 Modeling of fatigue test data

The stochastic modeling and analysis procedure described in the above is illustrated by fatigue test data from tapered composite laminate with pre-set delamination under load conditions: LCO and LCT, which are marked as Load Condition One and Two in sub-section 2.7. The compliance of composite laminate specimen corresponding to the load cycle is taken to be the fatigue response parameter and the *N-C* chart (compliances versus cycles) from 20 specimens under LCO is plotted in Fig. 4.3 and the original data are selected with 9 damage stages and they are used for further stochastic calculation is listed in table 4.1. The true probability distribution of fatigue response parameter at certain cycles and the estimated (predicted) probability distribution after certain cycles are presented in the following chapters.

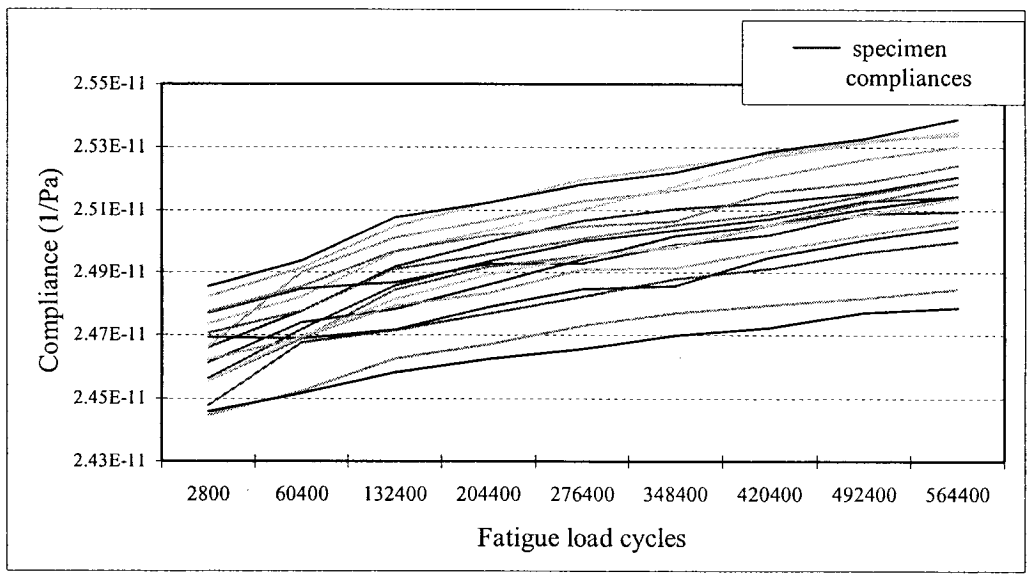

Figure 4.3 Specimens' compliances versus load cycles under load condition of LCO

Table 4.1: The 20 specimens' original compliance data (1×10^{-11} 1/Pa) and corresponding load cycles under the load condition of LCO

specimen	2800 cycles	60400 cycles	132400 cycles	204400 cycles	276400 cycles	348400 cycles	420400 cycles	492400 cycles	564400 cycles
1	2.4458	2.4514	2.4583	2.4624	2.4656	2.4699	2.4725	2.4772	2.4787
2	2.4445*	2.4522	2.4626	2.4669	2.4729	2.4769	2.4795	2.4817	2.4847
3	2.4476	2.4677	2.4714	2.4767	2.4822	2.4879	2.4912	2.4963	2.4997
4	2.4694	2.4689	2.4716	2.4790	2.4847	2.4856	2.4948	2.5004	2.5045
5	2.4623	2.4691	2.4792	2.4834	2.4910	2.4914	2.4968	2.5018	2.5067
6	2.4769	2.4846	2.4868	2.4927	2.4930	2.4989	2.5020	2.5088	2.5094
7	2.4555	2.4695	2.4814	2.4893	2.4950	2.4982	2.5054	2.5085	2.5139
8	2.4563	2.4718	2.4855	2.4934	2.4998	2.5035	2.5071	2.5126	2.5143
9	2.4613	2.4740	2.4782	2.4861	2.4942	2.5015	2.5052	2.5104	2.5143
10	2.4555	2.4687	2.4843	2.4918	2.4952	2.4980	2.5051	2.5122	2.5184
11	2.4706	2.4775	2.4909	2.4957	2.5007	2.5051	2.5086	2.5147	2.5205
12	2.4661	2.4775	2.4917	2.4997	2.5064	2.5103	2.5122	2.5156	2.5206
13	2.4579	2.4738	2.4886	2.4995	2.5063	2.5097	2.5110	2.5161	2.5210
14	2.4711	2.4798	2.4923	2.5001	2.5025	2.5077	2.5149	2.5200	2.5214
15	2.4773	2.4855	2.4966	2.5017	2.5046	2.5062	2.5157	2.5187	2.5243
16	2.4662	2.4900	2.5010	2.5066	2.5128	2.5162	2.5207	2.5262	2.5302
17	2.4821	2.4914	2.5047	2.5123	2.5198	2.5237	2.5280	2.5321	2.5340
18	2.4734	2.4821	2.4963	2.5033	2.5101	2.5175	2.5269	2.5314	2.5349
19	2.4911	2.4965	2.5115	2.5199	2.5232	2.5289	2.5303	2.5336	2.5377
20	2.4855	2.4936	2.5074	2.5122	2.5182	2.5221	2.5287	2.5327	2.5389**
STDEV*	0.013086	0.012231	0.014237	0.014873	0.015031	0.015378	0.015714	0.015655	0.016148

*: the minimum value of the specimen's compliance

**: the maximum value of the specimen's compliance

STDEV*: the standard deviation of specimen compliances at different load cycles

4.4.1 Case 1: Confrontation with test data corresponding to load condition LCO

The clear procedure for calculation of the true probability distribution of compliance at a certain load cycle and the prediction of probability distribution at further damage state corresponding to LCO according to MATLAB computing flow chart is listed below:

Step 1:

Determination of approximate constant DC: 9 damage stages are selected including initial damage stage, which are divided in the whole 564400 load cycles lifetime by approximately constant value of DC (It can be seen from the damage stage values, except the first value, that the approximate value of DC is 72000 cycles), that are 2800, 60400, 132400, 204400, 276100, 348400, 420400, 492400, 564400; that means 9 out of 40 groups of recorded data (mentioned in chapter 2) are selected for computing process.

Step 2:

Determination of damage states from the whole values of fatigue response parameter: 8 same size damage states are divided in the range from minimum value of compliance 2.4445×10^{-11} (1/Pa) to maximum value of compliance 2.5389×10^{-11} (1/Pa) of the test specimen, that is (2.4445, 2.4563), (2.4563, 2.4681), (2.4681, 2.4799),

(2.4799, 2.4917), (2.4917, 2.5035), (2.5035, 2.5153), (2.5153, 2.5271), (2.5271, 2.5389). The requirement of the selection of bounds or the number of damage states for the whole range of compliances is that the sum of probability densities in any row of transition matrix must be theoretically unity, or should be within 10% tolerance. If more damage states are used, the probability distribution will be more precise.

The following factors can largely affect the calculation results or the match percentages with the real distributions when one chooses the numbers of damage states:

- Dispersion of test data in each damage stage, and
- Computing methods, which are mentioned in sub-section 4.2.4.

For example, the damage states can be increased to 13 by the use of combined methods for calculation of joint probability density function and/or individual density function comparing with either only using MEM or Gaussian method and additionally, the damage states increase to 20 because of the dispersion of test data (smaller standard deviation) in LCT is declined at each damage stage (Examples are shown in sub-sections 4.5.1.3 and 4.5.2).

Step3:

Derive probability density functions based on the individual compliance values at each damage stage by using MEM of equation (4.4). The judgment of selection

numbers of damage states is prior to the sum of probability densities in any row of the transition matrix that must be theoretically unity, which however, for practical purposes may be within 10% tolerance range. The numerical integration method as well as the first four statistical moments is applied to calculate the probability distribution of single-variable of compliance C_{k-1} at a certain cycles of damage stage. The λ_i values, which are calculated by equation (4.4) in terms of 9 damage stages, are listed in Table 4.2 and probability density functions at damage stage of cycles 2800 can then be written by substitution of λ_i values from Table 4.2:

$$f_{c_{2800}}(c_{2800}) =$$

$$\exp\left[(-4.98\times10^{6})+(8.21\times10^{17})\times x+(-5.08\times10^{28})\times x^{2}+(1.40\times10^{39})\times x^{3}+(-1.44\times10^{41})\times x^{4}\right]$$

where x stands for a compliance value at any damage state.

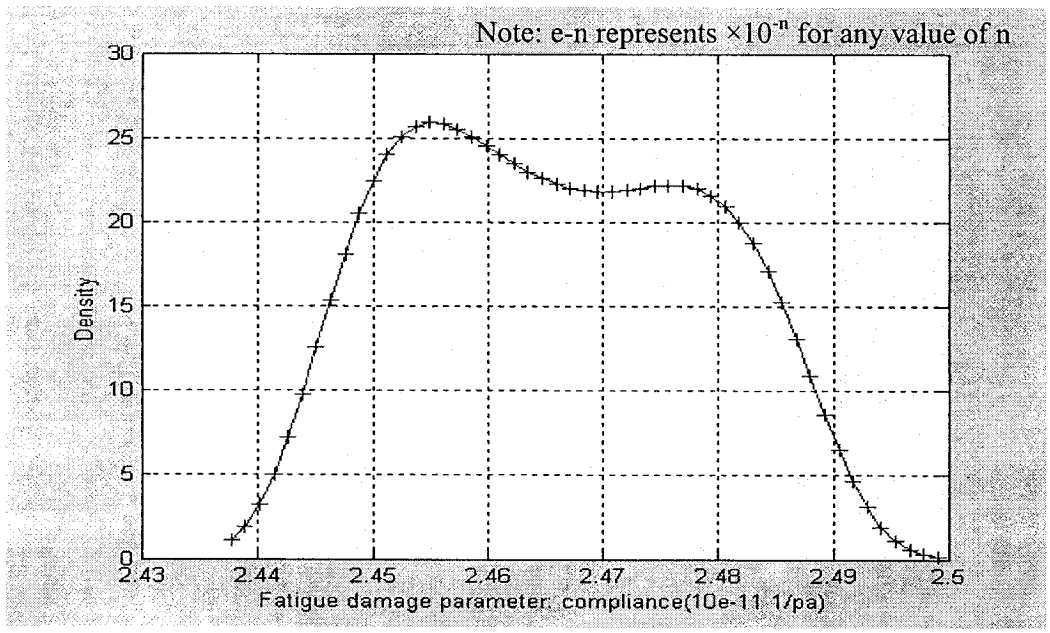

Figure 4.4 Maximum Entropy density function of damage stage at 2800 cycles

Table 4.2: The λ_i values at different damage stages under LCO based on the data from Table 4.1

Cycles(stages)	λ_0	λ_1	λ_2	λ_3	λ_4
2800	--2.2332E+8	3.6209 E+8	--2.2016 E+8	5.9493 E+7	-6.0287 E+6
60400	-5.153 E+7	8.3536 E+7	-5.0785 E+7	1.3722 E+7	-1.3905E+6
132400	-8.0949E+7	1.3044E+8	-7.8822E+7	2.1169E+7	-2.132E+6
204400	-4.9919E+7	8.0384E+7	-4.8541E+7	1.3028E+7	-1.3112E+6
276400	-3.4055E+7	5.4765E+7	-3.3027E+7	8.8524E+6	-8.898E+5
348400	-4.5092E+7	7.2306E+7	-4.348E+7	1.162E+7	-1.1646E+6
420400	-1.513E+7	2.4307E+7	-1.4644E+7	3.9213E+6	-3.9378E+5
492400	-1.1371E+7	1.8346E+7	-1.1099E+7	2.9844E+6	-3.009E+5
564400	-2.1026E+7	3.3752E+7	-2.0318E+7	5.4356E+6	-5.4532E+5

Note: E+n represents $\times 10^n$ for any value of n

The density function for each damage stage can then be plotted based on equation (4.4). For example, the two probability distribution charts (Figs. 4.4 and 4.5) plotted in MATLAB based on the function $f_{C_{2800}}(c_{2800})$ and $f_{C_{60400}}(c_{60400})$, which are the Maximum Entropy density functions for damage stages at 2800 cycles and 60400 cycles:

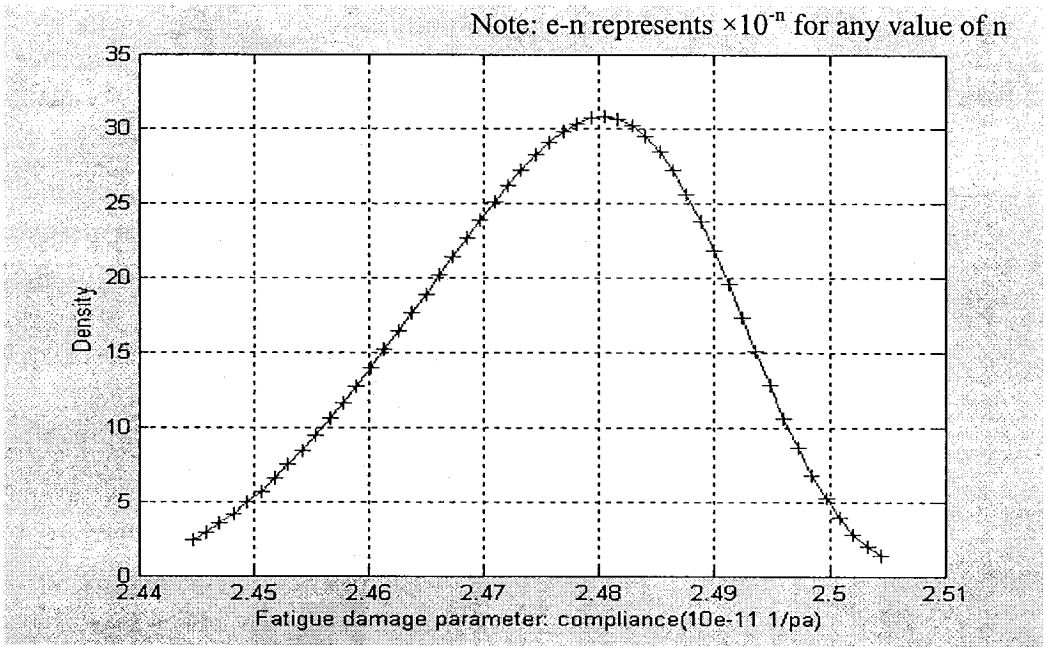

Figure 4.5 Maximum Entropy density function of damage stage at 60400 cycles

Step 4:

Determination of joint probability density functions. The 8 damage states mentioned in the above have to be used to define the rectangle regions to estimate the joint probability matrix at certain duty cycles by the following methods:

1) Joint probability density function estimation (refer to section 4.2.4.1): the integration of equation (4.7) can be written as

$$\iint f_{c_{k-1},c_k}(c_{k-1},c_k)dc_{k-1}dc_k = \int_{c_k}^{c_{k+1}} \int_{c_{k-1}}^{c_k} \frac{N_{c_{k-1},c_k}}{N} dc_{k-1}dc_k . \qquad (4.16)$$

where C_{k-1},C_k, C_k,C_{k+1} represent the damage state range from C_{k-1} to C_k and

from C_k to C_{k+1} respectively.

For example, at damage stage of fatigue cycle 2800, the numbers of specimen's compliances fall in the damage state rectangle range such as from 2.4445 to 2.4563 and from 2.4563 to 2.4681, or from 2.4563 to 2.4681 and from 2.4681 to 2.4799 ($\times 10^{-11}$ 1/Pa). Then in this case,

$$\frac{N_{(2.4378,2.4514),(2.4378,2.4514)}}{N}=\frac{1}{20}=0.05 \quad , \quad \frac{N_{(2.4378,2.4514),(2.4514,2.4651)}}{N}=\frac{1}{20}=0.05 \quad ,$$

$$\frac{N_{(2.4378,2.4514),(2.4651,2.4787)}}{N}=\frac{1}{20}=0.05.$$

2) Bivariate Gaussian distribution (refer to section 4.2.4.2): similarly, the integration of equation (4.8) can be rewritten as

$$\iint f_{c_{k-1}c_k}(c_{k-1},c_k)dc_{k-1}dc_k=\int_{C_i}^{C_{i+1}}\int_{C_j}^{C_{j+1}} f(c_{k-1},c_k)dc_{k-1}dc_k \qquad (4.17)$$

where $f(c_{k-1},c_k)=f(x,y)$.

3) Combined methods (refer to section 4.2.4.3): TPF $p_{ij}(n_{k-1},n_k)$ between damage states i and j at any load cycle k can be calculated by either method 1) MEM or method 2) Gaussian Distribution, in terms of the conditions for selecting the suitable methods as discussed in sub-section 4.2.4.4.

4.4.1.1 Calculation methods based on the ways of calculation of TPF

4.4.1.1.1 Method 1)

The following steps (from Step 5 to Step 8) are the calculation procedure by using joint probability density function estimation equation (4.16) for calculation of the numerator of equation (4.3) and MEM method for the individual probability density function calculation for the denominator of equation (4.3).

Step 5:

Calculation of transition probability matrices based on the calculation results in steps 3 and 4 by applying the equations (4.16), (4.3) and (4.9). The 6 non-zero entries of transition probability matrices at 7 damage stages in terms of 8 damage states are listed below (the numbers marked with underline are beyond the 10% tolerance):

Note: the rows that have all entries as zero are not given in the following

$[\Pi(2800,60400)] =$

Row1	0.3109	0.3109	0.3109	0	0	0	0	0
Row2	0	0	1.0421	0	0	0	0	0
Row3	0	0	0.3331	0.6661	0	0	0	0
Row4	0	0	0	0.5121	0.5121	0	0	0

$[\Pi(60400,132400)] =$

Row2	0	0.8983	0	0	0	0	0	0
Row3	0	0	0.2865	0.7163	0	0	0	0
Row4	0	0	0	0.5459	0.5459	0	0	0
Row5	0	0	0	0	1.0343	0	0	0

$[\Pi(132400,204400)] =$

Row2	0	0.6369	0.6369	0	0	0	0	0
Row3	0	0	0.2312	0.6937	0	0	0	0
Row4	0	0	0	0.3253	0.6505	0	0	0
Row5	0	0	0	0	0.6385	0.3192	0	0
Row6	0	0	0	0	0	1.1384	0	0

$[\Pi(204400,276400)] =$

Row2	0	0	1.0844	0	0	0	0	0
Row3	0	0	0.3544	0.7088	0	0	0	0
Row4	0	0	0	0.4024	0.6036	0	0	0
Row5	0	0	0	0	0.5811	0.4358	0	0
Row6	0	0	0	0	0	0.4748	0.4748	0

[Π(276400,348400)] =

Row3	0	0	1.0291	0	0	0	0	0
Row4	0	0	0	0.7422	0.2474	0	0	0
Row5	0	0	0	0	0.7805	0.3122	0	0
Row6	0	0	0	0	0	0.6764	0.3382	0
Row7	0	0	0	0	0	0	0	0.6701

[Π(348400,420400)] =

Row3	0	0	0.6653	0.6653	0	0	0	0
Row4	0	0	0	0.2839	0.5678	0	0	0
Row5	0	0	0	0	0.7206	0.3603	0	0
Row6	0	0	0	0	0	0.6191	0.3095	0
Row7	0	0	0	0	0	0	0	1.0524

The physical meaning of the numbers in the TPM: for instance, in the first row of [Π(2800,60400)] , it can be seen that p_{11}=0.3109, p_{12}=0.3109, p_{13}=0.3109, and so on. This means that, after DC (load cycle from 2800 to 60400) in the first state of specimens, 31.09% of specimens' compliances remain in the first damage state of the range from 2.4378 to 2.4514×10^{-11} 1/Pa, 31.09% of specimens display the compliances increase to the second damage state of the range from 2.4514 to 2.4651×10^{-11} 1/Pa, and another 31.09% of specimens display the compliances increase to the third damage state of the range from 2.4651 to 2.4787×10^{-11} 1/Pa, and

no specimen falls in higher level of damage state more than that, which are all represented as zero. In the same manner, the numbers in the second row and the rest of row of TPM can be interpreted.

Further observations from the above TPMs can be shown in below:

- The numbers of first row (Row1) of $[\Pi(60400,132400)]$ are all zero, which means that there are no specimens whose compliances fall in the first damage state after one Duty Cycle. As the Duty Cycle increases, the damage states as well as compliances of specimens increase, too. This also indicates that every specimen gets damaged when further DC is applied. Moreover, it can also be explained that any of $P_{ij}(n_{k-1}, n_k)$ are equal to zero when $i > j$.
- The range of maximum and minimum values of specimens' compliances can be easily obtained from the numbers of TPM at/between two conjunction damage stages. For example, from $[\Pi(60400,132400)]$, one can see that the specimens' damage state is from 2 to 5, and the corresponding compliance values are from 2.4514 to 2.5060×10^{-11} 1/Pa.
- The total of some of the rows are beyond 10% tolerance. The reasons are explained as follows:
  - ✓ Data collection (number of data): the more data we collected, the probability density function could better match the real distribution.
  - ✓ The dispersal of collected data could largely influence the estimated probability density functions, which could be more accurate if all the data are

within a small range (or relative low standard deviation).

- ✓ The selection of damage states also affects the transition probability matrix calculation results. In terms of small group of data or more dispersed data, we have to use small number of damage states for probability density function calculation, which would be better match the real distribution. So the finer the damage states we choose (in case the same group of data), the less accurate result may be obtained.

Step 6:

Calculation of m-step transition probability matrices. Based on the calculation results from step 5, the equation (4.12) then can be re-written:

$$[\Pi(2800,420400)] = [\Pi(2800,60400)] \times [\Pi(60400,132400)] \times ..... \times [\Pi(348400,420400)]$$

Then the non-zero entries of the transition probability matrices are given below:

$[\Pi(2800,420400)] =$

Row1	0.1802	0.2212	0.2096	0.1222	0.0516	0
Row2	0.0168	0.0652	0.4493	0.3718	0.1731	0
Row3	0.0054	0.0309	0.3655	0.3948	0.2740	0
Row4	0	0.0077	0.2811	0.4007	0.3724	0

Then the unconditional probabilities of compliance at load cycles 420400 in this case are listed below based on equation (4.13), and its histogram is presented in Fig. 4.6:

$$\left[\Pi^{U}(n_0, n_m)\right] = \left[\Pi^{U}(2800, 420400)\right] =$$

$$= \left[\Pi(2800)\right] \times \left[\Pi(2800, 60400)\right] \times \left[\Pi(60400, 13240)\right] \times \ldots\ldots \times \left[\Pi(276400, 348400)\right]$$

$$= [0 \quad 0 \quad 0.0345 \quad 0.0668 \quad 0.3546 \quad 0.3470 \quad 0.2250 \quad 0]$$

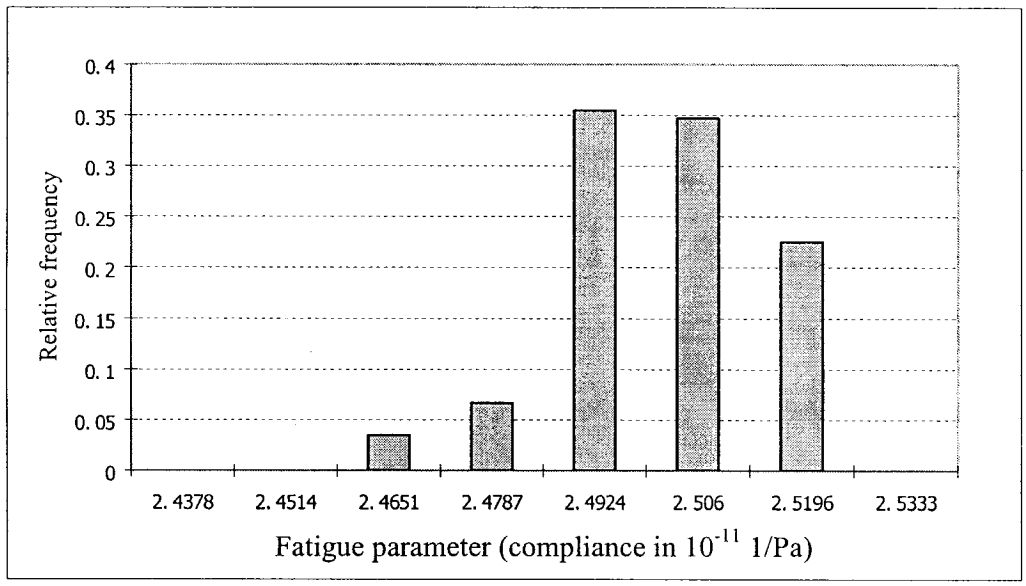

Figure 4.6 Histogram of unconditional probabilities at fatigue load cycle 420400 in terms of 8 damage states

The relative frequency of specimens' compliances at certain load cycles that is called the real distribution is defined based on the percentage of the number of specimens whose compliances at this load cycles fall in each range of damage states out of total specimens. For example, there is only one specimen whose compliance falls in the

third state at load cycle 420400, then the relative frequency at this state is 0.05 (1/20). In the same manner, the rest of relative frequency values at load cycle 420400 (or damage stage 6) with 8 damage states can then be calculated and listed below:

[0 0 0.05 0.10 0.30 0.35 0.20 0]

The histogram corresponding to these unconditional probabilities distribution compared with the real distribution is plotted in Fig.4.7.

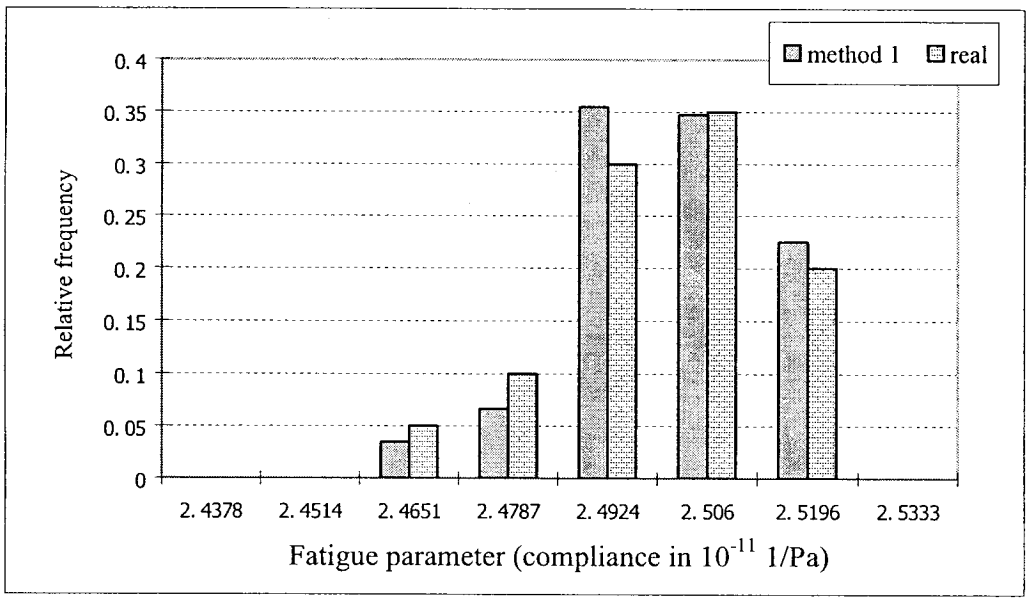

Figure 4.7 Histogram of unconditional probabilities versus histogram of real distribution at cycle 420400 in terms of 8 damage states

The match percentage at each damage state can be calculated using unconditional probabilities divided by real distribution at this state, that is:

$$p_m = \begin{cases} p_c / p_r ; p_c \geq p_r \\ [p_r - (p_c - p_r)] / p_r ; p_c < p_r \end{cases} \quad (4.18)$$

where the match percentage at certain damage state is p_m; p_c is unconditional probability at this state; p_r is real frequency at this state.

Then the overall match percentage is the average of non-zero match percentages corresponding to all damage states. For instance, the non-zero match percentages at damage states 3, 4, 5, 6, 7 are 0.69, 0.664, 0.987, 0.991, and 0.875 based on equation (4.18) at load cycle 492400 in terms of 8 damage states, so the overall match percentage with the real frequency is 84.14 % ((69%+66.4%+98.7%+99.1%+87.5%)÷5=84.14%).

Step 7:

Estimation of further damage stage probabilities after further DC at load cycle 449280. Based on the above processes, 6 TPMs are derived by using 6 sets of fatigue parameter values (compliance) that correspond to the 6 damage stages. And any 5 transition-probability-functions in 6 TPMs are assumed as constituting a random variable and shall follow a Gaussian distribution rule. For example, $1p_{ij}$, $2p_{ij}$, $3p_{ij}$, $4p_{ij}$, $5p_{ij}$ are assumed to be the constituting random variables, then $6p_{ij}$ is determined (estimated) by the following Gaussian distribution equation as the reliability is set to 90%:

$$p_{ij} = z_{90}\sigma_{ij} + \mu_{ij} \tag{4.19}$$

where z_{90} is approximately equal to 1.3 when the reliability is 90%, σ_{ij}, μ_{ij} are standard deviation and mean value of the above variables respectively. Then the estimation of transition probability matrix at load cycle 492400 can be finally determined. The non-zero entries of rows and columns are listed below:

$[\Pi(420400,492400)] =$

Row1	0.1216	0.1216	0.1216	0	0	0	0	0
Row2	0	0.4786	0.7511	0	0	0	0	0
Row3	0	0	0.6524	0.7304	0	0	0	0
Row4	0	0	0	0.5612	0.5995	0	0	0
Row5	0	0	0	0	0.8153	0.3421	0	0
Row6	0	0	0	0	0	0.7248	0.3039	0
Row7	0	0	0	0	0	0	0.5406	0

Step 8:

Calculation of the unconditional probabilities at load cycle 492400 by applying equation (4.13). The initial damage stage distribution $[\Pi(2800)]$, which is determined from relative frequency at full range of damage states (8 states), in this case is:

$[\Pi(2800)] = [0.15 \quad 0.35 \quad 0.30 \quad 0.20 \quad 0 \quad 0 \quad 0 \quad 0]$

Then the predicted unconditional probabilities of the specimen compliances at load cycle 492400 are given below by equation (4.13):

$$[\Pi^{U}(n_0, n_m)] =$$

[0 0 0.0225 0.0627 0.3292 0.3729 0.2271 0]

The histogram corresponding to the above result is showed in Figure 4.8.

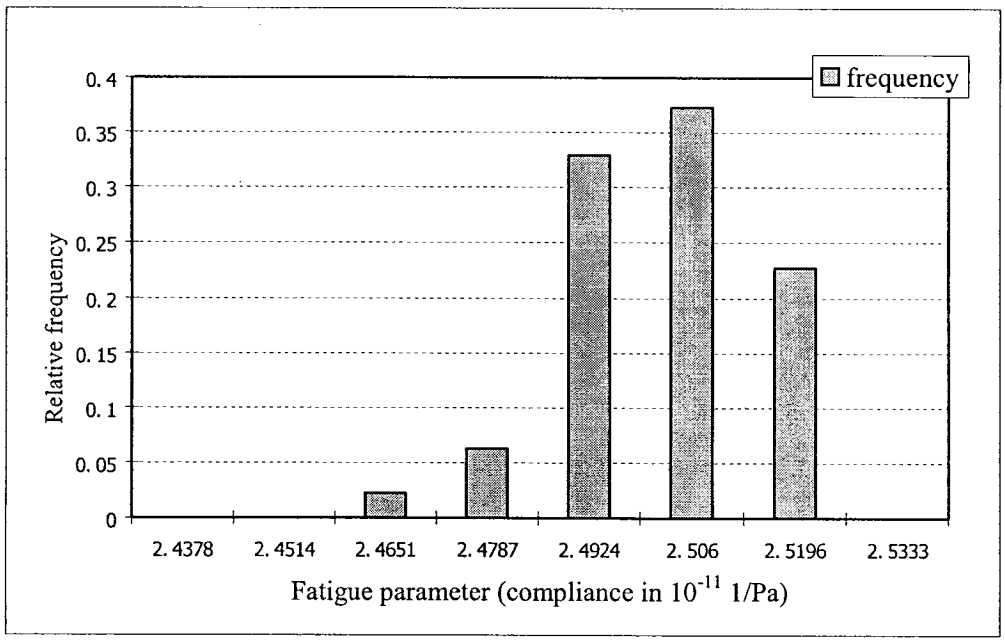

Figure 4.8 Histogram of predicted unconditional probabilities based on method 1 at load cycle 492400 in terms of 8 damage states.

By calculation of relative frequency, the real distribution of specimen compliances in

terms of 8 damage states at load cycle 492400 (or damage stage 6) is:

[0 0 0.05 0.05 0.30 0.35 0.25 0]

So in this way, the two probability distributions of fatigue parameter, which are obtained from (i) analytical estimation and (ii) from the test data, can now be compared and their histograms chart is shown in Figure 4.9.

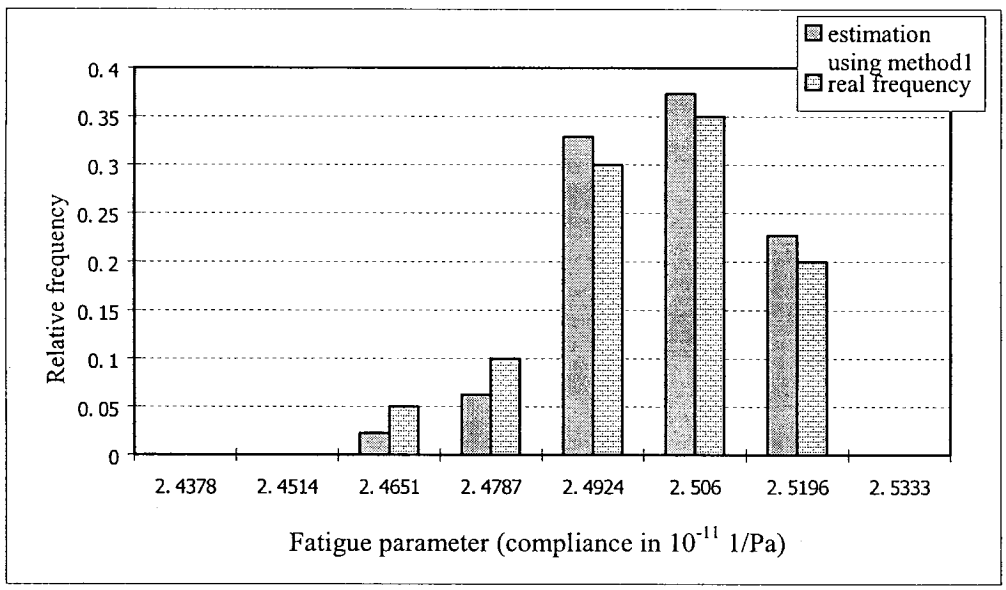

Figure 4.9 Histogram of predicted unconditional probabilities based on method 1 versus histogram of real distribution at load cycle 492400 in terms of 8 damage states

The overall match percentage of estimated probabilities distribution comparing with the real frequency distribution at load cycle 492400 in terms of 8 damage states based on Method 1) is 85%.

4.4.1.1.2 Method 2)

Gaussian probability distribution is used for TPM calculation of both individual probability density function and joint probability density function at each given specimen compliances at a certain damage stage. Then the equation (4.5) and the equation (4.9) are used to determine the individual and joint probability density function. The calculation procedure should follow the steps from 1 to 8 mentioned above.

For example, the detailed calculation of the individual and joint probability distribution at first damage stage of 2800 cycles is presented below in terms of 8 damage states, which are divided in the whole range of specimen compliances (2.4378 to 2.5469×10^{-11} 1/Pa). Since σ, μ are equal to 0.0131 and 2.4658based on the compliance data at cycle 2800 listed in table 4.1, then the individual probability at first damage state (from 2.4378 to 2.4514e-11 (1/Pa)) is equal to 0.1199 by integration of the equation (13) from 2.4378 to 2.4514e-11 (1/Pa). The joint probability distribution for the first damage state rectangle area, where X is from 2.4378 to 2.4514e-11 (1/Pa) and Y is from 2.4378 to 2.4514e-11 (1/Pa), is equal to 0.010 by integration of the equation (4.8) based on σ_x, σ_y, μ_x, μ_y and ρ are known from the compliance values at 2800 cycles and 60400 cycles, and they are 0.0131, 0.0122, 2.4658, 2.4763 and 0.9068 respectively. Finally, $p_{11}(2800,60400) = \frac{0.010}{0.1199} = 0.0838$ is determined according to equation (4.3).

Similarly, the rest of $p_{ij}(2800,60400)$ can be calculated and the probability transition matrix from load cycle 2800 to 60400 can be determined according to equation (4.11) as below (with non-zero entries):

$[\Pi(2800,60400)]=$

Row1	0.0838	0.7232	0.1924	0	0	0	0	0
Row2	0	0.1909	0.7212	0.0871	0	0	0	0
Row3	0	0	0.3544	0.6103	0.0316	0	0	0
Row4	0	0	0	0.5417	0.4352	0.0091	0	0
Row5	0	0	0	0	0.6954	0.2607	0	0

Then following the above mentioned steps, we can get the rest of the probability transition matrices as listed below (non-zero entries):

$[\Pi(60400,132400)]=$

Row1	0.2546	0.7214	0	0	0	0	0	0
Row2	0	0.2550	0.7083	0.0354	0.2438	0.0615	0	0
Row3	0	0	0.2462	0.6874	0.0473	0	0	0
Row4	0	0	0	0.2643	0.6812	0. 0542	0	0
Row5	0	0	0	0	0.2424	0.7019	0.0556	0
Row6	0	0	0	0	0	0.1985	0.7465	0

$[\Pi(132400,204400)] =$

Row1	0.3369	0.6630	0	0	0	0	0	0
Row2	0	0.3828	0.6172	0	0	0	0	0
Row3	0	0	0.4413	0.5587	0	0	0	0
Row4	0	0	0	0.5074	0.4926	0	0	0
Row5	0	0	0	0	0.5745	0.4255	0	0
Row6	0	0	0	0	0	0.6356	0.3644	0
Row7	0	0	0	0	0	0	0.6854	0.3145

$[\Pi(204400,276400)] =$

Row2	0.6747	0	0	0	0	0	0	0
Row3	0	0.3961	0.6038	0	0	0	0	0
Row4	0	0	0.4767	0.5232	0	0	0	0
Row5	0	0	0	0.5630	0.4368	0	0	0
Row6	0	0	0	0	0.6492	0.3506	0	0
Row7	0	0	0	0	0	0.7288	0.2708	0
Row8	0	0	0	0	0	0	0.7972	0.2024
Row8	0	0	0	0	0	0	0	0.8521

$[\Pi(276400,348400)] =$

Row2	0	0.5261	0.4735	0	0	0	0	0

Row3	0	0	0.5804	0.4191	0	0	0	0
Row4	0	0	0	0.6411	0.3582	0	0	0
Row5	0	0	0	0	0.7041	0.2952	0	0
Row6	0	0	0	0	0	0.7647	0.2346	0
Row7	0	0	0	0	0	0	0.8187	0.1807
Row8	0	0	0	0	0	0	0	<u>0.8634</u>

Then the unconditional probabilities of compliance at load cycles 420400 in terms of 8 damage states based on method 2 are calculated by using equation (4.12) and they are given below:

$$\left[\prod^{U}(n_0, n_m)\right] = \left[\prod^{U}(2800, 420400)\right] =$$

$$= \left[\prod(2800)\right] \times \left[\prod(2800, 60400)\right] \times \left[\prod(60400, 13240)\right] \times \ldots\ldots \times \left[\prod(276400, 348400)\right]$$

$$= [0 \quad 0.0051 \quad 0.0494 \quad 0.1882 \quad 0.3310 \quad 0.2818 \quad 0.1151 \quad 0.0211]$$

Similarly, the corresponding unconditional probabilities histogram versus real frequency histogram is plotted in Fig. 4.10.

As one can see, there is a big difference between the unconditional probabilities distribution calculated using method 2 and the real distribution from Fig. 4.10. the reason is because several numbers in its TPMs largely exceed the 10% tolerance, which are marked with underline.

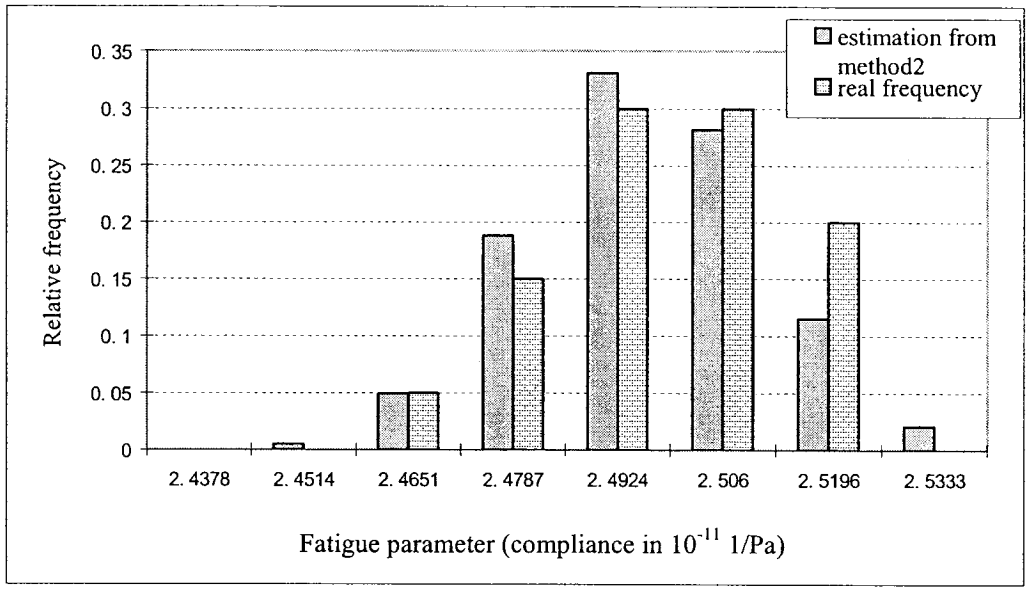

Figure 4.10 Histogram of unconditional probabilities based on method 2 versus histogram of real frequency at load cycle 420400 in terms of 8 damage states

Following the calculation steps of Step 7 and Step 8, the estimation of non-zero TPM at load cycle 492400 is presented below:

$[\Pi(420400,492400)] =$

Row1	0.1964	0.6814	0.0729	0	0	0	0	0
Row2	0	0.4026	0.6646	0.0398	0	0	0	0
Row3	0	0	0.4715	0.5998	0.0247	0	0	0
Row4	0	0	0	0.5605	0.5295	0.0221	0	0
Row5	0	0	0	0	0.6499	0.4773	0.0211	0
Row6	0	0	0	0	0	0.6035	0.4321	0.1944
Row6	0	0	0	0	0	0	0.6295	0.5310

Then the predicted unconditional probabilities of the specimen compliances at load cycle 492400 are given below by equation (4.15):

$$\left[\Pi^{U}(n_0, n_{m+1})\right] = [\Pi(0)] \times [\Pi(n_0, n_1)] \times [\Pi(n_1, n_2)] \times \ldots\ldots \times [\Pi(n_{m-1}, n_m)] \times [\Pi(n_m, n_{m+1})]$$

[0 0.001 0.0149 0.0918 0.2654 0.3604 0.2771 0.0704]

The histograms for the predicted unconditional probabilities obtained from method 2 comparing with that obtained from method 1 and the real frequency are plotted in Fig. 4.11.

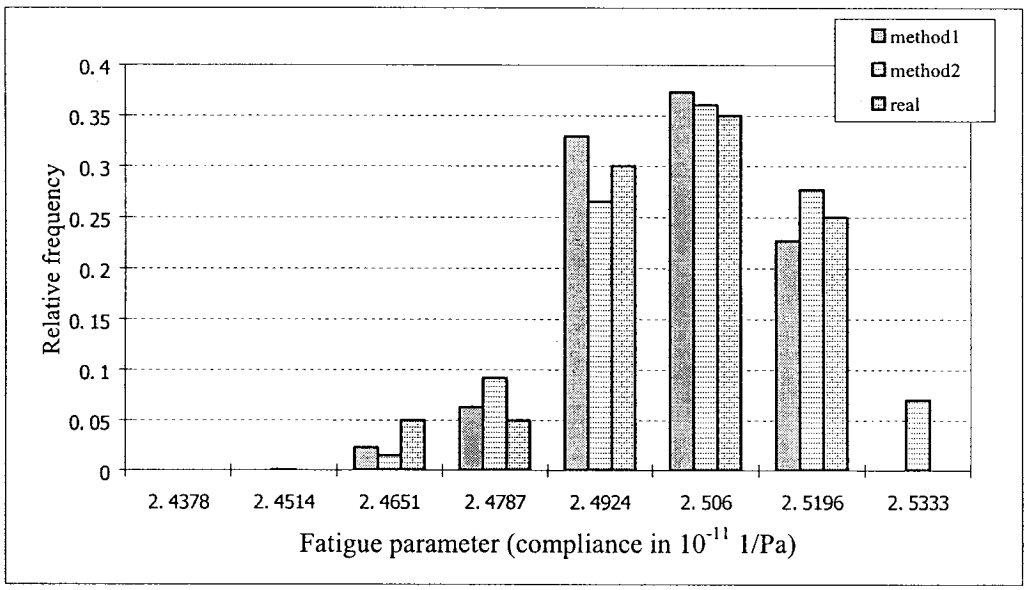

Figure 4.11 Histogram of predicted unconditional probabilities based on methods 1and 2 versus histogram of real distribution at load cycle 492400 in terms of 8 damage states

It is observed from Figs. 4.9 and 4.10 that there is a big difference between the estimated distribution and the real distribution, especially in the damage state, for which the real frequency is zero but the estimated frequency using method 2 is non-zero. The reasons for that are: 1) the specimen compliances distribution or joint distribution are assumed to follow Gausian distribution, but the reality is that the compliances at some damage stages follow and some do not; and 2) the data marked with underline from the above individual TPMs at different load cycles are far from 10% tolerance.

4.4.1.1.3 Method 3)

Combined method is the combination of method 1 and method 2. That is to select the more accurate TPMs from method 1 and method 2 or to select method 2 in the case where the frequency histogram charts are more like normal distribution (see Fig.4.4), then we could get the result closer to the real data.

For example, we select the following TPM from method 1:

$[\Pi(204400,276400)] =$

Row2	0	0	1.0844	0	0	0	0	0
Row3	0	0	0.3544	0.7088	0	0	0	0

Row4	0	0	0	0.4024	0.6036	0	0	0
Row5	0	0	0	0	0.5811	0.4358	0	0
Row6	0	0	0	0	0	0.4748	0.4748	0

The following TPMs have been selected from method 2:

$[\Pi(2800,60400)] =$

Row1	0.0838	0.7232	0.1924	0	0	0	0	0
Row2	0	0.1909	0.7212	0.0871	0	0	0	0
Row3	0	0	0.3544	0.6103	0.0316	0	0	0
Row4	0	0	0	0.5417	0.4352	0.0091	0	0
Row5	0	0	0	0	0.6954	0.2607	0	0

$[\Pi(60400,132400)] =$

Row1	0.2546	0.7214	0	0	0	0	0	0
Row2	0	0.2550	0.7083	0.0354	0.2438	0.0615	0	0
Row3	0	0	0.2462	0.6874	0.0473	0	0	0
Row4	0	0	0	0.2643	0.6812	0. 0542	0	0
Row5	0	0	0	0	0.2424	0.7019	0.0556	0
Row6	0	0	0	0	0	0.1985	0.7465	0

$[\Pi(132400,204400)] =$

Row1	0.3369	0.6630	0	0	0	0	0	0

Row2	0	0.3828	0.6172	0	0	0	0	0
Row3	0	0	0.4413	0.5587	0	0	0	0
Row4	0	0	0	0.5074	0.4926	0	0	0
Row5	0	0	0	0	0.5745	0.4255	0	0
Row6	0	0	0	0	0	0.6356	0.3644	0
Row7	0	0	0	0	0	0	0.6854	0.3145

$[\Pi(276400,348400)]=$

Row2	0	0.5261	0.4735	0	0	0	0	0
Row3	0	0	0.5804	0.4191	0	0	0	0
Row4	0	0	0	0.6411	0.3582	0	0	0
Row5	0	0	0	0	0.7041	0.2952	0	0
Row6	0	0	0	0	0	0.7647	0.2346	0
Row7	0	0	0	0	0	0	0.8187	0.1807
Row8	0	0	0	0	0	0	0	0.8634

The calculation results based on equation (4.12) and the corresponding histogram charts (Fig.4.12) based on methods 1, 2, and 3 are given below along with the histogram of real frequency at load cycles 420400:

$$\left[\Pi^{U}(n_0,n_m)\right]=\left[\Pi^{U}(2800,420400)\right]=$$

$$=[\Pi(2800)]\times[\Pi(2800,60400)]\times[\Pi(60400,13240)]\times.....\times[\Pi(276400,348400)]$$

= [0 0 0.0324 0.0929 0.3126 0.3565 0.1634 0.0182]

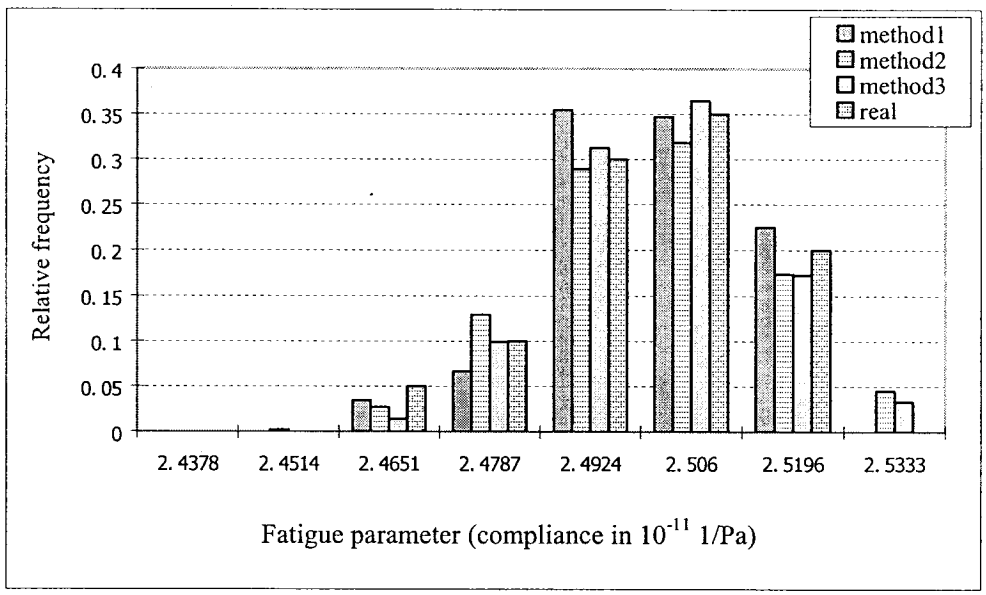

Figure 4.12 Histogram of unconditional probabilities based on methods 1, 2, and 3 versus histogram of real frequency at load cycle 420400 in terms of 8 damage states.

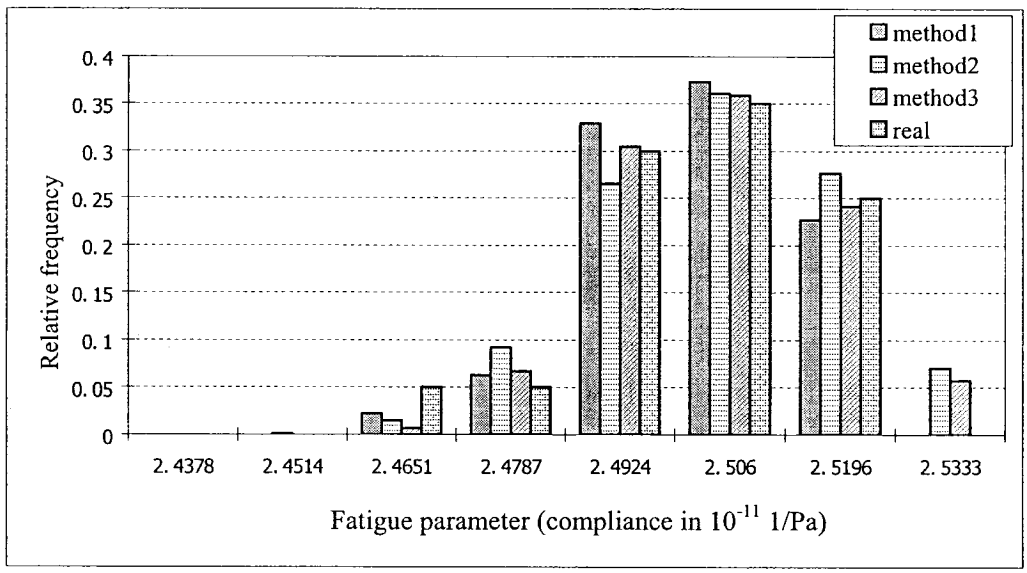

Figure 4.13 Histogram of predicted unconditional probabilities based on methods 1, 2, and 3 versus histogram of real frequency at load cycle 492400 in terms of 8 damage states

Similarly, the predicted unconditional probabilities distribution histogram obtained using combined method (method 3) at load cycle 492400 together with those obtained using other two methods are shown along with real frequency in Fig.4.13.

4.4.1.1.4 Method 4)

Another rule of calculating TPMs, that is by using Gaussian distribution to compute the joint probability density function and using MEM method to calculate the individual probability density function, is also conducted in the present thesis. But the result is far beyond the tolerance, and this method is therefore omitted for further discussion.

4.4.1.2 Discussion and conclusion

Gaussian method (method 2) calculation could be more accurate only if the individual and joint probabilities distribution of specimen compliances follow the normal distribution, while the MEM method (method 1) works very well in the condition of no big change of probabilities between any two conjunction damage stages, either increase or decrease. The probabilities distribution result calculated from method 3 (which is called a combined calculation method) by choosing the appropriate TPMs ($p_{ij}(n_{k-1}, n_k)$) from both methods 1 and 2 is closer to the real frequency compared

with that obtained using other two methods, as one can see from Figs.4.12 and 4.13.

Therefore, by using method 3, a good match with the real frequency can be shown when the damage states are increased. For example, the Figs.4.14 and 4.15 present the histogram of unconditional and predicted unconditional probabilities distribution based on method 3 compared with the results of other two methods along with real frequency at load cycle 420400 in terms of 13 damage states. The non-zero match percentages of method 3 (comparing with real frequency) versus that of the other two methods are presented in the table 4.3.

Table 4.3: Non-zero probability match percentage comparing with real frequency

Match percentage / Damage states(1×10^{-11} 1/Pa)	unconditional probability distribution at load cycle 420400			unconditional predicted distribution at load cycle 492400		
	method 1	method 2	method 3	method 1	method 2	method 3
2.4707~2.479	none	0.3860	0.9240	none	0.1920	0.5720
2.479~2.4873	0.3420	0.8320	0.6020	0.1380	0.7020	0.9700
2.4873~2.4955	0.6860	0.7530	0.8810	0.8380	0.1820	0.2320
2.4955~2.5038	0.6640	0.7220	0.7007	0.8820	0.8567	0.9560
2.5038~2.5121	0.6660	0.6071	0.9349	0.5397	0.7490	0.9750
2.5121~2.5203	0.7327	0.8293	0.8180	0.5750	0.8195	0.8015
2.5203~2.5286	0.6780	0.8840	0.5310	0.8193	0.7307	0.9787
2.5286~2.5368	0.3920	0.9020	0.4740	0.5100	0.2500	0.7300
overall match percentage	0.5944	0.7394	0.7332	0.6146	0.5602	0.7769

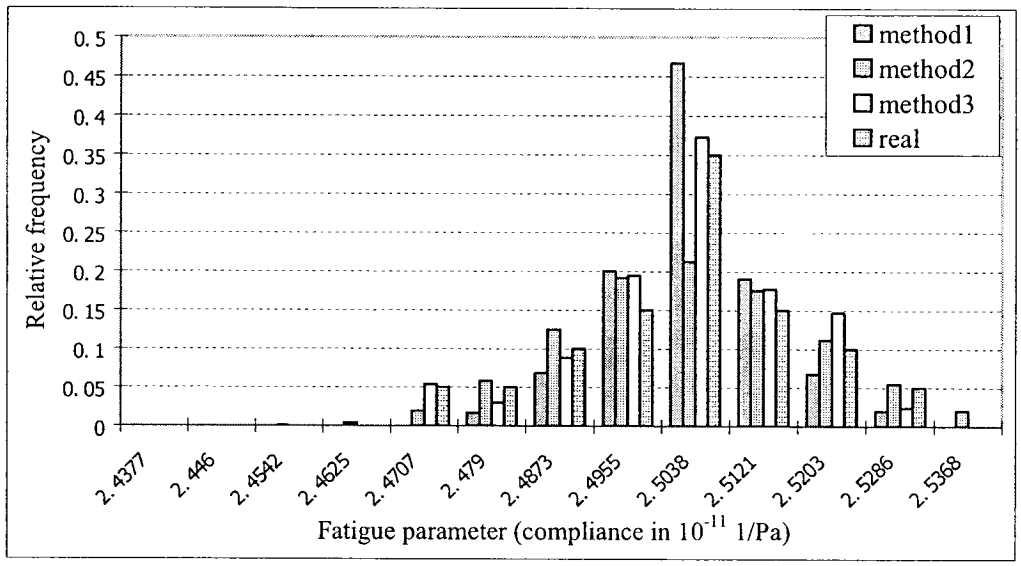

Figure 4.14 Histogram of unconditional probabilities based on 3 methods versus histogram of real frequency at load cycle 420400 in terms of 13 damage states

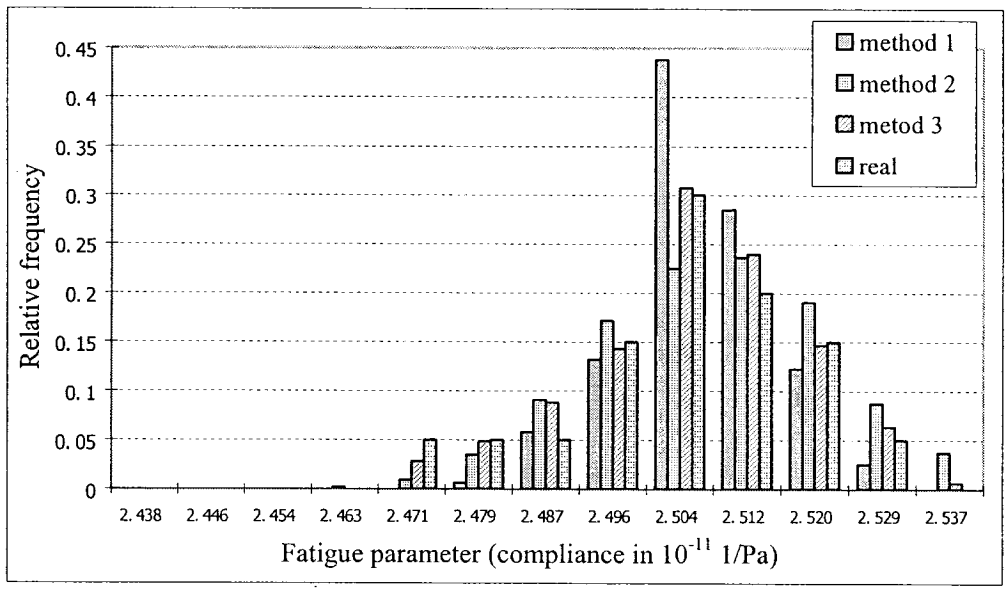

Figure 4.15 Histogram of predicted unconditional probabilities based on 3 methods versus histogram of real frequency at load cycle 492400 in terms of 13 damage states

As one can see from the above two charts, the result from either method 1 or method

2 is far from the real frequency distribution both in unconditional probabilities distribution and predicted unconditional probabilities distribution. Therefore, we may have the following conclusion from the above two charts:

- The calculation results from the dispersal data (with less standard deviation) will have good match with real frequency distribution in terms of higher number of damage states.
- The combined method (method 3) shows much improvement in matching with the real distribution even though some data from TPMs are still beyond the tolerance.
- If more specimens are tested, more accurate calculation result will be obtained according to statistical philosophy.

4.4.2 Case 2: Confrontation with test data corresponding to LCT

A total of 20 specimens were tested under LCT, which is the regular over tension load based on normal tension-compression load. The 20 specimens' compliances versus load cycles are listed in the table 4.4 and the plot of specimens' compliances versus load cycles is presented in Fig. 4.16.

Table 4.4: The compliances ($\times 10^{-11}$ 1/Pa) of tested specimens at different load cycles under LCT

Specimen	2800 cycles	60400 cycles	132400 cycles	204400 cycles	276400 cycles	348400 cycles	420400 cycles	492400 cycles
1	2.46516	2.49472	2.5141	2.53315	2.54449	2.55135	2.55869	2.56659
2	2.47768	2.5025	2.52778	2.54293	2.54842	2.5569	2.56407	2.56737
3	2.45482	2.48672	2.51867	2.53887	2.54617	2.55086	2.55844	2.56868
4	2.45784	2.49138	2.51243	2.53474	2.54757	2.56108	2.56567	2.57002
5	2.49246	2.52149	2.53908	2.5485	2.55282	2.55862	2.56138	2.5705
6	2.46982	2.498	2.53168	2.54346	2.55053	2.55575	2.56263	2.57066
7	2.46109	2.48593	2.50563	2.53034	2.54437	2.55166	2.56055	2.57185
8	2.45832	2.48859	2.52256	2.54162	2.55198	2.55705	2.56408	2.57226
9	2.47903	2.50852	2.52995	2.54089	2.55073	2.55521	2.56559	2.57377
10	2.44874	2.47422	2.5093	2.53239	2.54992	2.56764	2.57233	2.57645
11	2.48037	2.50965	2.53574	2.54841	2.55373	2.56094	2.56936	2.57691
12	2.46421	2.48605	2.52351	2.5399	2.55103	2.55658	2.56702	2.57702
13	2.47471	2.50453	2.53162	2.55295	2.55826	2.56438	2.57028	2.57781
14	2.46717	2.48903	2.52852	2.55084	2.56028	2.56958	2.57805	2.58266
15	2.4732	2.4944	2.53142	2.55183	2.5653	2.57586	2.57808	2.58451
16	2.48373	2.50777	2.53895	2.55906	2.56401	2.57041	2.57861	2.58811
17	2.4779	2.50655	2.54676	2.56387	2.57118	2.57714	2.58243	2.59029
18	2.45536	2.4857	2.53403	2.55733	2.57008	2.57738	2.58497	2.59063
19	2.48533	2.51657	2.54526	2.5637	2.5714	2.5849	2.58985	2.59183
20	2.48953	2.51236	2.5541	2.56408	2.57384	2.57997	2.58689	2.5932
STDEV*	0.01249	0.012458	0.0128	0.010834	0.009733	0.010514	0.009859	0.008874

STDEV*: the standard deviation of specimen compliances at different load cycles

As the value of standard deviation of fatigue parameter (specimen compliances) at each damage stage (load cycles) is reduced compared to the data from LCO, the calculation result of both unconditional and predicted unconditional probabilities distribution for Case 2, in terms of the same number of damage states used in the above, should be then much better than that of LCO. For example, with 13 damage states, the match percentages of the unconditional and predicted unconditional probabilities distribution for combined method (method 3), which are 94.67% and

95.02% respectively, are far better than that of LCO and their histograms obtained using the three methods versus real frequency distribution are presented in Figs. 4.16 and 4.17. Moreover, as one can also see from charts, the results calculated using the other two methods are also improved in this case.

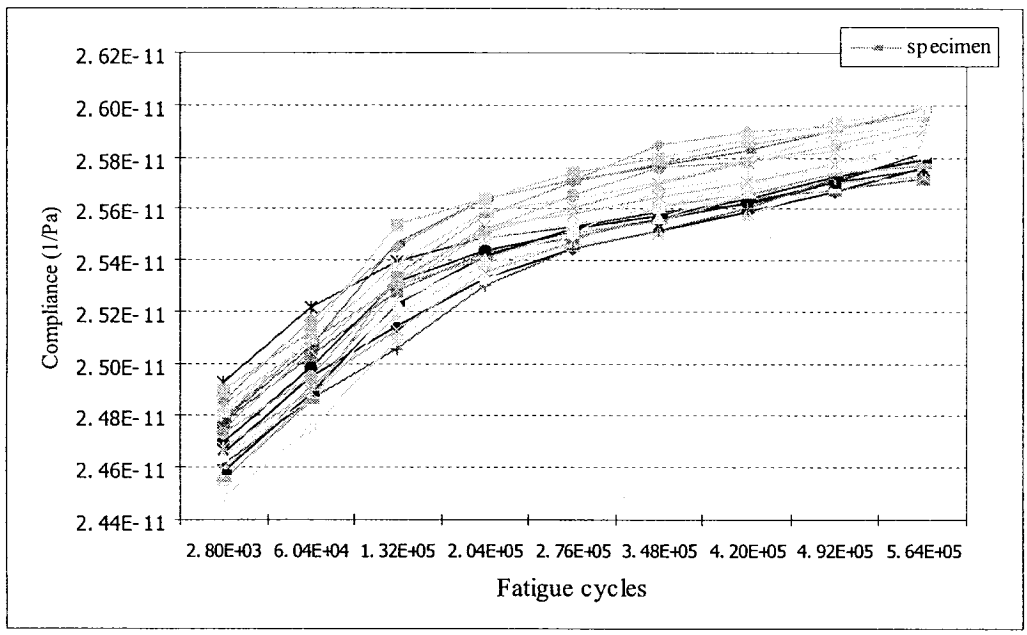

Figure 4.16 The plot of fatigue parameter (compliances) of 20 test specimens

Obviously, the test data from Case 2 is improved, i.e. the data dispersal declined, so that the number of damage states can be further divided into 20 states (or even more). The histogram charts of unconditional and predicted unconditional probabilities for specimen compliances at load cycles 420400 and 492400 in terms of 13 and 20 damage states are plotted in Figs. 4.18 and 4.19.

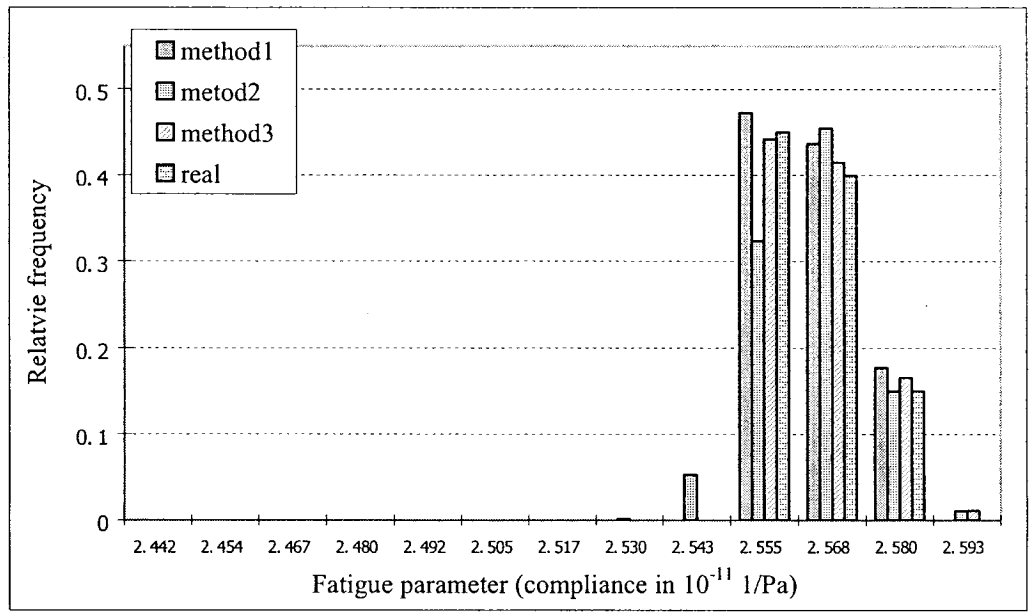

Figure 4.17 Histogram of unconditional probabilities based on 3 methods versus histogram of real frequency at load cycle 420400 in terms of 13 damage states

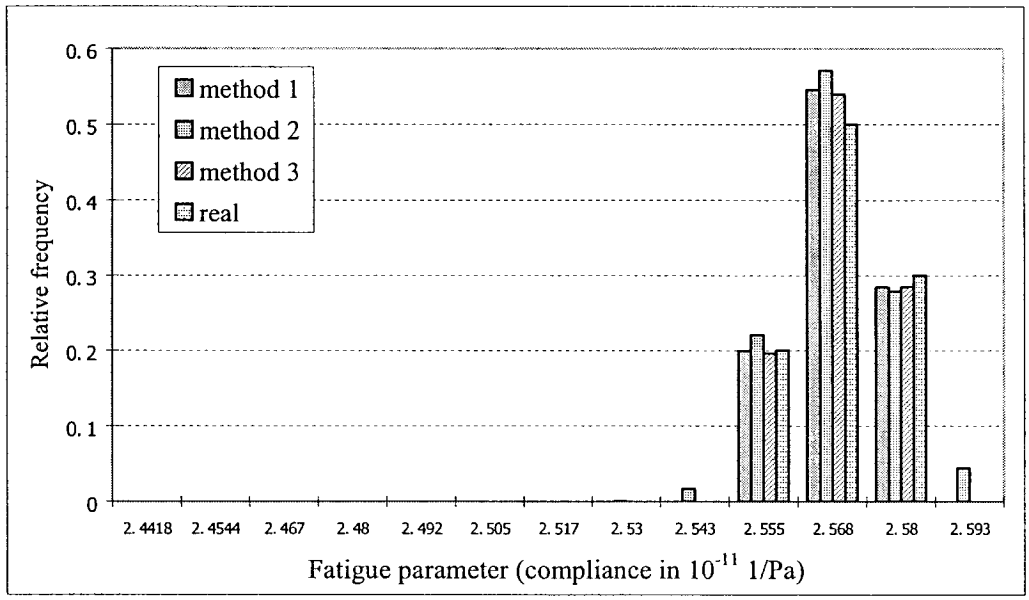

Figure 4.18 Histogram of predicted unconditional probabilities based on 3 methods versus histogram of real frequency at load cycle 492400 in terms of 13 damage states

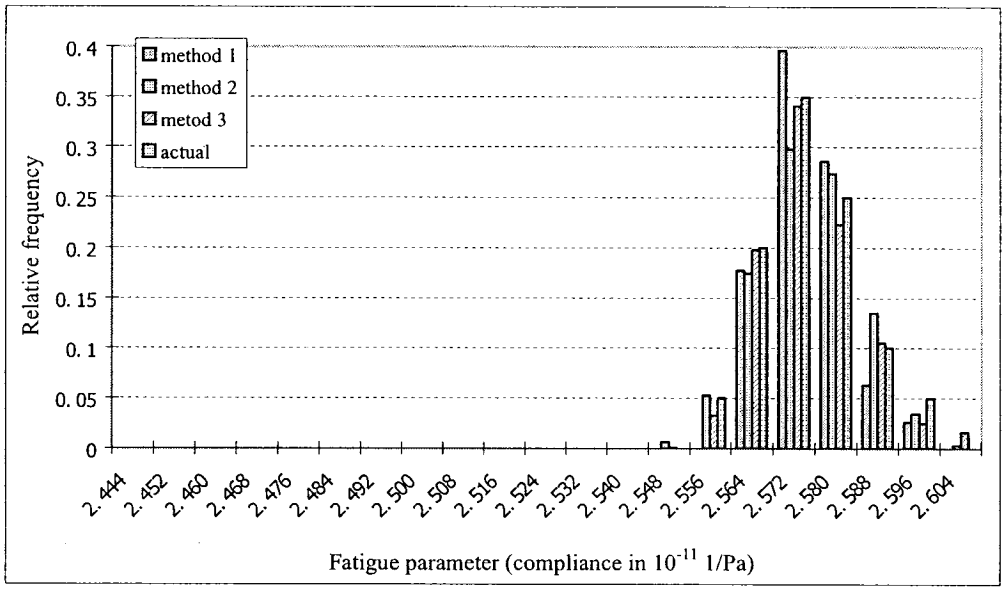

Figure 4.19 Histogram of unconditional probabilities based on 3 methods versus histogram of real frequency at load cycle 420400 in terms of 20 damage states

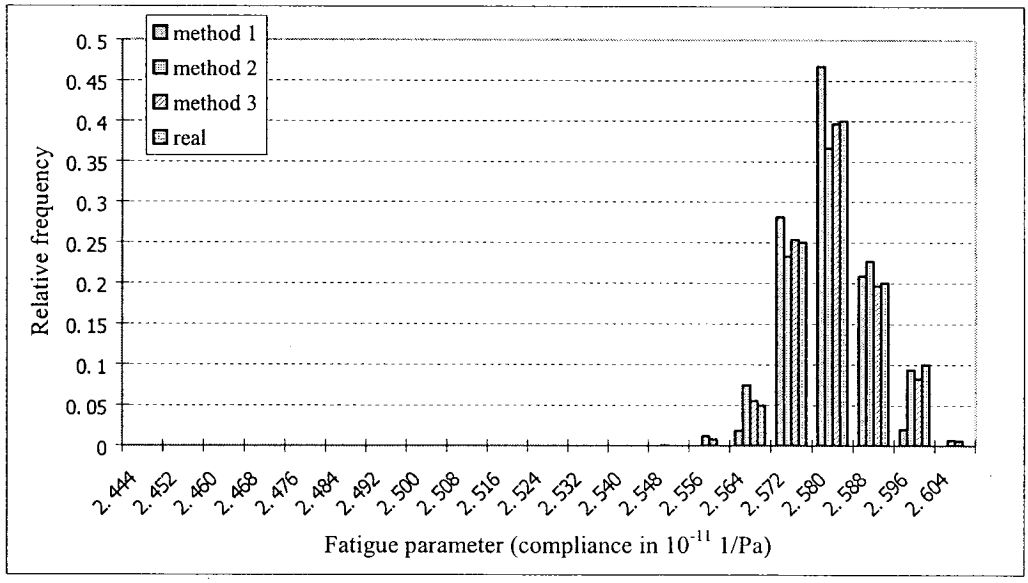

Figure 4.20 Histogram of predicted unconditional probabilities based on 3 methods versus histogram of real frequency at load cycle 492400 in terms of 20 damage states

4.5 Discussion and conclusion

A stochastic approach [35] to model and analyze the test data on the fatigue response parameter of composite laminate is used in the present thesis. The fatigue damage accumulation process can be well represented by Markov process modeling subjected to the structural-level fatigue response parameter. Four calculation methods of the true probabilities distribution regarding fatigue response parameter in terms of the number of damage states are also described and discussed in the present thesis, that are Maximum Entropy Method (MEM), Gaussian (single and Bivariate) probability distribution for individual and joint probability density function, and combined method.

The summary of improving the probability distribution compared to the real distribution is listed below:

- Improving the dispersal of data: which could have a closer result comparing with the real frequency if all the data are within a small range.

  The value of standard deviation of compliances at different damage stages with two load conditions are listed in the Table 4.5. As one can see from Table 4.6, the estimated probability distribution results from load case 2 are much better than that from load case 1 as the data from load case 2 has less dispersal.

- Combined method is considered as an efficient way to improve the estimated probability distribution if the test data can not be improved.

  For example, Method 3) always has better results compared with the other two methods, which are presented in the histogram charts in the above.

- Data collection (number of data): the more we collect, the probability density function could better represent the real distribution of data.

In another words, the number of damage states (which can be precisely quantified the fatigue damage accumulation process as the number of damage states increase.) can be increased by improving the dispersal of data, using combined method and increasing the number of test specimens.

Table 4.5: The specimens' compliance standard deviations versus damage stages in two loading conditions

damage stage	2800 cycles	60400 cycles	132400 cycles	204400 cycles	276400 cycles	348400 cycles	420400 cycles	492400 cycles
case 1: compliance STDEV under LCO	0.013086	0.012231	0.014237	0.014873	0.015031	0.015378	0.015714	0.015655
case 2: compliance STDEV under LCT	0.01249	0.012458	0.0128	0.010834	0.009733	0.010514	0.009859	0.008874

Table 4.6: The match percentages under two loading conditions in terms of 3 numbers of damage states

Match percentage / Damage states		Unconditional probabilities distribution at load cycle 420400	Predicted unconditional probabilities distribution at load cycle 492400
13 damage states	LCO: match percentage with actual frequency	0.7332	0.7743
13 damage states	LCT: match percentage with actual frequency	0.9467	0.9502
20 damage states	LCO: match percentage with actual frequency	Far from the actual distribution	Far from the actual distribution
20 damage states	LCT: match percentage with actual frequency	0.8263	0.9357

Chapter 5

Reliability analysis of tapered composite laminate under cyclic tension-compression loading

5.1 Introduction

There is no doubt that it is important to evaluate the damage and degraded properties accurately to ensure that the structures or components operate with high reliability during their service lives. It is also important to evaluate the performance of the structure in advance so that the maintenance or replacement of components can be scheduled before catastrophic failure. Therefore, the fatigue data as well as reliability data of the system plays an important role in engineering design phase regarding the safety purposes, especially for the system that could not be repaired or reworked after start of service. And the analysis and quantification of hazard rate (or failure rate), which is one of the very important terms of system reliability indices is also necessary and needed before further reliability discussion.

5.2 Typical reliability index: Hazard Rate

The basic concept of hazard rate is described as the instantaneous percentage of the numbers of failed specimens in Δt_i period to the number of survived specimens at time t_i, which is expressed by formula:

$$\lambda_{t_i} = \frac{N_S(t_i) - N_S(t_i + \Delta t_i)}{N_S(t_i) \times \Delta t_i} \tag{5.1}$$

where $N_S(t_i)$ represents the number of survived specimens at time t_i, and $N_S(t_i + \Delta t_i)$ stands for the number of survived specimens at time $t_i + \Delta t_i$.

Based on the above description, the hazard rate between two conjunction damage stages in present tests can then be rewritten in terms of composite laminate specimen compliances:

$$\lambda_i = \frac{(C_i - C_{i-1})}{C_{i-1} \times (n_i - n_{i-1})} \tag{5.2}$$

where λ_i is the hazard rate from load cycle n_i to n_{i+1}, C_i, C_{i+1} are specimen compliances at load cycles n_i and n_{i+1} respectively.

Unlike the specimen compliances, the individual specimen hazard rates under LCO

computed by equation (5.2) do not show either continuous decrease or increase in Fig. 5.1. But, when we look at the average hazard rates of 20 specimens at each damage stage load cycles for both loading cases, a continuous decrease is observed as the load cycle values increase. The average hazard rate at one load cycle value is calculated as the sum of individual hazard rates divided by 20 (20 specimens). One can assume that this trend will somehow be coincident with the typical U-shaped hazard rate of component service life that is shown in Fig. 5.4 when the test specimens are continuously tested until total failure [34, 38].

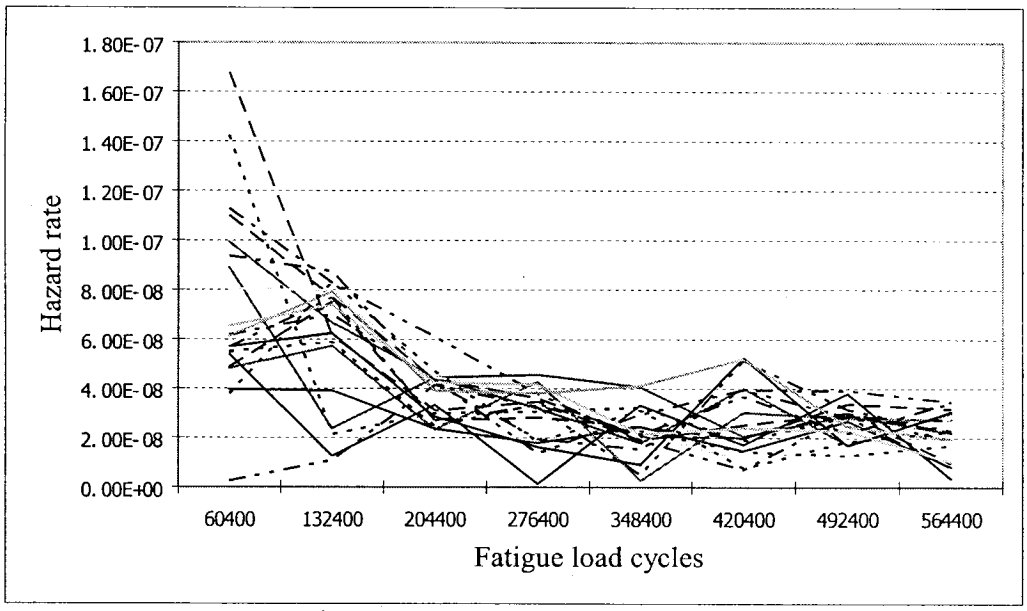

Figure 5.1 The individual hazard rates of 20 specimens under load condition LCO

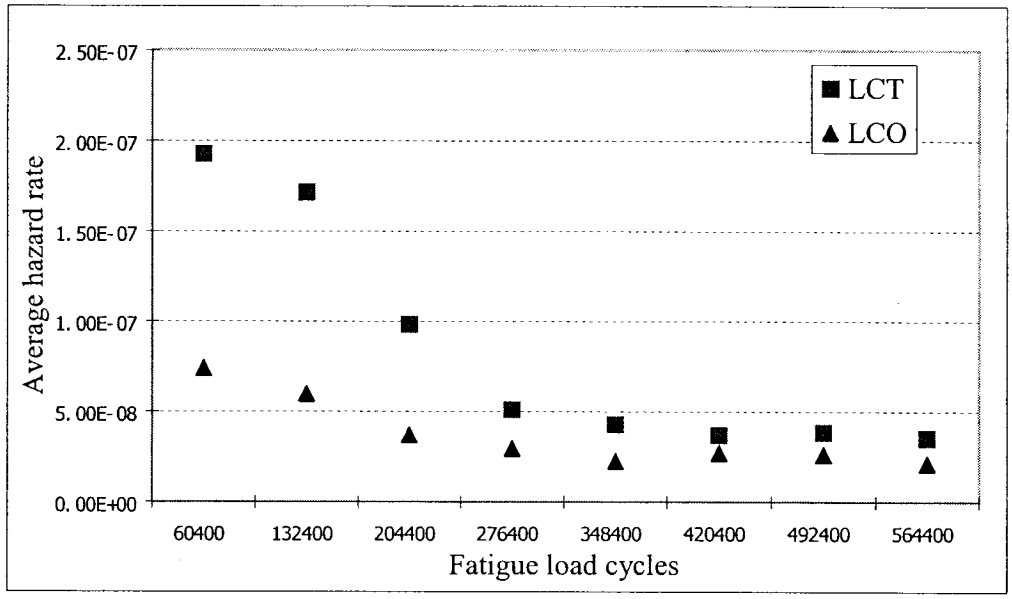

Figure 5.2 The average hazard rates under two load conditions (LCO and LCT)

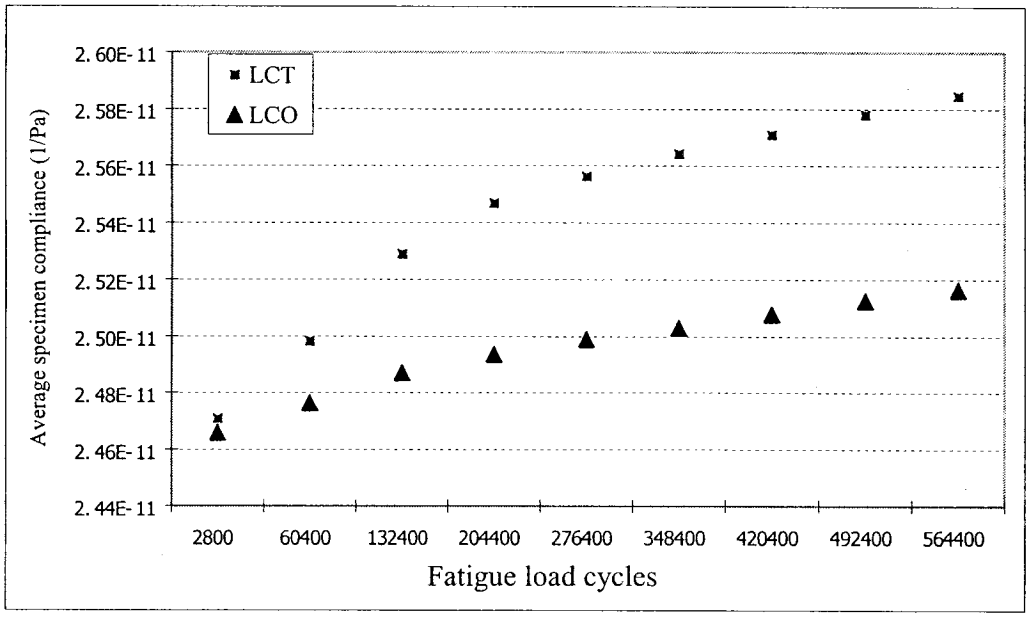

Figure 5.3 The average compliance under LCO and LCT

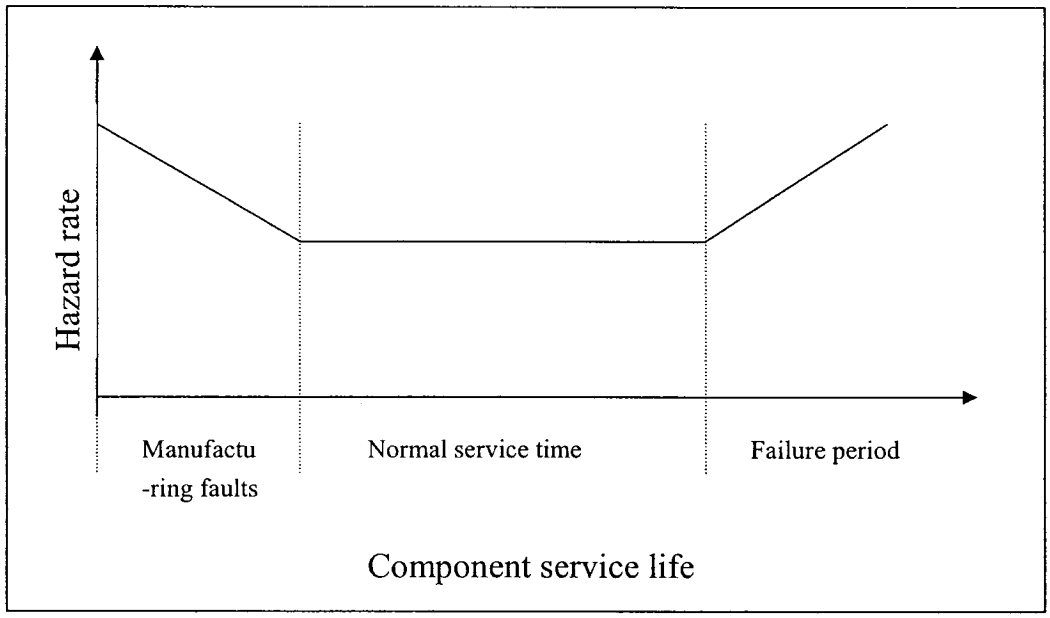

Figure 5.4 Typical chart of hazard rate in component service life

It can also be observed that:

i) The Hazard Rate value for LCT (with over tension load) is three times than that of LCO. In the graph (Fig.5.2), the slope of the line of load condition 2 is more when compared to load condition 1 during the manufacturing faults phase, which indicates that the damage speed with over tension load condition is fast when compared with normal tension-compression load condition during the same period.

ii) In the two damage process phases(Fig.5.2) , the phase I from start of test to about 300,000 (or) 400,000 cycles where the hazard rate decreases continuously is called the "manufacturing faults" or "burning-out" process ,which happens due to some early failures such as matrix crack, de-bonding, etc. Then the phase

II which starts from about 400,000 cycles is called as the "normal service life" process, where the hazard rate remains constant and will last for a quite long time. This process is also called as the typical damage accumulating process which indicates that specimen's damage keeps constant at each Duty Cycle. In the phase III (which cannot be seen in Fig5.2 but in Fig.5.4) the hazard rate will continue to increase until final failure that is called "wearing" or "failure" process.

iii) The initial failures or manufacturing faults occur regardless of the loading conditions within some range of load.

iv) The hazard rates in both cases become stable and constant at almost same level and same load cycles and also the damage accumulation speed of both cases remain at the same level, but their compliance values are at different ranges as shown in Fig.5.4.

v) Although the hazard rates from both cases remain constant at same level after some load cycles, the reliability from load case 2 will be less than that of load case 1 because of the high hazard rate during the manufacturing fault phase, which means more damage occurred at that period.

5.3 Markov process modeling of hazard rate

In order to simplify the results of unconditional and predicted unconditional

probabilities distribution of specimen hazard rates, the data only from over tension load condition (load case 2) is considered and presented hereafter in present thesis.

Based on equation (5.2), 20 specimens' Hazard Rates from various load cycles under LCT are computed and presented in Table 5.1.

Table 5.1 HRs* under LCT at different cycles (1×10^{-8} 1/cycle):

specimen	132400 cycles	204400 cycles	276400 cycles	348400 cycles	420400 cycles	492400 cycles	564400 cycles
1	21.4525	27.0045	12.7706	6.9245	3.9450	4.0901	3.0411
2	15.3869	20.9279	9.0207	6.0862	3.0217	5.6716	5.4105
3	20.2207	9.6889	5.1528	2.3543	3.1556	1.4982	4.9453
4	14.8818	20.6128	11.1982	7.3313	5.7173	1.1970	3.4640
5	18.0648	19.6920	12.7802	9.6143	9.6517	2.5369	2.2245
6	23.6912	11.7349	12.3331	7.0301	7.3654	2.4892	2.3548
7	21.8225	15.8339	10.0623	4.1715	7.2918	2.6597	1.0618
8	15.3826	22.0356	12.2601	5.1399	5.0450	4.5781	2.4836
9	17.3914	14.0304	8.3242	2.9985	4.6216	3.8947	1.7875
10	20.6524	11.8651	6.0058	5.3787	2.4394	5.6421	4.4283
11	22.5605	17.8448	11.1390	3.9935	2.5583	4.1272	5.5589
12	19.8086	18.7261	6.4626	3.8607	2.8426	3.7389	4.3521
13	16.8038	17.2686	11.0008	2.6865	3.4668	4.4308	5.1169
14	20.4943	14.4387	6.9397	2.8994	3.9213	4.5665	4.0812
15	20.9200	15.0228	11.7020	2.8888	3.3226	3.1955	4.0690
16	20.8179	10.7895	10.5240	6.2176	3.7445	3.9957	4.2882
17	20.0733	22.2805	9.3310	3.9599	3.2195	2.8509	4.2273
18	17.5227	11.0064	13.6969	7.7010	3.9794	4.8389	6.1293
19	21.3772	18.9587	10.4942	5.6613	2.7593	3.8184	4.4309
20	15.9208	23.0748	5.4270	5.2867	3.3079	3.7253	3.3878

HR*: Hazard Rate

Then the same rule of 8-step TPM calculation procedure mentioned in the previous chapter is followed, but here $p_{ij}(n_k, n_{k-1})$ will have some difference comparing to the cases in chapter 4, that it is not always zero when $i > j$ since the individual hazard rate doesn't decrease continuously. For example, the numbers marked with underline in non-zero TPM under LCT in terms of 10 hazard rate divisions should be zero if the hazard rate continuously decreases:

$[\Pi(2800,60400)]=$

Row 1	0	0	0.4772	0	0	0.4772	0
Row 2	<u>0.1263</u>	0.1263	0.1263	0.2527	0.1263	0.2527	0.1263
Row 3	0	0	<u>0.5235</u>	0	0.2617	0.2617	0
Row 4	<u>0.1776</u>	<u>0.5328</u>	0	0.1776	0	0	0

Then one can get the unconditional and predicted unconditional probabilities of specimen hazard rate corresponding to load cycles 420400 and 492400 in terms of 10 divided states, which are illustrated in Figs.5.5 and 5.6.

$[\Pi^U(2800,420400)]=$

[0 0 0 0 0 0 0 0.1049 0.7627 0.1457]

Predicted $[\Pi^U(2800,492400)]=$

[0 0 0 0 0 0 0.0098 0.1976 0.6303 0.1605]

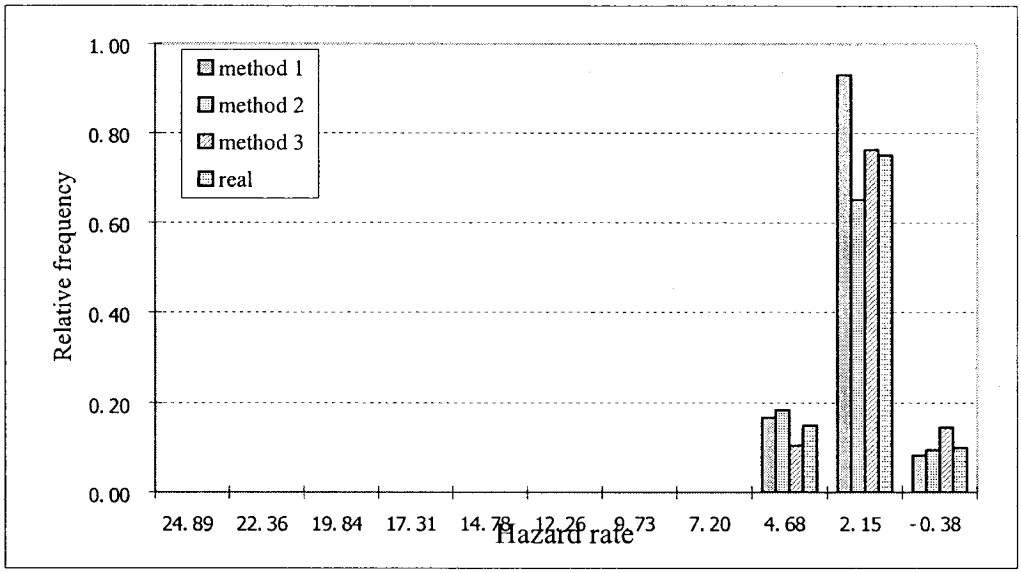

Figure 5.5 Histogram of unconditional probabilities of HR at load cycle 420400 in terms of 10 divisions

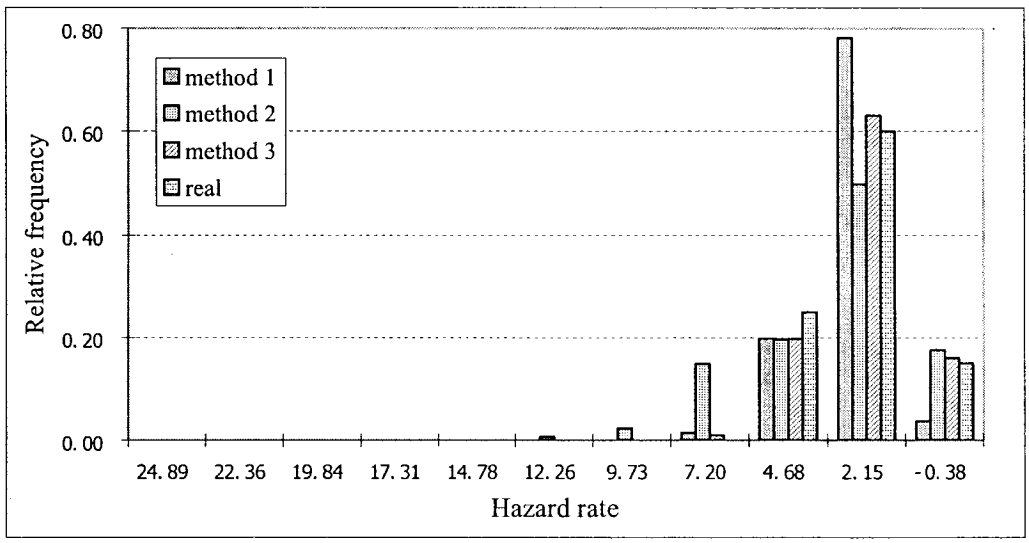

Figure 5.6 Histogram of predicted unconditional probabilities of HR at load cycle 492400 in terms of 10 divisions

5.4 Markov process modeling of reliability

Markov process modeling of reliability can be done according to the procedure mentioned in chapter 4. The true unconditional probabilities distribution and predicted unconditional probabilities distribution for composite laminate fatigue reliability at a given load cycle can be computed from three methods of reliability calculation, which are basically calculated from basic reliability concept, hazard rate and failure density function. Furthermore, the results under both cases of load conditions are also considered in present thesis.

5.4.1 Markov process modeling of reliability function

From strict probabilistic concept, the reliability is defined as the probability of a system's ability to perform its operations, or probability of loss of a system's property as time goes [38, 44].

In case of the composite laminate fatigue test, using the strict probabilistic concept the following formula in terms of the initial Young's modulus E_0 at load cycle 0 (i.e., Young's Modulus at the beginning of fatigue test) and the modulus at any load cycle E_n is derived:

$$R(n) = \frac{E_n}{E_0} \tag{5.3}$$

Therefore, the reliabilities at different load cycles are computed and listed in table 5.2 based on equation (5.3) (E_0 is considered as Young's Modulus at load cycle 2800 as it may not be stable at exactly 0 cycle):

Table 5.2 Reliabilities at different load cycles based on basic reliability concept under LCT:

Specimen	2800 cycles	60400 cycles	132400 cycles	204400 cycles	276400 cycles	348400 cycles	420400 cycles
1	0.9878	0.969	0.9601	0.9554	0.9527	0.9499	0.9478
2	0.9912	0.9765	0.9702	0.966	0.9639	0.9599	0.9562
3	0.9885	0.9816	0.978	0.9764	0.9741	0.9731	0.9696
4	0.99	0.9822	0.9726	0.9673	0.9645	0.9612	0.9569
5	0.9897	0.9759	0.967	0.9603	0.9537	0.952	0.9504
6	0.9865	0.9783	0.9697	0.9648	0.9597	0.958	0.9563
7	0.9876	0.9765	0.9694	0.9665	0.9615	0.9596	0.9589
8	0.9912	0.9757	0.9672	0.9636	0.9601	0.957	0.9553
9	0.9901	0.9802	0.9743	0.9722	0.969	0.9663	0.9651
10	0.9882	0.9799	0.9757	0.9719	0.9702	0.9663	0.9632
11	0.9872	0.9747	0.9669	0.9641	0.9624	0.9595	0.9557
12	0.9887	0.9756	0.971	0.9684	0.9664	0.9638	0.9608
13	0.9904	0.9783	0.9706	0.9687	0.9663	0.9632	0.9597
14	0.9883	0.9782	0.9733	0.9713	0.9685	0.9654	0.9625
15	0.9881	0.9775	0.9694	0.9673	0.965	0.9628	0.96
16	0.9882	0.9805	0.9732	0.9688	0.9662	0.9634	0.9605
17	0.9886	0.973	0.9665	0.9637	0.9615	0.9595	0.9566
18	0.9915	0.977	0.9692	0.9641	0.9601	0.9593	0.9569
19	0.9878	0.9745	0.9672	0.9633	0.9614	0.9588	0.9557
20	0.9909	0.9747	0.9709	0.9672	0.9649	0.9624	0.96

Then again following the 8-step probabilities distribution calculation procedure, the

unconditional and predicted unconditional probabilities distribution of reliability at load cycles 420400 and 492400 are illustrated in the Figs.5.7 and 5.8.

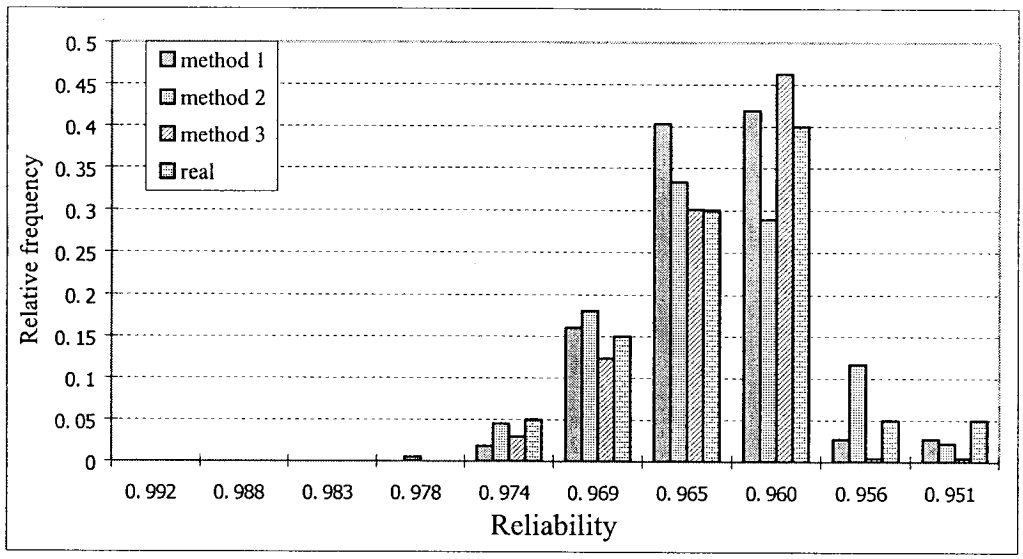

Figure 5.7 Histogram of unconditional probabilities of reliability at load cycle 420400 based on reliability function in terms of 10 divisions

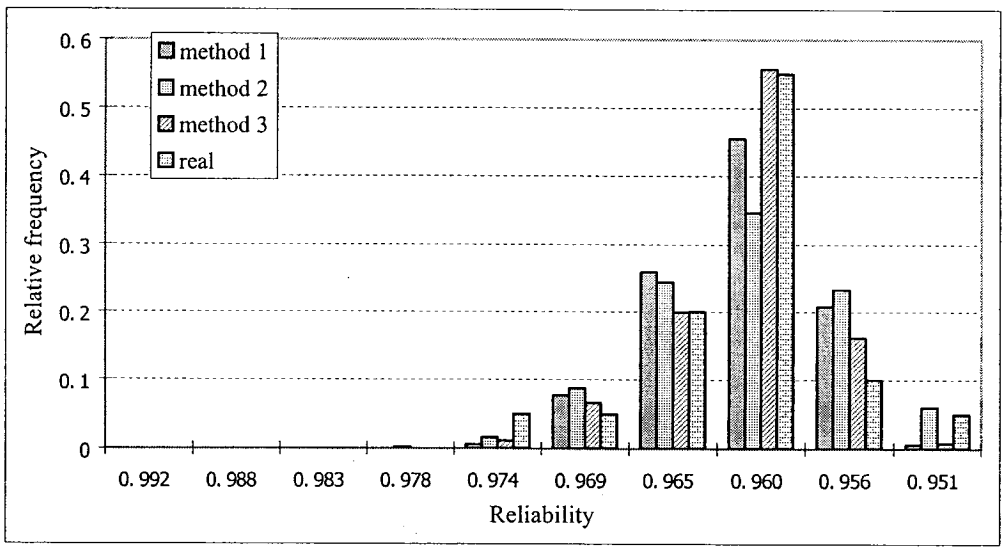

Figure 5.8 Histogram of predicted unconditional probabilities of reliability at load

cycle 492400 based on reliability function in terms of 10 divisions

The change in laminated specimen reliability as the load cycle increases can be expressed from Fig.5.9 that 2.94% of specimen's reliability falls in the range of 0.969 to 0.974 at load cycle 420400 while only 1.06% of specimen's reliability in that range at load cycle 492400; 12.36% of specimen's reliability falls in the range of 0.965 to 0.969 at load cycle 420400 while only 6.28% of specimen's reliability in that range at load cycle 492400; similarly, 46.29% of specimen's reliability falls in the range of 0.956 to 0.960 at load cycle 420400 but 58.32% of specimen's reliability is in that range of load cycle 492400, and so on. It can be noticed from fig.5.9 that the maximum relative frequency of reliability falls under the low range of reliability as the no. of load cycles increases.

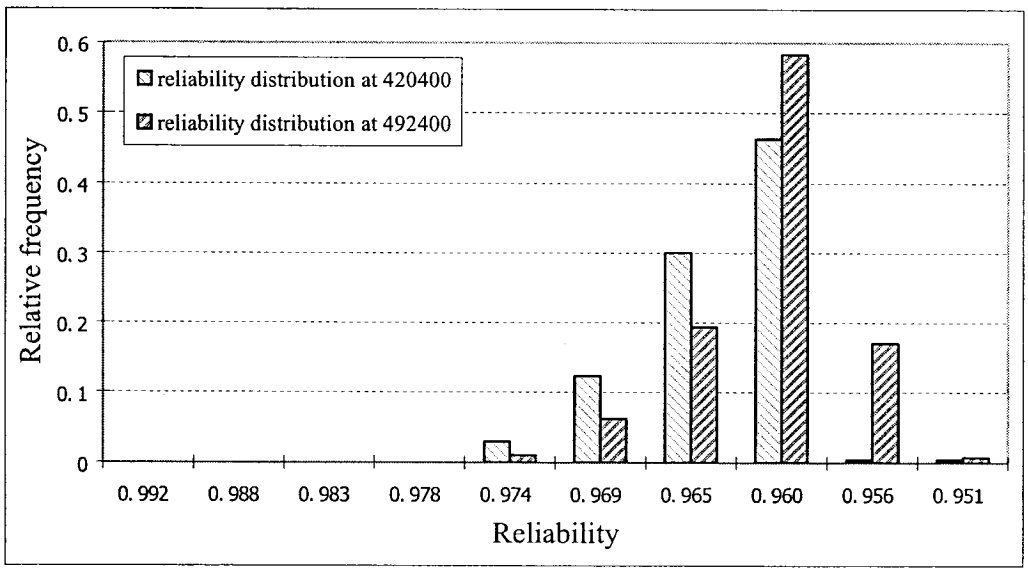

Figure 5.9 Comparison of reliability distribution at load cycles 420400 and 492400 in terms of 10 divisions

5.4.2 Markov process modeling of reliability based on hazard rate

The reliability of specimen at any load cycles can be expressed by knowing λ_i from equation (5.1):

$$R(n) = \exp[-\int_0^{n_n} \lambda(\xi)d\xi] \tag{5.4}$$

where $R(n)$ is the reliability at load cycle n_n, the $-\int_0^{n_n} \lambda(\xi)d\xi$ can be rewritten in terms of various hazard rates at different damage stages as following:

$$\int_0^{n_n} \lambda(\xi)d\xi = \int_{n_1}^{n_2} \lambda_1(\xi)d\xi + \int_{n_2}^{n_3} \lambda_2(\xi)d\xi + \int_{n_3}^{n_4} \lambda_3(\xi)d\xi + \ldots + \int_{n_{n-1}}^{n_n} \lambda_n(\xi)d\xi \tag{5.5}$$

where $n_1, n_2, \ldots, n_n$ denote the load cycles at damage stages 1, 2, 3,…, n.

Then based on the hazard rates data from table 5.1, the reliabilities corresponding to the load cycles based on equations (5.4) and (5.5) are calculated and listed below.

Table 5.3 The specimen reliabilities at different load cycles based on hazard rates under LCT:

Spec.	2800 cycles	60400 cycles	132400 cycles	204400 cycles	276400 cycles	348400 cycles	420400 cycles
1	0.9877	0.9687	0.9598	0.9551	0.9524	0.9496	0.9475
2	0.9912	0.9764	0.97	0.9658	0.9637	0.9598	0.956
3	0.9884	0.9815	0.9779	0.9763	0.974	0.973	0.9695
4	0.9915	0.9769	0.969	0.9639	0.96	0.9591	0.9567
5	0.9896	0.9757	0.9668	0.9601	0.9535	0.9517	0.9502
6	0.9864	0.9781	0.9695	0.9646	0.9595	0.9578	0.9562
7	0.9875	0.9763	0.9693	0.9664	0.9613	0.9595	0.9587
8	0.9912	0.9756	0.967	0.9634	0.9599	0.9568	0.9551
9	0.99	0.9801	0.9742	0.9721	0.9689	0.9662	0.9649
10	0.9882	0.9798	0.9755	0.9718	0.9701	0.9661	0.9631
11	0.9871	0.9745	0.9667	0.9639	0.9622	0.9593	0.9555
12	0.9887	0.9754	0.9709	0.9682	0.9662	0.9636	0.9606
13	0.9904	0.9781	0.9704	0.9685	0.9661	0.963	0.9595
14	0.9883	0.978	0.9732	0.9711	0.9684	0.9652	0.9624
15	0.988	0.9774	0.9692	0.9672	0.9649	0.9627	0.9598
16	0.9881	0.9804	0.973	0.9687	0.9661	0.9633	0.9603
17	0.9885	0.9728	0.9663	0.9635	0.9613	0.9593	0.9564
18	0.99	0.9821	0.9725	0.9671	0.9644	0.961	0.9568
19	0.9878	0.9744	0.967	0.9631	0.9612	0.9586	0.9555
20	0.9909	0.9745	0.9707	0.9671	0.9648	0.9622	0.9598

Again, the Markov process modeling is done using the above reliability data. The 8-step calculation method written in chapter 4 is followed here. The unconditional and predicted unconditional reliability probabilities histogram with 10 reliability divisions at load cycles 420400 and 492400 are shown in Figs. 5.10 and 5.11.

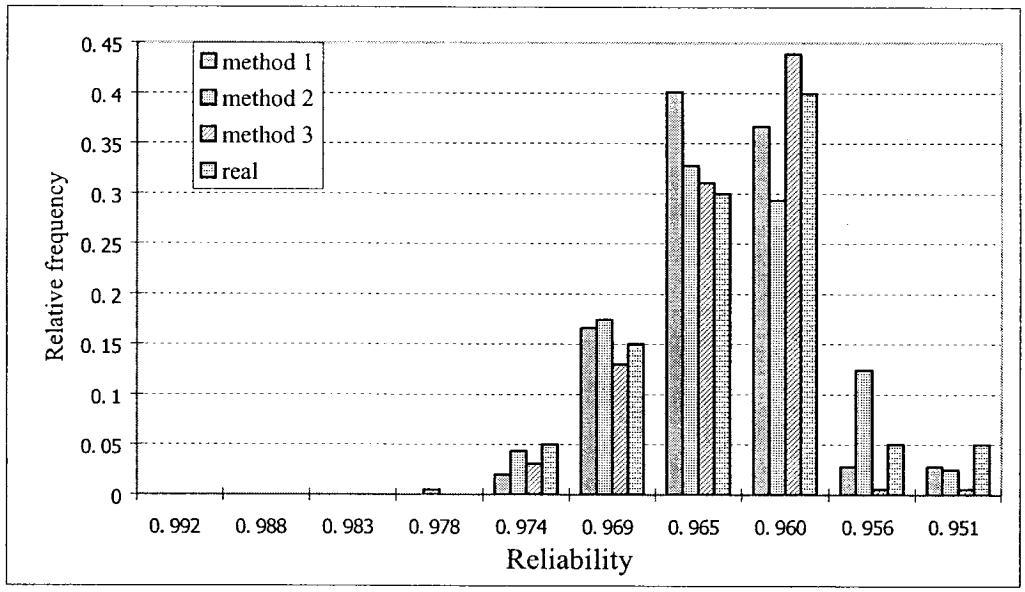

Figure 5.10 Histogram of unconditional probabilities of specimen reliability at load cycle 420400 in terms of 10 divisions

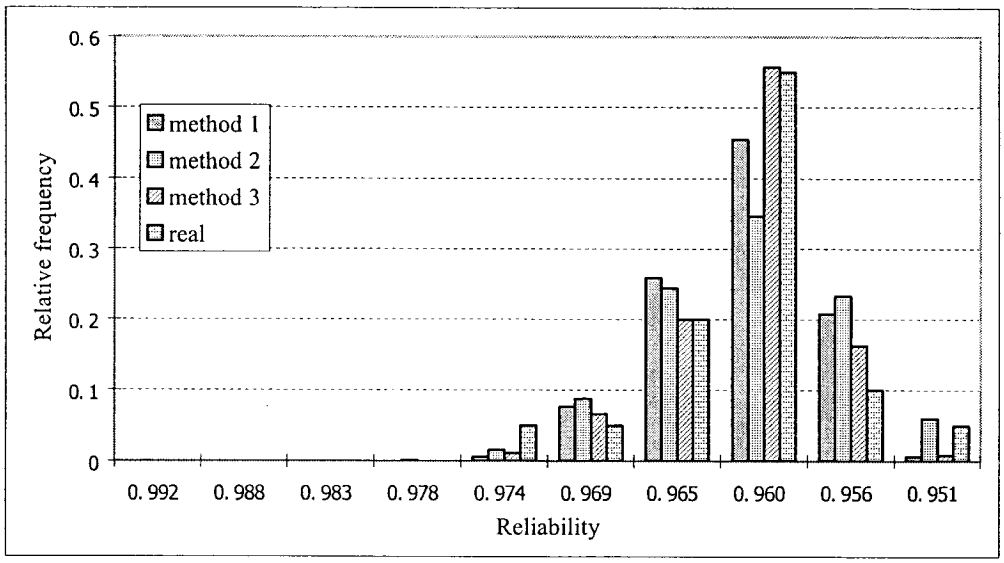

Figure 5.11 Histogram of predicted unconditional probabilities of specimen reliability at load cycle 492400 in terms of 10 divisions

5.4.3 Markov process modeling of reliability based on failure density function

In the same manner, the failure density function at load cycle n can be written as below based on its definition:

$$f_n = \frac{E_n - E_{n+1}}{E_0 \times \Delta N} \tag{5.6}$$

where E_0, E_n, E_{n+1} stand for initial Young's modulus, Young's modulus at load cycles n & $n+1$ respectively. ΔN denotes the load cycle deviation between n and $n+1$.

The failure probability at load cycle n is determined by:

$$F_n = \int_{n_1}^{n_2} f_1 d\xi + \int_{n_2}^{n_3} f_2 d\xi + \int_{n_3}^{n_4} f_3 d\xi + \ldots + \int_{n_n}^{n_{n+1}} f_n d\xi \tag{5.7}$$

where $n_1, n_2, \ldots n_n$ denote the load cycles at damage stages 1,2,3...n.

Then the reliability at load cycle n in this case is given by:

$$R(n) = 1 - F_n \tag{5.8}$$

Based on the equations (5.6), (5.7), and (5.8), the following reliabilities data can be calculated from the original data listed on the table 4.1:

Table 5.4 The specimen reliabilities at different load cycles based on failure density function under LCT:

specimen	2800 cycles	60400 cycles	132400 cycles	204400 cycles	276400 cycles	348400 cycles	420400 ccycles
1	0.9878	0.969	0.9601	0.9554	0.9527	0.9499	0.9478
2	0.9912	0.9765	0.9702	0.966	0.9639	0.9599	0.9562
3	0.9885	0.9816	0.978	0.9764	0.9741	0.9731	0.9696
4	0.9915	0.977	0.9692	0.9641	0.9601	0.9593	0.9569
5	0.9897	0.9759	0.967	0.9603	0.9537	0.952	0.9504
6	0.9865	0.9783	0.9697	0.9648	0.9597	0.958	0.9563
7	0.9876	0.9765	0.9694	0.9665	0.9615	0.9596	0.9589
8	0.9912	0.9757	0.9672	0.9636	0.9601	0.957	0.9553
9	0.9901	0.9802	0.9743	0.9722	0.969	0.9663	0.9651
10	0.9882	0.9799	0.9757	0.9719	0.9702	0.9663	0.9632
11	0.9872	0.9747	0.9669	0.9641	0.9624	0.9595	0.9557
12	0.9887	0.9756	0.971	0.9684	0.9664	0.9638	0.9608
13	0.9904	0.9783	0.9706	0.9687	0.9663	0.9632	0.9597
14	0.9883	0.9782	0.9733	0.9713	0.9685	0.9654	0.9625
15	0.9881	0.9775	0.9694	0.9673	0.965	0.9628	0.96
16	0.9882	0.9805	0.9732	0.9688	0.9662	0.9634	0.9605
17	0.9886	0.973	0.9665	0.9637	0.9615	0.9595	0.9566
18	0.99	0.9822	0.9726	0.9673	0.9645	0.9612	0.9569
19	0.9878	0.9745	0.9672	0.9633	0.9614	0.9588	0.9557
20	0.9909	0.9747	0.9709	0.9672	0.9649	0.9624	0.96

When compared with the reliability data based on hazard rate, it is observed that reliability data got from both methods have only minor difference. For example, the reliability is 0.9885 for specimen #3 at load cycle 2800 calculated from failure density function and 0.9884 calculated from hazard rate. Therefore, the unconditional and predicted unconditional probabilities distribution at load cycles 420400 and

492400 in terms of 10 reliability divisions based on failure density function are exactly the same as the results from hazard rate indicated in Figs. 5.10 and 5.11.

5.5 Discussion and conclusion

One can observe that not only the reliability results at a given load cycles are almost the same, which were obtained from three methods namely the basic concept, hazard rate function and failure density function, but also the results of unconditional and predicted unconditional probabilities distribution based on the above three methods are the same as seen in Figs.5.12 and 5.13.

Comparing the reliability results from load condition one (normal tension-compression load) and load condition two (over tension load) in Fig. 5.14, it shows that the average reliability corresponding to load cycles for load condition two (the average value of reliability is determined by sum of 20 specimens' reliabilities divided by 20) drops faster than that for load condition one, although both of them have same level of hazard rate after about 200,000 cycles.

It is more interesting to compare the reliability and hazard rate for both load conditions from Fig.5.15 (combination chart of Figs. 5.2 and 5.14). One can see that the reliabilities from both load conditions keep on decreasing as load cycle increases no matter whether the hazard rates decrease, remain stable, or even increase.

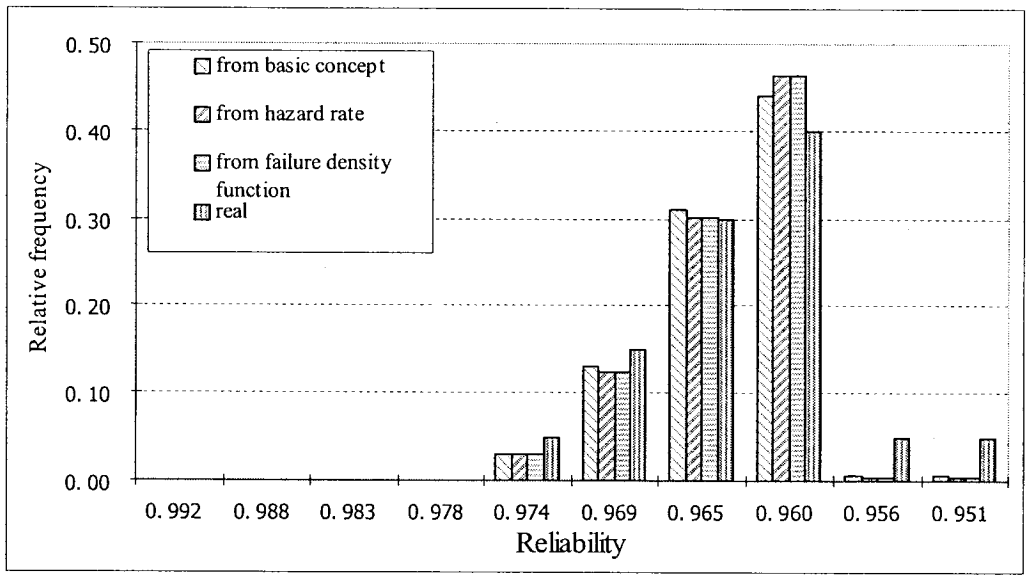

Figure 5.12 Histogram of unconditional probabilities based on three calculation methods in terms of 10 divisions

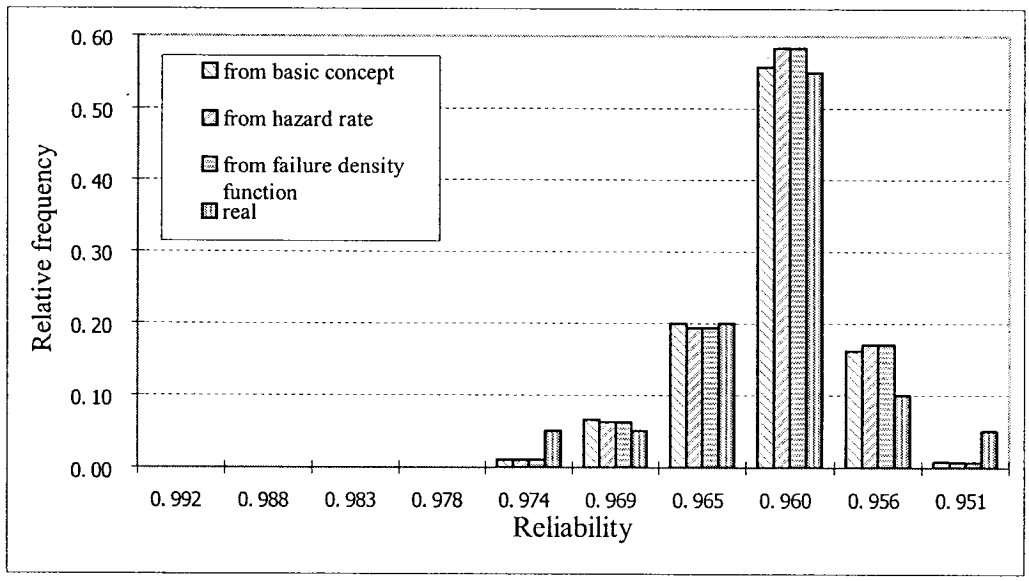

Figure 5.13 Histogram of predicted unconditional probabilities based on three calculation methods in terms of 10 divisions

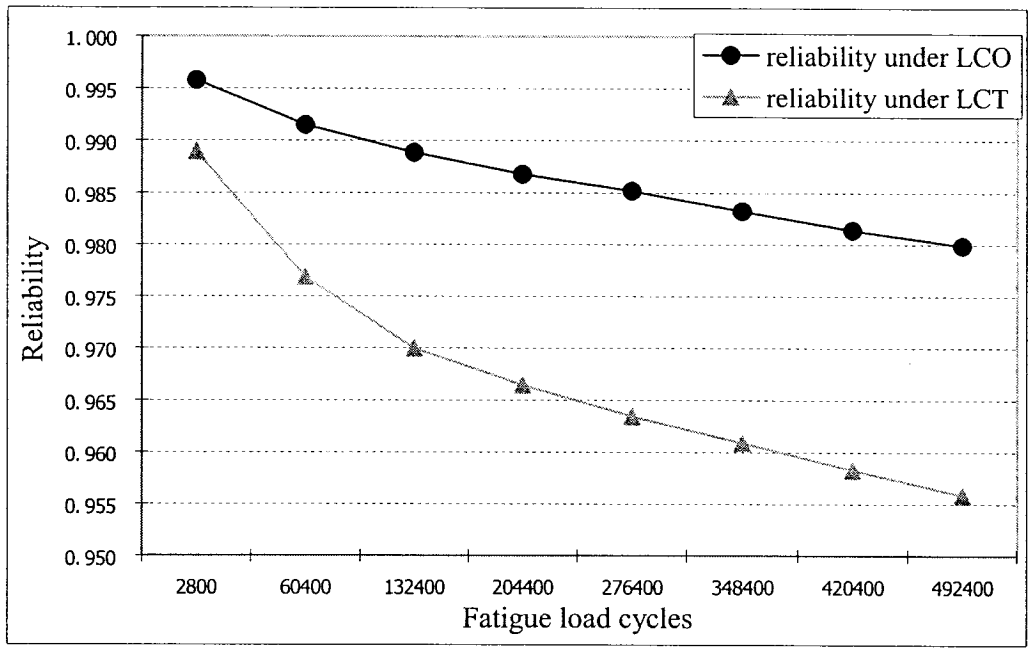

Figure 5.14 Comparison of reliability from load conditions LCO and LCT

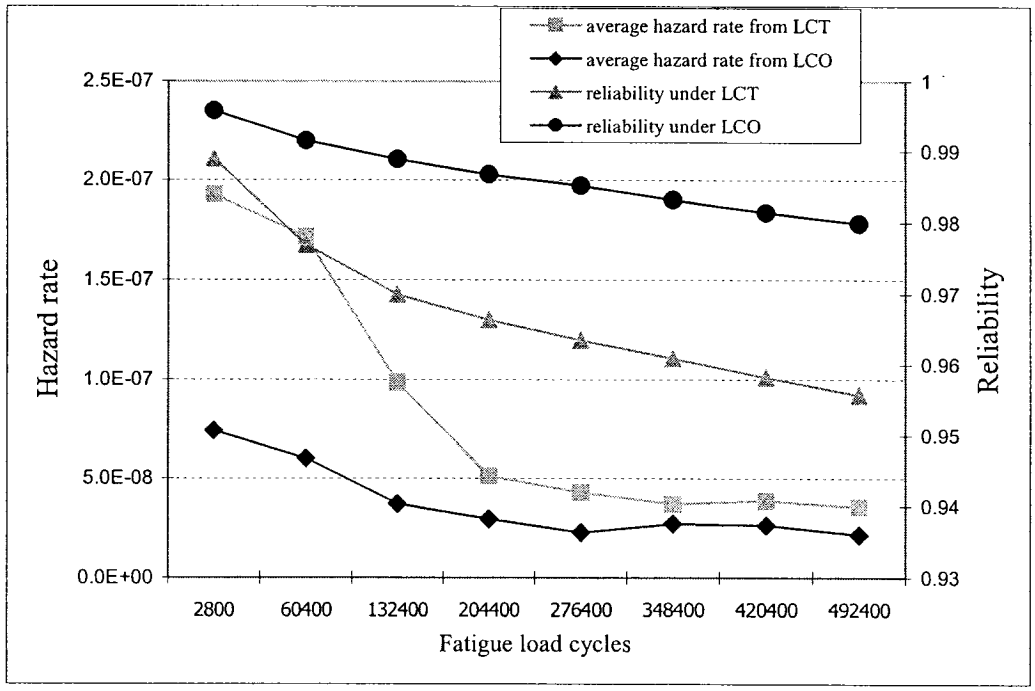

Figure 5.15 Comparison of average hazard rate and reliability

Chapter 6

Conclusions and Recommendations

6.1 Conclusions

The symmetric tapered composite laminates were made using Graphite/Epoxy with manual lay-up and with variety of configurations and different locations of pre-set delamination, and tested under two fatigue load conditions. In the present thesis, a stochastic and reliability approach has been used based on the test data, with the aim of determining the composite laminates fatigue behavior and the statistical distribution of fatigue damage accumulation process. The conclusions are listed below:

- ✓ It has been proved from test results that the strength and stiffness of symmetric tapered composite laminates with lay-up A ($[0/\pm45/0/(\pm45)_3/\pm45/0_7]_S$ laminate that reduced to $[0/\pm45/0/\pm45/0_7]_S$) that has a thicker core layer but thinner belt layer is much stronger than lay-up B ($[0_7/\pm45/0/(\pm45)_3/\pm45/0]_S$ laminate that reduced to $[0_7/\pm45/0/\pm45/0]_S$)

which has a thinner core layer but thicker belt layer.

- ✓ It has been proved from test results that the locations of pre-set delamination in composite laminate specimen will affect the fatigue test results largely. It has been shown that when the location of pre-set delamination is closer to the middle of the symmetric tapered laminate, the damage is more severe and damage speed is faster.
- ✓ Unlike metallic materials, the over tension load will produce the broad failure of composite laminates instead of building-up plastic zone to resist further growth of crack. The test data corresponding to any load cycles in chapter 3 show that the strength and stiffness of composite laminate with over-tension load is less when compared with normal tension-compression load and from chapter 5 the test data show that the specimen's reliability with over-tension load drops faster when compared with normal tension-compression load.
- ✓ Markov Chain modeling of fatigue damage accumulation process has been carried out based on fatigue parameter (specimen compliance) as well as the true probability distribution. The probability distribution at a given load cycle is computed and presented in present thesis. Four methods have been used in calculating TPMs based on appropriate number of damage states, such as the Maximum Entropy Method (MEM), Gaussian (single and Bivariate) probability distribution and joint probability density function, and combination method. The results show a reasonable match

with the actual probability distribution.

- ✓ The reliability of test specimens is computed and analyzed using three parameters, which are reliability function, hazard rate (or failure rate function), and failure density function. The results show very good match with the actual reliability status.
- ✓ The Markov Chain modeling for hazard rate and reliability of test specimens is also established and developed in present thesis, and the results illustrate that the reliability for the specimens under load condition two (with over tension load based on normal tension-compression load) drops faster when compared with that of load condition one (with normal tension-compression load), no matter whether the hazard rate decreases, increases or remains stable.

6.2 Recommendations

It would be very interesting if one can go for further research focusing on the following related works:

- ✓ The laminate specimen can be tested until total failure under the two loading conditions. Based on this, we can get the complete hazard rate and reliability curve instead of getting just a part of these curves as presented in the present thesis.

- ✓ Estimate the number of cycles at which the Young's modulus (or compliance) of specimen will drop below the critical Young's modulus (or exceed critical compliance), and determine the corresponding probability distribution.
- ✓ Predict the reliability distribution at the load cycles when the laminate specimen fails completely.

References

[1] K. L. Reifsnider, *Fatigue of Composite Materials*, 1990, Elsevier Science Publishers B. V.

[2] Jie Tong, "Three stages of fatigue crack growth in GFRP composite laminates", Journal of Engineering Materials and Technology, Vol. 123, 01/ 2001, pp.139-143.

[3] Ramesh Talreja, *Fatigue of Composite Materials,* 1987, Lancaster Technomic Pub. Co.

[4] WoonBong Hwang and Kyung S. Han, "Fatigue of composite materials-damage model and life prediction", Composite Materials: Fatigue and Fracture, Vol. 2, 1989, pp. 87-102.

[5] T. K. O'Brien, M. Rigamonti and C. Zanotti "Tension fatigue analysis and life prediction for composite laminates", International Journal of Fatigue, Vol.11, 11/1989, pp. 379-393.

[6] T. K. O'Brien, "Towards a damage tolerance philosophy for composite materials and structures", Composite Materials: Testing and Design, Vol. 9, 1990, pp. 7-33.

[7] J. N. Yang, "Fatigue and residual strength degradation for graphite/epoxy composites under tension-compression cyclic loading," Journal of Composite Materials, Vol. 12, 1978, pp.19-39.

[8] J. N. Yang, S. H. Yang and D. L. Jones, "A statistical model for predicting fatigue life of graphite/epoxy laminates," Journal of Composite Technology and Research, Vol. 11, 1989, pp.129-134.

[9] Wen-Fang Wu, L. J. Lee and S. T. Choi, "A study of fatigue damage and fatigue life of composite laminates", Journal of Composite Materials, Vol. 30, No.1/1996, pp. 123-139.

[10] J. R. Schaff and B. D. Davidson, "Life prediction methodology for composite structures. Part I-Constant amplitude and two-stress level fatigue", Journal of Composite Materials, Vol. 31, 2/1997, pp. 128-157.

[11] Jerzy P. Komorowski, Dminique Lfebvre, Clermount Roy and Catherine Randon, "Stacking sequence effects and delamination growth in graphite/epoxy laminates under compression-dominated fatigue loading", Composite Materials: Fatigue and Fracture, Vol. 5, 1995, pp. 249-267.

[12] G. Meirinhos, J. Rocker, J-P. Cabanac and J.-J. Barrau, "Tapered laminates under static and fatigue tension loading", Composite Science and Technology, Vol. 13, 2001, pp. 26-41.

[13] M. W. Hyer, *Stress Analysis of Fiber-Reinforced Composite Materials,* 1998, Boston, USA.

[14] Kan He, *Interlaminar Stresses and Fracture Behavior in Thickness-Tapered Composite Laminates*, Ph. D. Thesis, 2002, Concordia University, Montreal.

[15] O. O. Ochoa and W. S. Chan "Tapered laminates: A study on

delamination characterization" Proceedings of the American Society for Composites third conference, 1988.

[16] Gretchen Bostaph Murri, Satish A. Salpekar and T. Kevin O'Brien, "Fatigue delamination onset prediction in unidirectional tapered laminates", Composite Materials: Fatigue and Fracture, Vol. 3, 1991, pp. 312-339.

[17] S. A. Salpekar, I. S. Raju, and T. K. O'Brien, "Strain-energy-release rate analysis of delamination in tapered laminate subjected to tension load", Journal of Composite Materials, Vol. 25, 02/1991, pp. 118-139.

[18] Erian A. Armanios and Levend Parnas, "Delamination analysis of tapered laminated composites under tensile loading", Composite Materials: Fatigue and fracture, Vol. 3, 1991, pp. 340-358.

[19] Gretchen Bostaph Murri, T. Kevin O'Brien and Satish A. Salpekar, "Tension fatigue of glass/epoxy and graphite/epoxy tapered laminates", Journal of Composite Materials, Vol. 12, 06/1987, pp. 105-117.

[20] T. K. O'Brien, "Local delamination in laminates with angle ply matrix cracks, part II: Delamination fracture analysis and fatigue characterization", Composite Materials: Fatigue and Fracture, Vol. 4, 1993, pp. 507-538.

[21] V. M. Harik, J. R. Klinger and T. A. Bogetti, "Low-cycle fatigue of unidirectional composites: Bi-linear S-N curves", International Journal of Fatigue, Vol. 24, 2002, pp. 455-462.

[22] A. Rotem, "The fatigue behavior of orthotropic laminates under tension-compression loading", International Journal of fatigue, 13, 1991, pp.209-215.

[23] V. M. Harik, J. R. Klinger and T. A. Bogetti, "Low cycle fatigue of unidirectional laminates: stress ratio effects", Journal of Engineering Materials and Technology, Vol. 122, 10/2000, pp. 415-419.

[24] Woo-Min Kyoung, Chun-Gon Kim and Chang-Sun Hong, "Modeling of composite laminates with multiple delaminations under compressive loading", Journal of Composite Materials, Vol.32, 10/1998, pp.951-969.

[25] Hiroshi Suemasu, "Effects of multiple delaminations on compressive buckling behaviors of composite panels", Journal of Composite Materials, Vol. 27, No.12/1993, pp.1172-1191.

[26] Wayne W. Stinchcomb and Charles E. Bakis, "Fatigue behavior of composite laminates", Fatigue of composite materials, 3/1990, pp.125-146.

[27] Joakim Schoen, "Model for predicting the load ratio for the shortest fatigue life", Composite science and technology, 05/2001, pp.135-158.

[28] J. Payan and C. Hochard "Damage modeling of laminated carbon/epoxy composites under static and fatigue loadings" International Journal of Fatigue, 24/2002, pp. 299-306.

[29] J. N. Yang and M. D. Liu, "Residual strength degradation model and theory of periodic proof test for graphite/epoxy laminates," Journal of

Composite Materials, Vol. 11, 1977, pp. 176-203.

[30] Ying-Jin Lo, Ching-Ho Liu, Diing-Guey Hwang, Jin-Fu Chang, Jong-Cheng Chen, Wen-Yin Chen, and Shu-En Hsu, "High-temperature behaviors of an innovative polymeric matrix composite", ASTM STP 1174, 1993.

[31] W. W. Stinchcomb, K. L. Reifsnider, L. A. Marcus and R. S. Williams "Effects of frequency on the mechanical response of two composite materials to fatigue loads" ASTM STP569, 1975.

[32] G. C. Tsai, J. F. Doyle and C. T. Sun, "Frequency effects on the fatigue life and damage of graphite/epoxy composites", Journal of Composite Materials, Vol. 21, Jan. 1987, pp.2-13.

[33] V. Barron, M. Buggy and N. H. McKenna, "Frequency effects on the fatigue behavior on carbon fiber reinforced polymer laminates", Journal of Material Science, Vol. 36, 2001, pp.1755-1761.

[34] J. L. Bogdanoff and F. Kozin, "Probabilistic Models of Cumulative Damage", 1985, Wiley, New York.

[35] R. Ganesan, "A data-driven stochastic approach to model and analyze test data on fatigue response", Computers and Structures, Vol. 76, 2000, pp. 517-531.

[36] James N. Siddall, *Probabilistic Engineering Design: Principles and Applications*, 1983, Marcel Dekker, New York.

[37] J. S. Bendat and A. G. Piersol, *Random Data: Analysis and*

Measurement Procedures, 1986, Wiley-Interscience, New York.

[38] Boris Gnedenko, Igor Ushakov and James Falk, *Probabilistic Reliability Engineering*, 1995, John Wiley & Sons.

[39] K. Schulte, "Compressive static and fatigue loading of continuous fiber-reinforeced composites", Compression Response of Composite Structures, ASTM STP 1185, 1994, pp. 278-305.

[40] Gretchen Bostaph Murri and Roderick H. Martin, "Effect of initial delamination on Mode I and Mode II interlaminar fracture toughness and fatigue fracture threshold", Composite Materials: Fatigue and Fracture, Vol. 4, 1993, pp. 239-256.

[41] H. Mao and S. Mahadevan "Fatigue damage modeling of composite materials", Composite Structures, Vol. 14, 2002, pp. 201-216.

[42] Bangyan Liu and Larry B. Lessard "Fatigue and damage-tolerance analysis of composite laminates: stiffness loss, damage-modeling, and life prediction", Composite Science and Technology, 5/1994, pp. 57-72.

[43] K. L. Reifsnider and A. Talug, "Analysis of fatigue damage in composite laminates", International Journal of Fatigue, Vol. 2, 01/1980, pp. 3-11.

[44] Lakshmi Vara Prasad Pondugala, *Stochastic J-integral and Reliability of Composite Laminates Based On A Computational Methodology Combining Experimental Investigation, Stochastic Finite Element Analysis And Maximum Entropy Method*, M. A. Sc Thesis, 2000, Concordia University, Montreal.

[45] Valeria La Saponara and George A. Kardomateas, "Statistical considerations in the analysis of data from fatigue tests on delaminated cross-ply graphite/epoxy composites", Journal of Engineering Materials and Technology, Vol.122, 10/2000, pp.409-414.

[46] Prakash Chandra Gope, "Determination of minimum number of specimens in S-N testing", Journal of Engineering Materials and Technology, Vol.124, 10/2002, pp.421-427.

[47] Vasyl Michael Harik, "Control of damage in composite laminates by ply-stacking designs: characteristic failure signatures and safety criteria", Journal of Engineering Materials and Technology, Vol.125, 10/2003, pp. 385-393.

[48] Assimina A. Pelegri and Diwakar N. Kedlaya, "On the energy release rate of fatigued composites subjected to compressive overloads", Journal of Engineering Materials and Technology, Vol. 122, 10/2000, pp. 443-449.

[49] H. Mao and S. Mahadevan, "Fatigue Damage Modeling of Composite Materials", 2000, Vanderbilt University, P.O. Box 1831B, Nashville, TN 37235, USA.

Appendix A

MATLAB program

```
^^^^^MAIN PROGRAM^^^^

%%Method 2: Gaussion calculation method for both joint and individual probabilities%%

clear all;
clc;
global p1 p2 p3 p4 ww o o1 o2 o3 o4 o5;
format long;
KIC=1;
fl=0;


%%%%%%%   INPUT THE NO. OF MOMENTS      %%%%%%%%%%%%
for KIC=1:6


    d = datakic(KIC);     % Supply the data
    D=d(KIC,:)
    M = 4;                    % Number of Moment
    Nsamp = length(D);      % Total number of samples
    Nrecd = 1;
    i= 1:Nsamp;
    X= D(Nrecd,i);

%%%%%%%%%%%%%%%%%%%%%%%%%%%%%%%%%%%%%%%%%%%%%%%%%%%%
    g = datakjc(KIC);
    G = g(KIC,:);
    Nsamp1 = length(G);
    Nrecd1=1;
    j= 1: Nsamp1;
    Y= G(Nrecd1,j);
%%%%%%%%%%%%%%%%%%%%%%%%%%%%%%%%%%%%%%%%%%%%%%%%%%%%
```

```
%%%%%%%symbol defined for Gaussian joint probability density function
 P6 = corrcoef(D,G)                    %correlation coefficients of two variables
 ww = P6(1,2)
 p1=mean(D)
 p2=std(D)
 p3=mean(G)
 p4=std(G)
%--------------------  PLOT  ----------------------------------------------
%   subplot(311)
%         plot(ARG(:,4),DENS(:,4),'-+')
%
%
%       % Plot the density curves for "n" iterations %
%       xlabel('fatigue damage parameter: compliance(10e-11/pa)') %
%   ylabel('Density Function')
%   grid
%
%       subplot(312)
%       hist(D,7);
%       grid
%----------------------- define damages stages limits-----------------------------------------------

 %%%transition probability matrix%%%%%

T1=0;                                 %%% to check whether the individual probability density at a certain cycles is equal to unity
Q1=0;                                 %%% to check that whether the whole area integration are becoming to unity for joint gaussian distribution
QA1=0;                                %%% (actually b matrix) to check whether the sum of each row is equal to unity

X1max=2.6006;                         %%% the range of damage states
X1min=2.4478;

%%%% transition probability matrix calculation

    N=8                 %the number of damage states
    p=X1min;

    for k=1:N

        T = quad(@myfun1,p,p+(X1max-X1min)./N)
```

```
            T1 = T1 + T

            r=X1min

            QA1=0

            for m=1:N

                if   m>=k;

                    Q = dblquad(@myfun,p,p+(X1max-X1min)./N,r,r+(X1max-X1min)./N)
                    if 0.001>Q; Q>=100
                        Q=0
                    end

                    Q1=Q1+Q
                else
                    Q=0
                end

                  QA=Q./T

                  a(k,m,KIC)=QA;                                    %%%transition
probability matrix%%%%%

                  QA1=QA1+QA;
                  r=r+(X1max-X1min)./N
            end

          b(1,k,KIC)=QA1;
          p=p+(X1max-X1min)./N

      end

end

 %%% prediction calculation%%%%%%%

    for u=1:N
          for v=1:N
              for w=1:6
              C=a(u,v,:)

              end
```

```
            f(u,v)=0.78*std(C)+mean(C)          %% calculation of probability matrix
prediction

        end

    end
a1=[0.4,0.45,0.15,0,0,0,0,0]
a
a0=a(:,:,1)*a(:,:,2)*a(:,:,3)*a(:,:,4)*a(:,:,5)*a(:,:,6)*f   %%m-step transition probability matrix
b
f
a2=a1*a0                                  %% unconditional probability at last load cycle

%%%%%%%%%%%%%%%%%%%%%%%%%%%%%%%%%%%%%%%%%%%%
```

^^^^SUB PROGRAM^^^

```
function s = myfun(x,y)
global p1 p2 p3 p4 ww;
s=
exp((-1./(2*(1-ww.^2)))*(((x-p1)./p2).^2-2*ww*(((x-p1)./p2)*((y-p3)./p4))+((y-p3)./p4).^2))./
(2*pi*p2*p4*sqrt(1-ww.^2));
```

```
function t = myfun1(x)
global p1 p2;
t = (1./(p2*sqrt(2*pi)))*exp (-0.5*((x-p1)./p2).^2);
```